2-P

CR-115761

MSC-04800
FZK-390
15 March 1972

STUDY OF ACOUSTIC EMISSION DURING MECHANICAL TESTS OF LARGE FLIGHT WEIGHT TANK STRUCTURE

(NASA-CR-115761) STUDY OF ACOUSTIC EMISSION DURING MECHANICAL TESTS OF LARGE FLIGHT WEIGHT TANK STRUCTURE Final Report, Y. Nakamura, et al (General Dynamics/Fort Worth) 15 Mar. 1972 95 p CSCL 20A G3/23

N72-31667

Unclas
39393

GENERAL DYNAMICS
Convair Aerospace Division
P.O. Box 748, Fort Worth, Texas 76101

95

MSC-04800
FZK-390

STUDY OF ACOUSTIC EMISSION DURING MECHANICAL TESTS OF LARGE FLIGHT WEIGHT TANK STRUCTURE

By

Y. Nakamura
B. O. McCauley
C. L. Veach

March 1972

Prepared for

National Aeronautics and Space Administration
Manned Spacecraft Center

GENERAL DYNAMICS
Convair Aerospace Division
P.O. Box 748
Fort Worth, Texas 76101

PREFACE

This is the final report on a study of acoustic emission during mechanical tests of large flight weight tank structure carried out by the Convair Aerospace Division of General Dynamics Corporation. The major portion of the study was supported by the National Aeronautics and Space Administration, Manned Spacecraft Center, under Contract NAS9-12229, covering the period from September 1971 to February 1972. Dr. James L. Youngblood was the Technical Monitor of the Contract.

The program was conducted by the Research and Engineering Department of the Convair Aerospace Division with R. T. Anderson of San Diego Operation and Y. Nakamura of Fort Worth Operation as Co-Program Managers. The study described in this report was performed by Y. Nakamura, B. O. McCauley, and C. L. Veach of the Fort Worth Operation.

Assistance in various forms offered by Messrs. R. T. Anderson, W. M. Thomas, C. F. Johnson, and other personnel of the San Diego Operation during the study is appreciated. We also wish to thank J. W. Hagemeyer of the Fort Worth Operation for his valuable discussions during this study and critical review of the draft of this report.

ABSTRACT

A PPO-insulated, flight-weight, subscale, aluminum tank was monitored for acoustic emissions during a proof test and during 100 cycles of environmental test simulating space flights. The use of a combination of frequency filtering and appropriate spatial filtering to reduce background noise was found to be sufficient to detect acoustic emission signals of relatively small intensity expected from subcritical crack growth in the structure. Several emission source locations were identified, including the one where a flaw was detected by post-test x-ray inspections. For most source locations, however, post-test inspections did not detect flaws; this was partially attributed to the higher sensitivity of the acoustic emission technique than any other currently available NDT method for detecting flaws. For these non-verifiable emission sources, a problem still remains in correctly interpreting observed emission signals.

TABLE OF CONTENTS

LIST OF FIGURES

SUMMARY

A PPO-insulated flight-weight, subscale, 2219 aluminum tank was monitored for acoustic emissions in order to evaluate the applicability of the technique to testing of such an internally insulated, thin-walled tank structure. The study was performed in three phases: pre-test preparation, proof test, and environmental test.

During the pre-test preparation,various specimen tests were conducted in the laboratory, methods of mounting acoustic transducers to the tank were investigated, and monitoring equipment to be used for the tank test was assembled and checked out. The primary data obtained from the specimen tests were, first, the amplitude distribution and absolute intensity of acoustic emission signals from subcritical and near-critical crack growth in 2219-T81 aluminum and,second, attenuation of acoustic waves in a PPO-foam-insulated aluminum plate. These data were used for planning the monitoring and for interpreting the monitoring results. The most satisfactory transducer-to-structure acoustic coupling agent to withstand the expected temperature cycles was found to be a mixture of Dow-Corning 33 wide-temperature bearing grease and Cerac SP102 fluorocarbon telomer dry lubricant. Dow-Corning 92-024 aerospace adhesive/sealant was chosen for bonding the transducer housing to the tank structure.

The proof test was monitored using six arrays of acoustic sensors to cover the entire tank structure. The test consisted of pressurization in water of the,as yet,uninsulated tank up to 75 psi (517 kN/m^2) in three stages. The presence of water on both sides of the thin aluminum structure caused severe attenuation of acoustic signals. Water was also considered responsible for a large number of small emission signals observed during the test. A group of emission sources was located in a region where a post-proof-test x-ray inspection detected a flaw. Several other emission signals were also observed. However, the result of the proof test was judged rather inconclusive primarily because of the following two reasons: The sensor distribution used was not dense enough to permit effective detection of weak signal sources, and the interpretation of detected signals as to the nature of their source was uncertain.

The environmental test was monitored after the monitoring setup was modified rather extensively based on the results of the proof test and specimen tests. The test consisted of thermal and pressure cycling of the insulated tank for one hundred times to simulate repeated space flights. The presence of the insulation was found to cause a large number of spurious acoustic emissions of small intensity whenever the tank pressure varied even slightly. Additional modifications of the monitoring setup were therefore necessary during the environmental test to overcome the problem. The signal processing technique most useful was the coincidence detection of signals to eliminate spurious signals originating near the sensors. By using a combination of this spatial filtration technique and narrow-band filtering of signals, several groups of emission signals of interest were detected. These could be classified into two major groups: extremely large amplitude signals and small amplitude signals. The former group of signals was too large to be caused by a growing crack in the aluminum structure and thus was suspected of being generated by partial breaking of material at or near the aluminum-insulation interface. The latter group of signals had its intensity in the range expected for subcritical crack growth in an aluminum sheet. However, since there were also other possible sources of these small amplitude emissions and since our present knowledge of the acoustic emission phenomenon is not sufficient to tell one from the other, their interpretation was uncertain. None of the consistently observed groups of small signals, however, showed a steady increase of activity with life cycles, indicating that none of these signals represented crack growth approaching its critical level. The post-environmental-test nondestructive inspection did not detect any significant crack growth in the structure.

From the results of this study two things are clear as to the application of acoustic emission technique for nondestructive inspection of complex structures. First, the current technology is adequate to detect and locate, but not to identify, small acoustic emission signals expected from subcritical crack growth in structures. Therefore, with appropriate equipment development, the technique can be used as a surveillance tool for nondestructive inspection. Second, for acoustic emission to be useful as an independent NDI tool, more research work on acoustic emission phenomenon itself is needed.

I. INTRODUCTION

The potential of the acoustic emission technique as a tool of nondestructive inspection and evaluation of structures and materials has been increasingly recognized by many in recent years as evidenced by the great interest demonstrated in a symposium held in late 1971 on this subject (Ref. 1). However, because of the newness of this technique, there are no established procedures universally applicable to all situations, and each new type of application requires special considerations of its own. An application of the technique to fracture control to assure safe structural life of spacecraft structures such as large, thin-walled, foam-insulated aluminum pressure vessel type fuel tanks is no exception. Although the acoustic emission technique has been applied quite extensively to testing of large, thick-walled pressure vessels in the past, particularly in nuclear applications, no data has been available to date on a thin-walled, foam-insulated pressure vessel.

In order to evaluate applicability of the acoustic emission technique to such a vessel used for holding liquid hydrogen for Space Shuttle vehicles, the present study was conducted. The test article used as a test bed for this investigation was a flight-weight, subscale insulated liquid hydrogen test tank fabricated at a San Diego plant of the Convair Aerospace Division of General Dynamics under Contract NAS9-10960, North American Rockwell P.O. MON7BMX-587600H. A detailed description of the test tank is available elsewhere (Ref. 2). Briefly, it is a 2219 aluminum tank of 69 in. (175 cm) diameter and 87 in. (220 mm) length with a wall thickness typically 1/16 in.(1.6 mm). After the initial proof test of the tank, the interior of the tank was insulated with PPO (polyphenylene oxide) foam, 1 to 1.8 in. (25-46 mm) thick.

The test of the tank was performed in two phases: a proof test, in which the, as yet, uninsulated tank was pressurized to 75 psi (516 kN/m^2) in water and an environmental test in which the insulated tank was thermally and pressure cycled for 100 times to simulate conditions expected in repeated space flights. The proof test of the tank was conducted at the Kearny Mesa Plant, and the environmental test of the insulated tank was conducted at the Sycamore Canyon Hydrogen Test Site, both at Convair Aerospace Division of General Dynamics in San Diego, California.

Several problems which were peculair to a monitoring of such a test were anticipated before the test. Because of the wide range ($-100^{\circ}F$ to $+300^{\circ}F$; $-73^{\circ}C$ to $+145^{\circ}C$) and rapid variation of

expected temperatures of the tank structure, the problem of selecting and mounting sensors to withstand and perform satisfactorily in such an adverse condition was anticipated. Another expected problem was the attenuation of acoustic signals by the presence of the PPO foam insulation. In addition, noise interference of various kinds was expected as usual with a monitoring of any structure. To find out how these problems could be solved, therefore, was one of the objectives of the present study.

The study was performed in three phases. In the first phase of the study, small specimens were tested in the laboratory to examine acoustic emission and signal attenuation properties of the material, several sensor mounting materials and mounting techniques were investigated, and the equipment was prepared for the monitoring of the actual tank structure. In the second phase of the study, the proof test of the uninsulated tank was monitored and the data were analyzed. In the third phase of the study, the environmental test of the insulated tank was monitored and the data were analyzed. In the following sections, details of these three phases and results are described and discussed.

Amplitudes of acoustic emission signals and threshold of signal detection are referred to repeatedly in this report. Unless specified otherwise, these quantities refer to electrical signals either at the output of the transducer or at the input to the preamplifier, both of which are practically the same for most cases. The amplitude is measured from the quiescent level to the peak of the signal envelope, and is sometimes referred to as half-peak amplitude in order to distinguish it from peak-to-peak amplitude.

Another forewarning: The reader may notice that many of the monitoring results described in this report are inconclusive. This is primarily because the acoustic emission technique is far more sensitive than any other currently available NDI method for detecting subcritical flaw growth, and therefore, monitoring results often cannot be substantiated by other methods. This is common to many applications of this new technique. In the following sections, a negative NDI result is implied unless otherwise stated. Detailed NDI results are also found in Ref. 2.

II. PRE-TEST PREPARATIONS

Specimen Tests

Basic Acoustic Properties - The compressional and shear wave velocities of a 1/16 in. thick 2219-T81 aluminum sheet specimen were measured using the pulse transit technique. These data were considered to be essential to the interpretation of monitoring results. The results are given below in Table 1.

Table 1

COMPRESSIONAL AND SHEAR WAVE VELOCITIES
OF 2219 ALUMINUM THIN SHEET

Compressional Wave Velocity (first longitudinal mode)	At Room Temperature	5.42 mm/μs
Shear Wave Velocity	At Room Temperature	3.16 mm/μs

The dispersive characteristics of acoustic waves propagating through a thin sheet of 2219 aluminum were examined. These properties are partially responsible for defining the character of observed emission waveforms. A 0.2 in. (5 mm) wide acoustic sensor mounted flat on a surface of an aluminum sheet has a high frequency cut-off at about 400 kHz in its response to compressional acoustic waves propagating in the direction parallel to the plane of the sheet. Since the wavelength of compressional waves in this frequency range is much larger than the thickness of the aluminum plate used for the test tank, compressional waves experience very little dispersion (Ref. 3). As a result, unlike thick-walled structure where dispersion of waves is appreciable, a compressional pulse propagating through a thin-walled tank remains impulsive for a long distance. This eliminates an effective use of the signal rise-time criterion for spatial discrimination of signals in the present application. These properties were confirmed experimentally on a specimen.

Precracked Specimen Tests - Eight single-side-notch tension specimens of 2219-T81 aluminum were prepared and three were tested by loading to failure. The objectives of the tests were to obtain amplitude-distribution data of acoustic emissions from

subcritical and critical crack growths and to compare the effectiveness of various types of spatial discrimination techniques for noise rejection.

Specimens of two different sizes were tested. Figure 1 shows the specimen configuration and approximate dimensions of the larger-sized specimens. The smaller-sized specimens were approximately half of the larger specimens in all dimensions except the thickness. Specimens of both 1/16 in. (1.6 mm) and 1/8 in. (3.2 mm) thicknesses were prepared for each specimen size , although not all of the prepared specimens have been tested because of time limitations.

Figure 1 also shows the locations of the acoustic sensors on a specimen. These locations are typical; exact locations differed for different specimens because of accessibility to sensors when the specimen was in the loading machine. Sensors used for these tests were the same as those used for the later tank tests. They were lead-zirconate-titanate piezoelectric plates, 0.05 in. (1.27 mm) thick, polarized in the thickness direction,and cut to 0.2 in. (5 mm) squares and were mounted directly onto the specimen with a minimum amount of backloading.

A block diagram of the experimental setup typically used for these tests is shown in Fig. 2. Amplified signals from transducers were fed into three different acoustic emission signal processing units, marked AEM for Acoustic Emission Monitor in this diagram. The M/S (Master/Slave) AEM (Ref. 4) receives signals from multiple master and slave sensors (marked M and S, respectively, in Figs. 1 and 2) and performs a logic processing such that a count output is produced only when a master sensor receives an acoustic signal prior to any of the slave sensors. When used in this test with the sensor arrangement as shown, it performs a type of spatial filtration to eliminate acoustic noise generated in the loading pin areas. The C (coincidence) AEM receives signals from a pair of oppositely polarized transducers and performs another kind of logic processing such that a count output is produced only when signals from both transducers are coincident within a pre-determined resolution time. By placing the transducers in symmetrical positions about the plane of crack propagation, as shown in Figs. 1 and 2, only those signals generated around this plane are detected, providing another type of spatial filtration of signals for noise rejection. Filters were used to obtain the best possible signal-to-noise ratio. The Beta-AEM is a unit to measure the amplitude distribution of acoustic emission signals in real time. It determines the peak amplitude of each acoustic event, and prints out the accumulated result

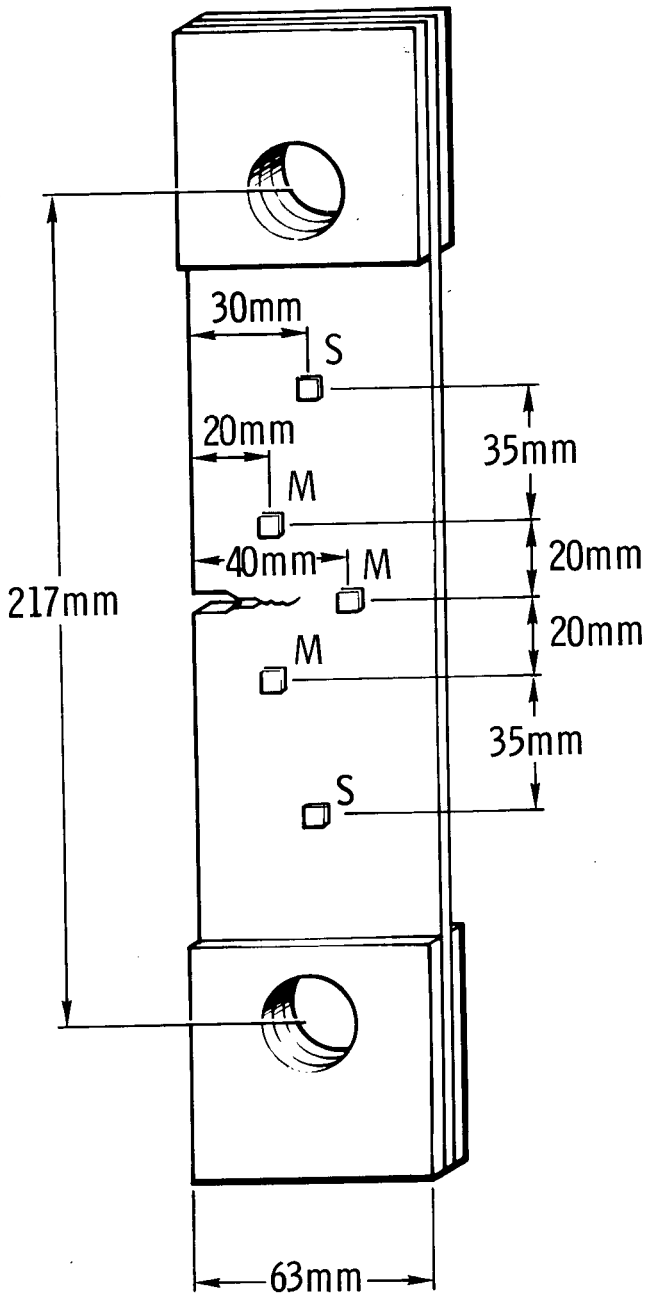

Fig. 1. Precracked 2219 aluminum specimen and sensor locations. Dimensions shown are approximate for the larger specimens. Sensor locations are typical. M = master sensor, S = slave sensor.

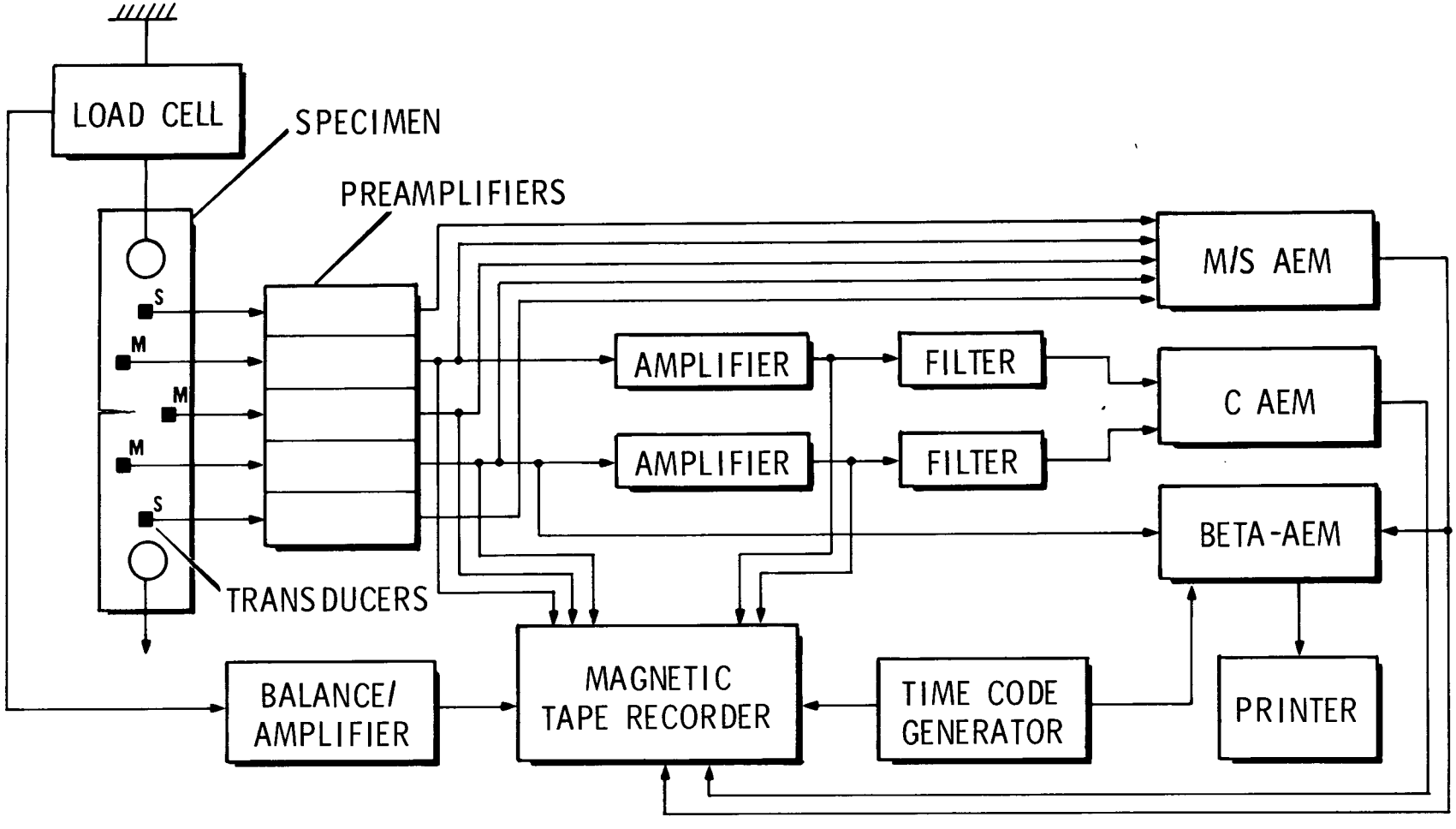

Fig. 2. Experimental setup for precracked specimen tests.

periodically. In this test, the result was gated by the count output from the M/S-AEM to eliminate the contamination of the data by noise. All the data were recorded on a magnetic tape recorder for post-test analyses, except the amplitude distribution data, which were printed out in real time.

The descriptions of the three specimens tested are given in Table 2, below. All the specimens were tensile loaded in a Baldwin testing machine at a nearly constant loading rate of approximately 1 kip/min (75 N/sec) until complete failure.

Table 2

DESCRIPTION OF FLAWED SPECIMENS

Specimen	Specimen Size (mm)	Type of Flaw	Depth of Flaw (mm)	Failure Load (kN)
5-1	1.55 x 63.3 x 305	Elox Slot	20.49	11.82
2-2	3.20 x 63.0 x 305	Elox Slot	20.88	22.69
4-1	3.22 x 31.5 x 152	Fatigue Precrack	6.23	19.65

In Fig. 3, the cumulative numbers of acoustic emission events detected by the master/slave and coincidence units for specimen 4-1 are plotted against time. The results of the other two specimens were similar. The load levels in percent of failure load are also indicated. The higher sensitivity for the coincidence unit was made possible by the use of a set of filters before the AEM unit. Even with the higher sensitivity of detection, however, the coincidence unit detected only about one-half of the events detected by the master/slave unit. The difference was even larger for the thin specimen 5-1. This is because of the asymmetry of the acoustic energy emitted from a crack tip. Unlike that from plane-strain crack growth, the acoustic energy emitted from a crack in a thin plate, where the plane-stress condition prevails, has a radiation pattern which is far from symmetric about the plane of the crack. Because of this asymmetry, a pair of acoustic sensors located at symmetrical positions about the plane of the crack may not receive signals at equal strength. Consequently, the coincidence detection logic, where signals are detected at a

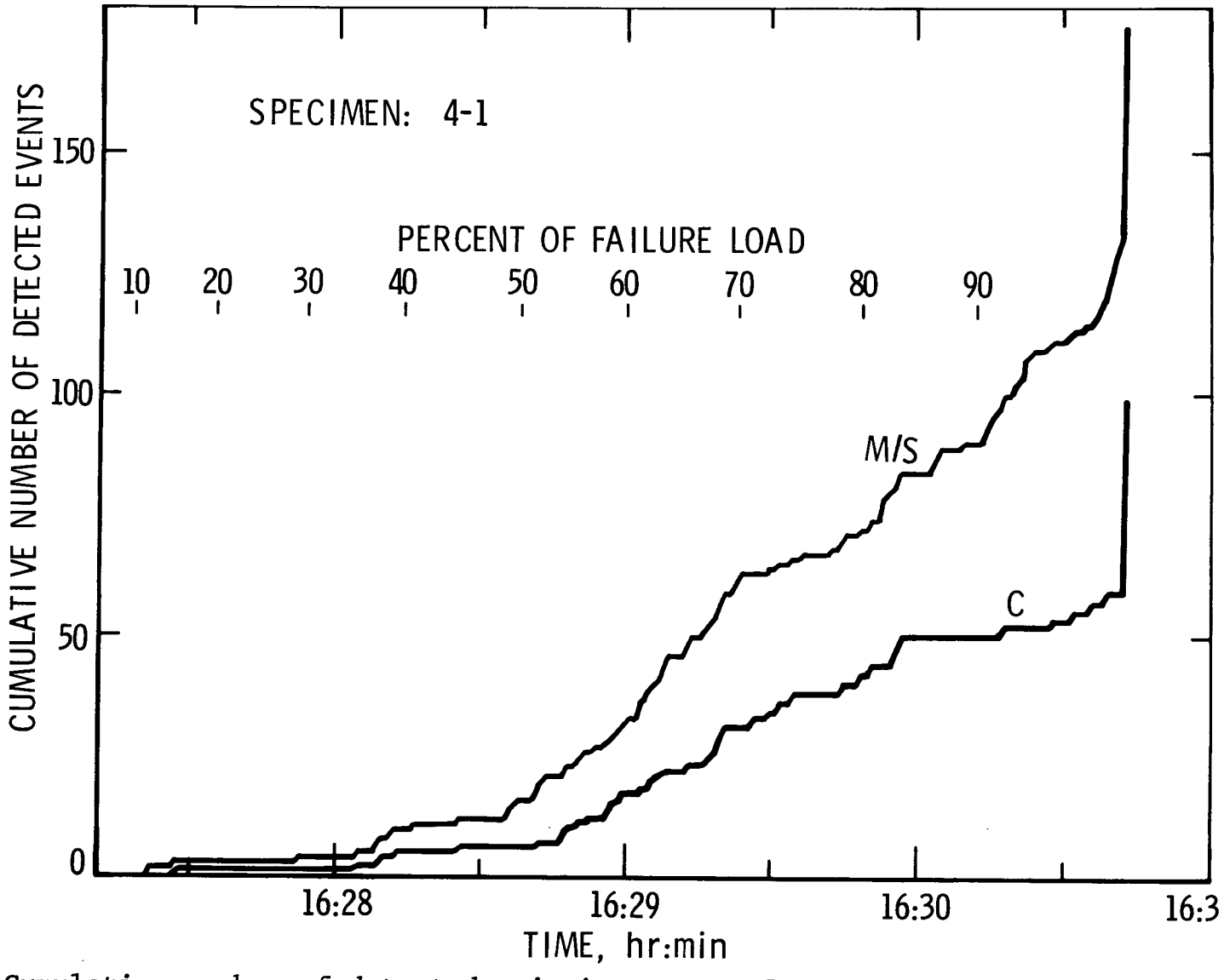

Fig. 3. Cumulative number of detected emission events from a specimen. The detection thresholds were 75 μV and 18.5 μV for the master/slave (M/S) and coincidence (C) detections, respectively.

constant detection threshold at the pair of sensors, often fails to register signals arriving coincidently. It is clear that the master/slave noise rejection logic is superior to the coincidence logic when such a situation exists.

Another property of the acoustic emission from these specimens seen on these cumulative plots is that emissions are first observable at a very low loading level. The emission rate, which is the slope of the cumulative curve, generally increases with increasing load, but not in any regular manner. Therefore, the increase of the emission rate is not a reliable indicator of the imminence of failure.

The amplitude distributions of acoustic emission signals from these specimens, obtained by the Beta-AEM unit, are shown in Figs. 4a through 4b. The distributions are presented in the log-cumulative form as described in Ref. 5. The quantity plotted in these figures is the cumulative number, in a logarithmic scale, of emission events of amplitude greater than a given value, also in the same logarithmic scale. Data for three time/load level intervals are plotted separately to show the shift of the distribution with loading level. Those intervals are (a)below 95% of the failure load, (b) above 95% of the failure load excluding the final second, and (c) the final one second including the event leading directly to the failure. In agreement with our past experiences with emission signals from crack growths in various metals, the slopes of these distribution curves generally lie in the neighborhood of 1.0 ± 0.5. The decrease of the slope with increasing loading level is again observed. For emission signals generated at load levels below 95% of failure load, representing subcritical slow crack growth, the slope is about 2.0. As the loading level approaches the critical level, the slope decreases to 1.0 or less, as represented by the curves for loading levels above 95% of failure load. The slope of the log-cumulative amplitude distribution, therefore, can be used as an indicator of (1) existence of a growing crack and (2) criticality of its growth rate.

In Table 3, below, the ranges of the peak amplitudes of the largest observed signals are listed with values reduced to a unit distance of 1 cm. The distance correction applied to the observed amplitudes is a multiplication factor of the square root of the distance, thus correcting for the geometrical spreading of the acoustic energy in a plane without dispersion. The effect of the absorption of energy is negligible at these distances.

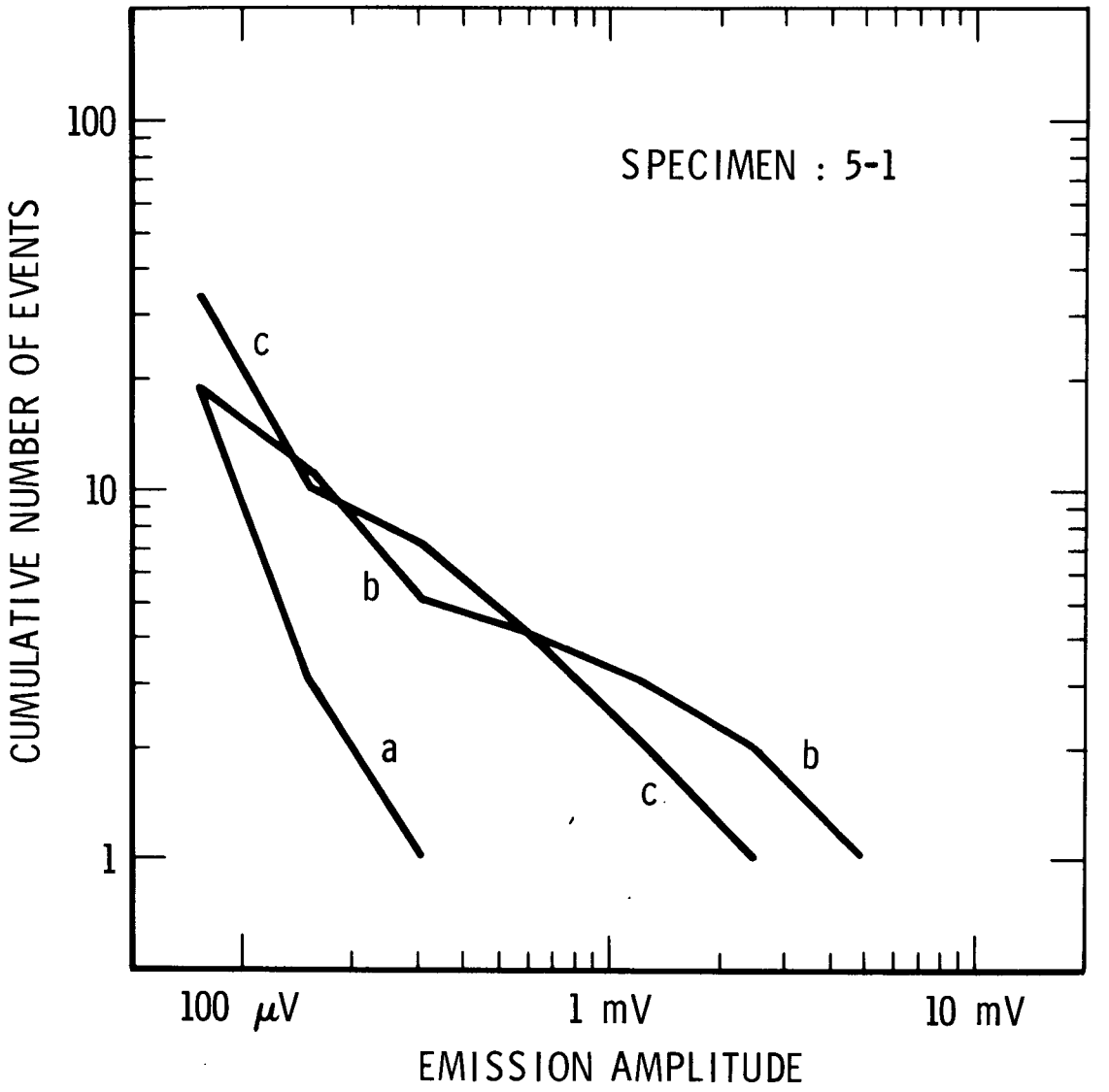

Fig. 4a. Amplitude distribution of emission signals from crack growth in specimen 5-1. (a) Below 95% of the failure load. (b) Above 95% of the failure load. (c) During the final one second.

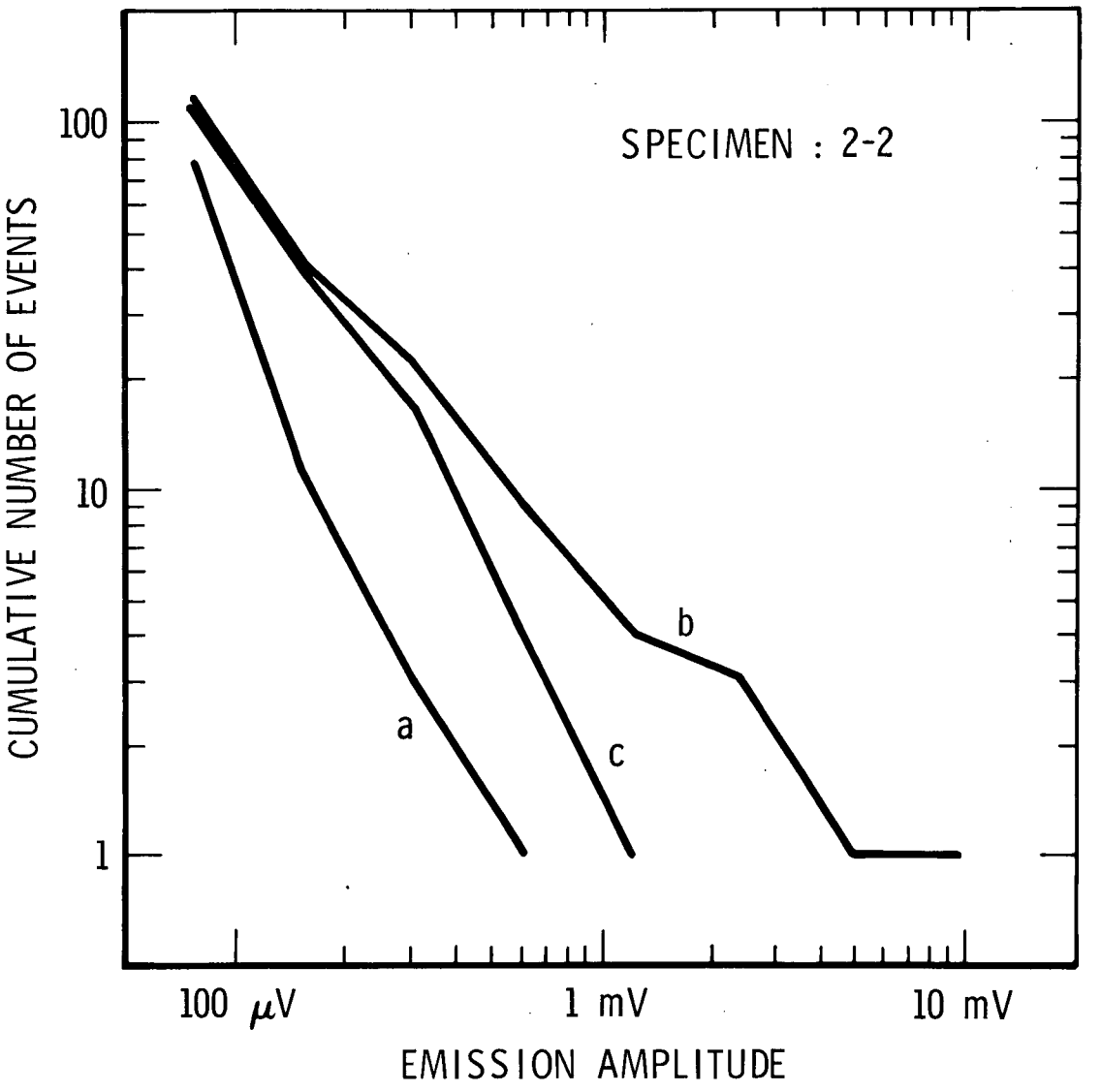

Fig. 4b. Amplitude distribution of emission signals from crack growth in specimen 2-2. See note for Fig. 4a.

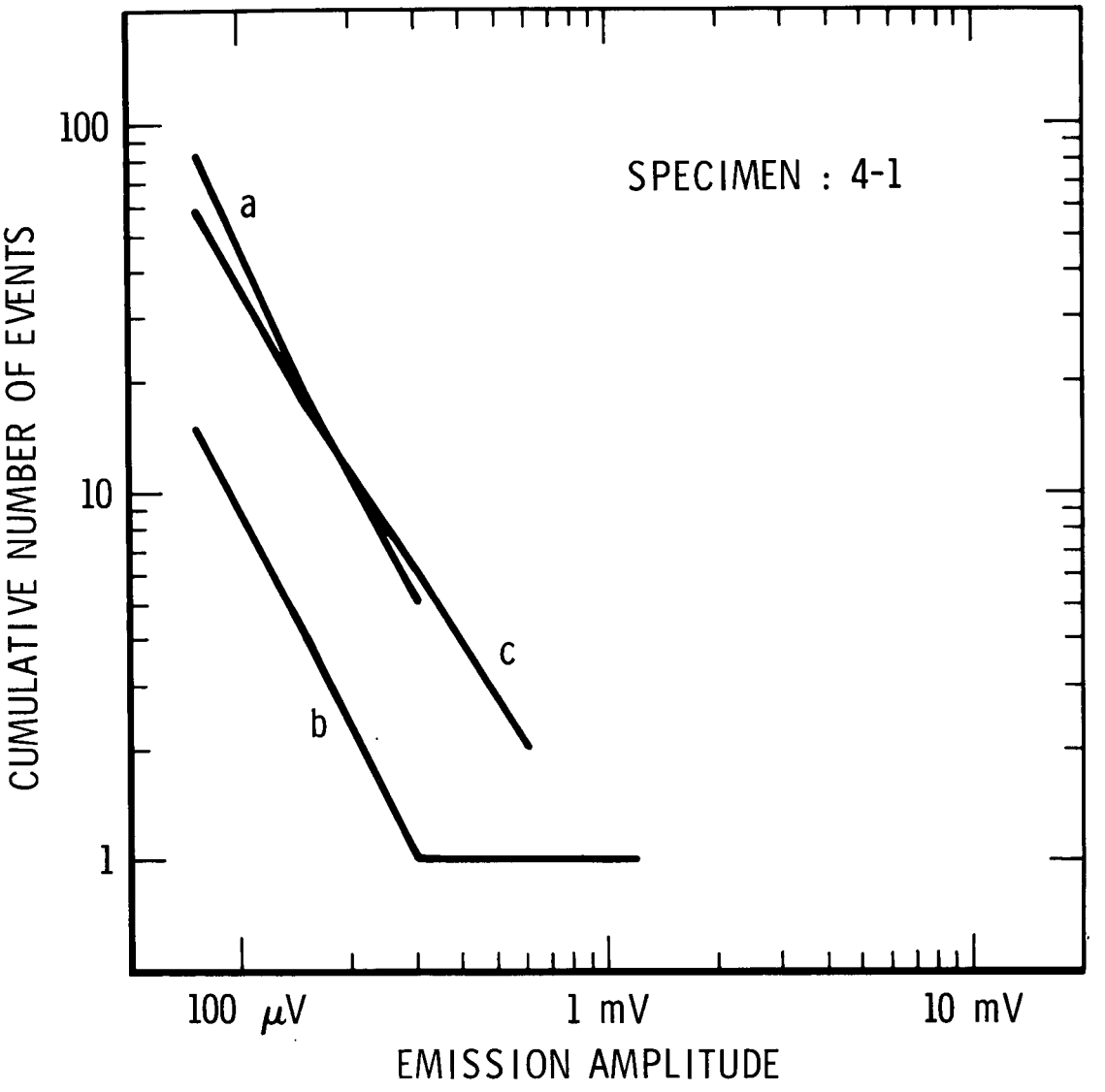

Fig. 4c. Amplitude distribution of emission signals from crack growth in specimen 4-1. See note for Fig. 4a.

Table 3

AMPLITUDE RANGES OF LARGEST EMISSION SIGNALS FROM CRACK GROWTH

Specimen	5-1	2-2	4-1
Observed amplitude at distances of	2.0 cm	2.0 cm	1.2 cm
below 95% of failure load	0.3-0.6 mV	0.6-1.2 mV	0.3-0.6 mV
above 95% of failure load	5-10 mV	10-20 mV	1.2-2.4 mV
Reduced to Unit distance	(1 cm)		
below 95% of failure load	0.42-0.85 mV	0.85-1.7 mV	0.33-0.66 mV
above 95% of failure load	7-14 mV	14-28 mV	1.3-2.6 mV

The amplitude of the largest emission signals is on the order of 1 mV at a distance of 1 cm at loading levels below 95% of the failure load, representing subcritical crack growth. At loading levels above 95% of the failure load, representing a near-critical condition, the amplitude of the largest emission signals is an order of magnitude greater than that at a subcritical condition. The observed data suggest that there may be an effect of the size of the specimen on these values, but the limited data obtained during this study do not warrant a firm conclusion of this property.

PPO foam-lined specimen - The wave propagation characteristics of 2219 aluminum sheet lined with a PPO foam were examined because knowledge of these characteristics was considered to be essential to the planning and performance of the monitoring of the environmental test. The first property examined was the attenuation of acoustic waves. The setup used for this test is shown in Fig. 5. The specimen was a 14 in. (35.5 cm) square sheet of 2219 aluminum, 1/16 in. (1.6 mm) thick, with a 12 in. (30.5 cm) square piece of PPO foam, 1.75 in. (44.5 mm) thick, bonded on one side in the same way as was done for the test tank. Two acoustic transducers were placed on a diagonal line of the

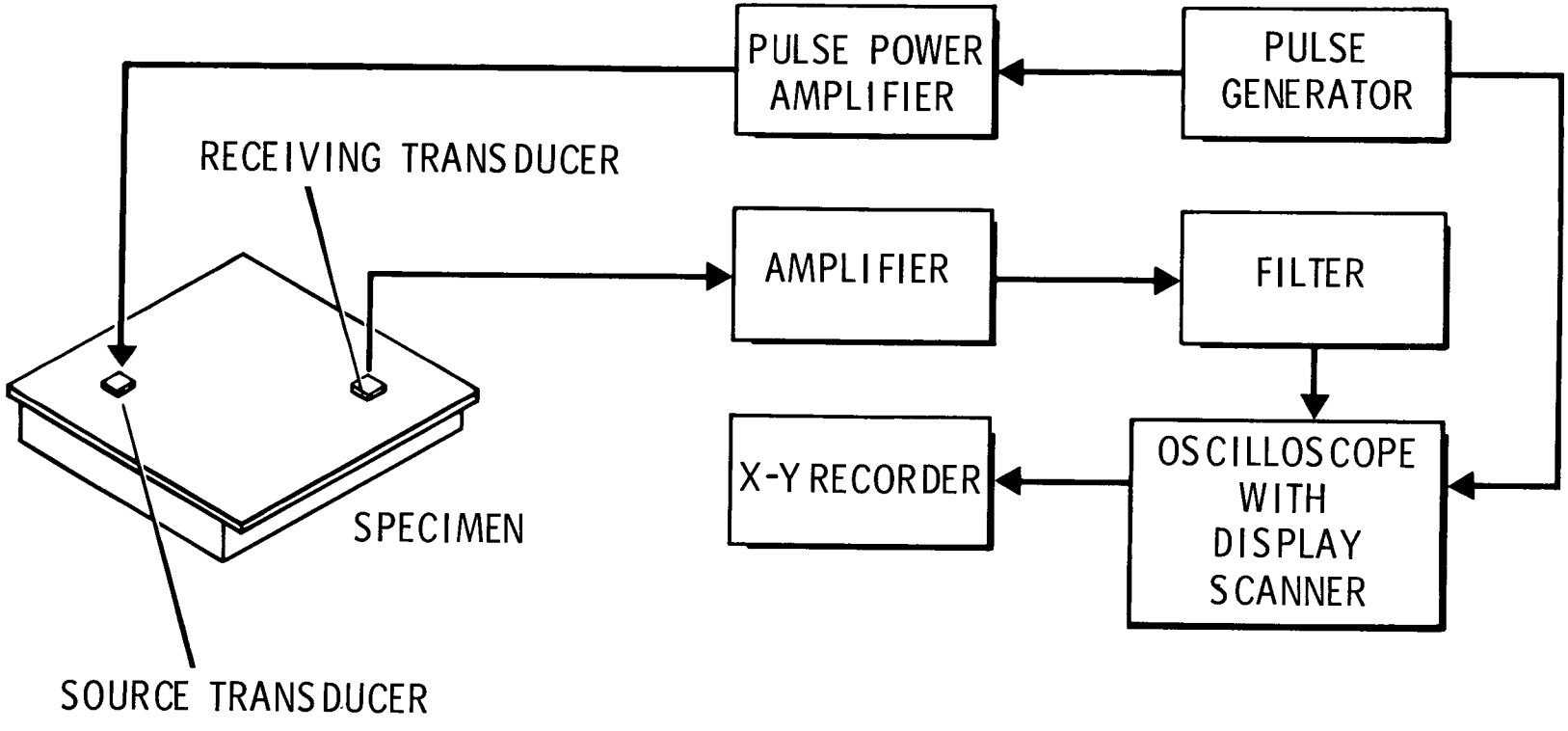

Fig. 5. Experimental setup for testing a PPO foam lined aluminum specimen for signal attenuation.

sheet as shown in the figure, and were moved along the line for various separations between them. One of the transducers was excited by pulsing it with a high voltage, short duration square pulse from the pulse power amplifier; the acoustic waves generated in the specimen were detected by the other transducer; and the signal was amplified, filtered, and recorded on a X-Y recorder through an oscilloscope with a display scanner. Recordings were made at various distances of sensor separations and at several narrow-band settings of the filter and with several different sensors to cover a wide range of frequencies. The amplitudes of signals were read from these recordings, corrected for the geometrical spreading of the signal, and plotted on a semi-log graph paper against distance to find the attenuation factor. In addition to the attenuation property, such other properties as dispersion characteristics and group and phase velocities were also examined on these recordings.

At frequencies below 1 MHz, the dominant modes of acoustic wave propagation through the specimen, detected by a thickness-mode transducer, were found to be the fundamental symmetric, or longitudinal, mode, M_{11}, and the fundamental anti-symmetric, or flexural, mode, M_{21}. The group and phase velocities of these modes were found to be little affected by the presence of the PPO insulation, showing practically the same dispersion characteristics as those for a bare aluminum plate. The M_{11} mode showed negligible dispersion in the frequency range of observation of 75 kHz to 1 MHz, while the M_{21} mode showed strong dispersion in the lower part of this frequency range. The group velocity of the M_{21} mode reached a maximum at around 900 kHz.

Although the velocities were little affected by the presence of the PPO foam insulation, the waves were found to be severely attenuated by the presence of the PPO insulation because of energy absorption into the PPO foam. The attenuation factors at room temperature were found to be 0.04 Np/cm and 0.10 Np/cm for the M_{11} and M_{21} modes, respectively. In other words, the amplitudes of M_{11} and M_{21} modes were attenuated by a factor of 1/e every 25 cm and 10 cm, respectively, of propagation in the PPO insulated aluminum plate, in addition to the amplitude decay due to the geometrical spreading and dispersion of waves. These attenuation factors were found to be independent of frequency within the frequency range of the present observation. The frequency-independent attenuation is in contrast to the normal attenuation behavior of acoustic waves in metals, where the attenuation factor increases nearly in proportion to increasing frequency. For a monitoring of a large PPO-insulated structure, this means that lowering of operating frequency does not contribute favorably to

obtaining a long-range detection of emission signals as is the case with ordinary metal structures.

The resulting decay of amplitudes of these two modes of wave propagation in an aluminum sheet insulated by a PPO foam is therefore estimated to be given by the following formulae:

M_{11} Mode: $$A = A_o\, r^{-\frac{1}{2}}\, e^{-0.04r}$$

M_{21} Mode below 400 kHz: $$A = A_o\, r^{-1}\, e^{-0.10r}$$

M_{21} Mode at Around 900 kHz: $$A = A_o\, r^{-\frac{1}{2}}\, e^{-0.10r}$$

where A is the amplitude at a distance of r cm and A_o is the amplitude without attenuation at 1 cm of distance. These realtions are shown in Fig. 6 with extrapolations to include distances appropriate for the insulated tank structure. These attenuation properties were later confirmed on the real tank up to a range of 133 cm within a frequency range of 50 to 400 kHz. Because of the greater decay of amplitude of the flexural mode over that of the longitudinal mode, only the fundamental longitudinal mode wave can be expected to reach far distances, and it is often the only arrival observable. This fact was also confirmed on the real tank.

By combining this result of attenuation coefficients with the amplitude range of the emission signals observed during the precracked specimen tests, a rough estimate of the range of detection of each sensor on the real tank can be made. From the result of the precracked specimen tests, the largest acoustic emission signals expected from subcritical crack growth have an amplitude at 1 cm of distance in the neighborhood of 1 mV, while the largest signals expected at a near-failure condition have an amplitude at 1 cm in the neighborhood of 10 mV. The amplitude decay curves of emission signals having these two signal strengths are shown in Fig. 7. The detection ranges of a sensor can be easily obtained from this diagram. For example, at a detection threshold sensitivity of 50 microvolts, the detection range for the largest signals from a subcritical crack growth is 32 cm, while that from a near-failure crack growth is 78 cm. It is clear that a high sensitivity and closer sensor separations are essential to the detection of subcritical crack growth.

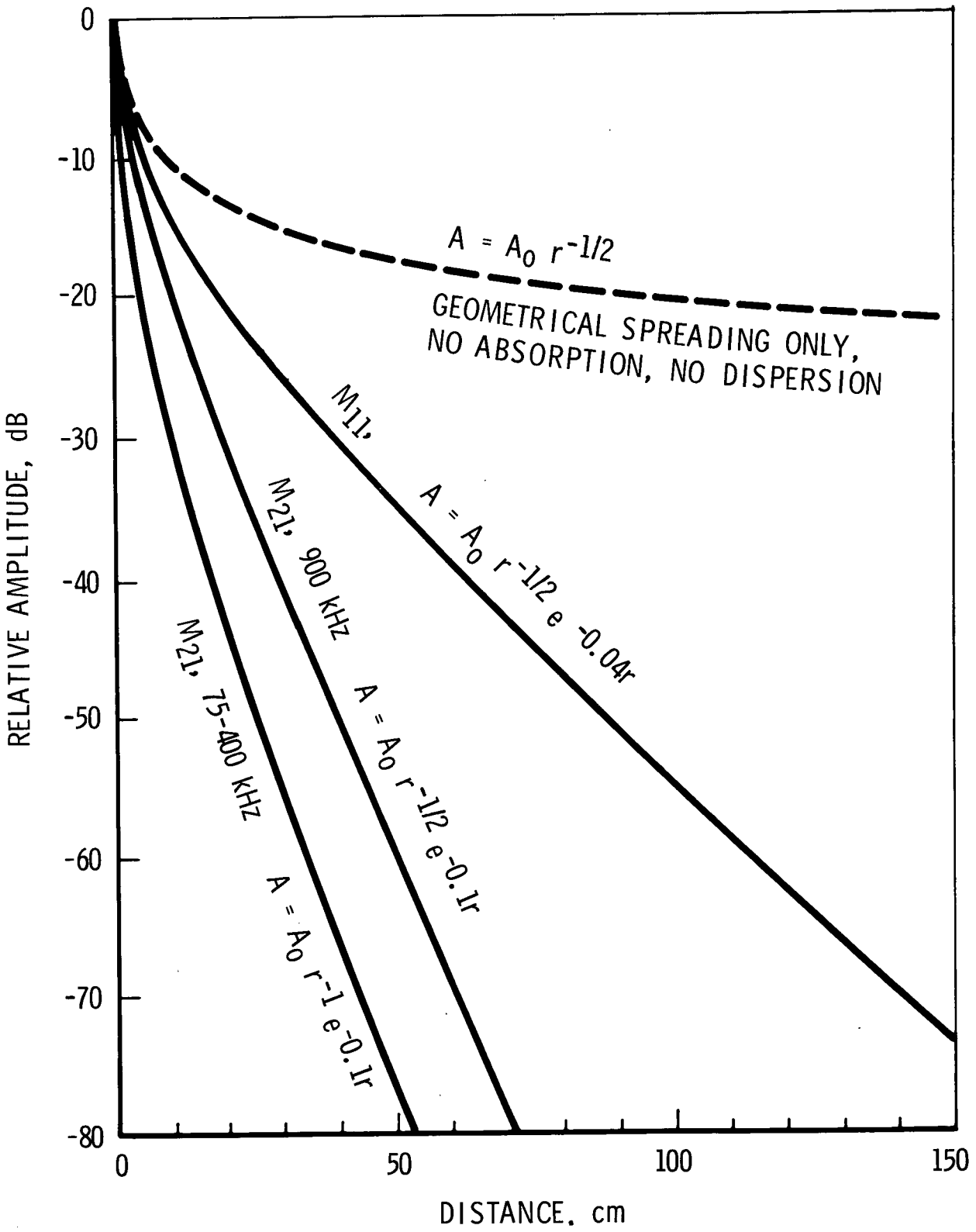

Fig. 6. Extrapolated acoustic signal attenuation curves for a PPO foam insulated aluminum plate. Amplitudes are relative to those at 1 cm without absorption. See text for notations for various modes.

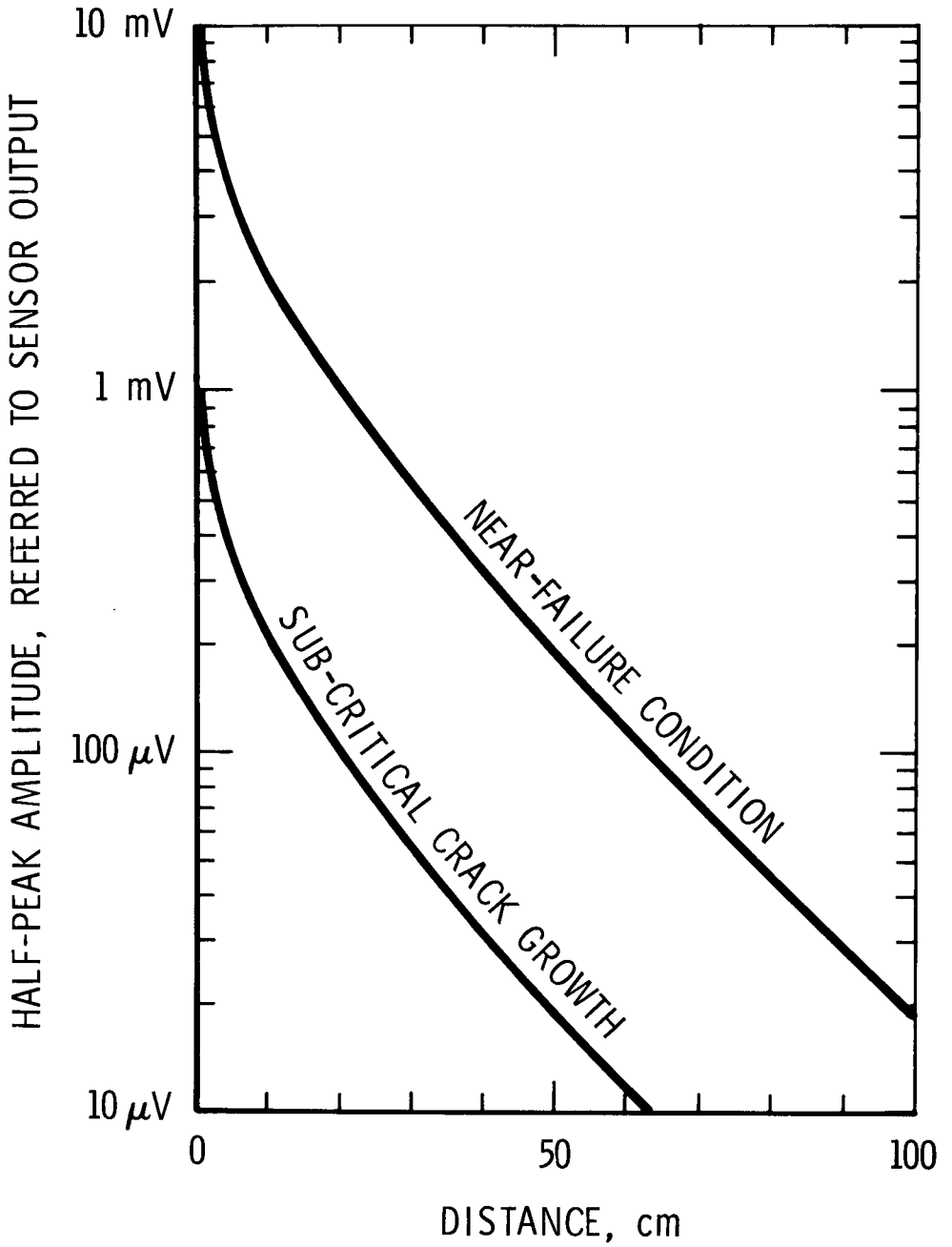

Fig. 7. Amplitude decay of maximum expected emission signals.

The velocity and attenuation measurements were also conducted on the same PPO-lined specimen in an environment chamber to obtain the effect of temperature variation on these quantities in the temperature range of -75°C to +125°C. The velocity of the M_{11} mode was found to decrease with increasing temperature at a rate of approximately 0.001 mm/μs °C over this temperature range. The attenuation factor of the M_{11} mode was found to be nearly constant at 0.04 Np/cm from room temperature up to +125°C, but at low temperatures it increased with decreasing temperature, reaching 0.06 Np/cm at -75°C.

Another potential problem anticipated for the PPO-foam insulated structure was the possible generation of spurious emission signals from the PPO foam and from the foam-aluminum interface. In order to examine this possibility, the PPO foam lined specimen described above was thermally cycled in the laboratory by cooling the specimen rapidly from the insulated side by liquid nitrogen down to -75°C followed by heating it rapidly from the aluminum side by infrared heat lamps up to +125°C. The spurious signals generated during this process were detected by three acoustic sensors mounted on the specimen at three corners of a triangle of sides 151, 210, and 301 mm. The amplitude distribution of these signals was measured using the Beta-AEM described earlier. The data were also recorded on a magnetic tape recorder, and were analyzed later for the locations of the noise sources. The temperature of the specimen was monitored by a chromel-alumel thermocouple placed at the center of the aluminum sheet. This experiment was performed for a total of five temperature cycles.

During the rapid cooling a large number of emission signals were observed. Most of these signals were too small to be observable by more than one sensor, but several signals were large enough to be observable by all three sensors. Typical waveforms of a signal observed by all three sensors are shown in Fig. 8. It is seen that these spurious signals have all the characteristics of an acoustic emission signal.

The observed amplitude distributions of these spurious signals are shown in Fig. 9. Large signals were observed only during the rapid cooling of the specimen. During holding at a low temperature, rapid heating and subsequent air cooling of the specimen no significant emission signals were observed. The slope of the distribution curves as seen on this figure are relatively steep compared with those of crack-generated emission signals. Although the observed amplitudes of some of the signals

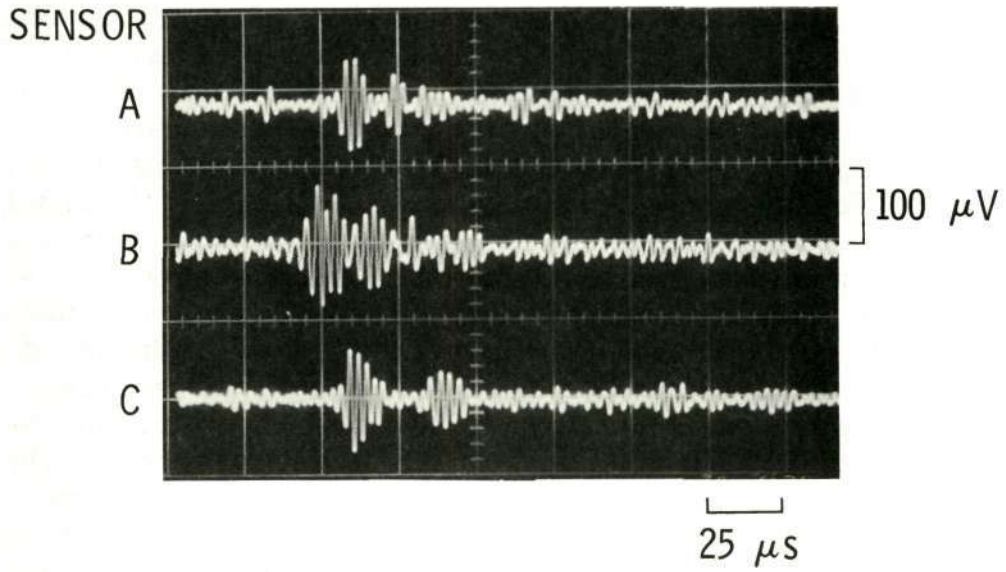

Fig. 8. Typical spurious emission signals from a PPO foam lined aluminum specimen. Three traces represent a single event observed by three sensors separated by 301 mm, 210 mm, and 151 mm from A to B to C to A, respectively.

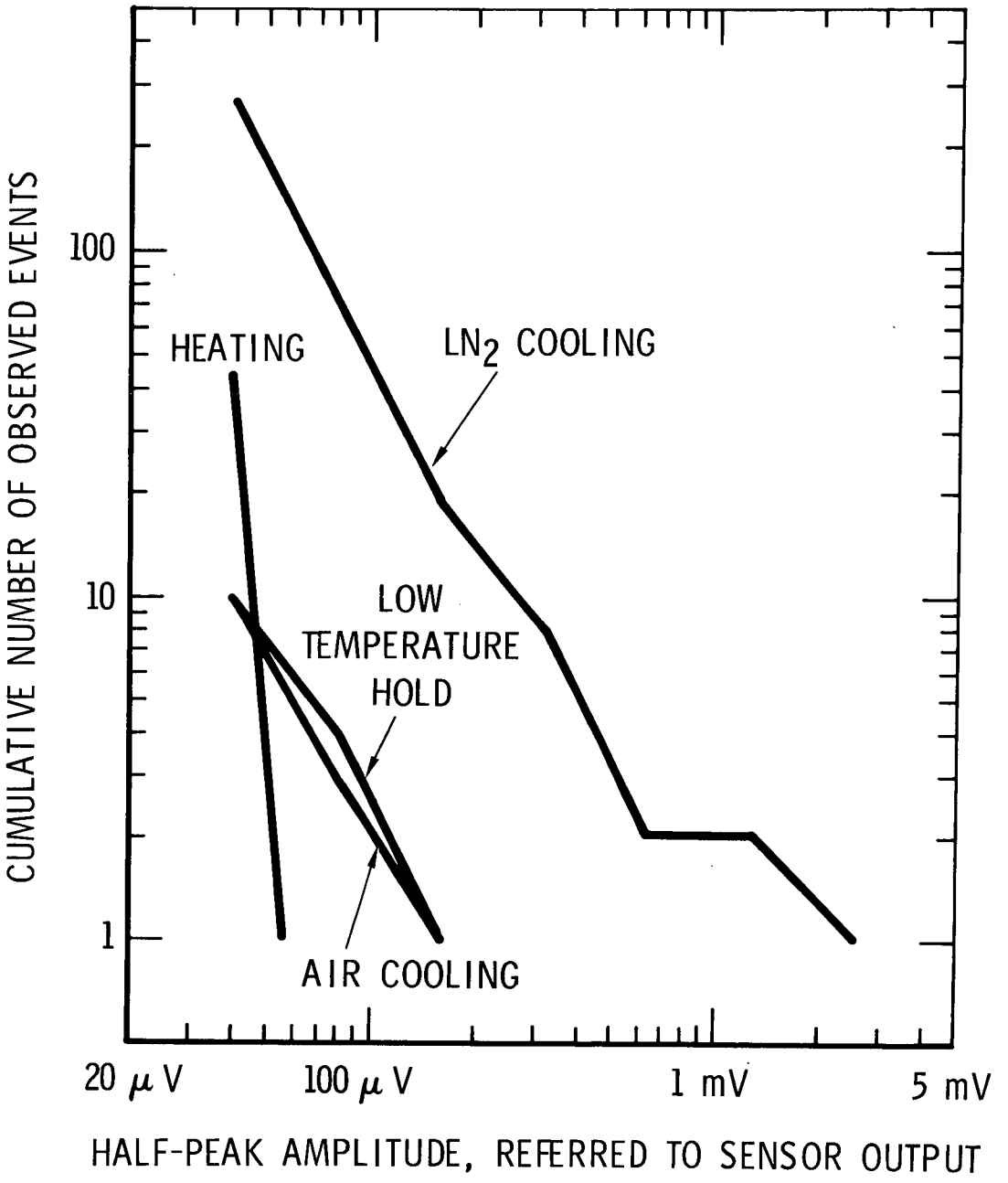

Fig. 9. Amplitude distribution of spurious emission signals from a PPO-lined aluminum specimen. The data were taken during the 4th and 5th temperature cycles of the experiment.

were relatively large, they were the ones which originated in a very close proximity of a sensor. Those signals large enough to be detected by all three sensors, and thus were located, indicated that the maximum source strengths of these spurious signals were somewhat smaller than those of the largest acoustic emissions from a subcritical crack growth.

The exact cause of these spurious emission signals remains to be determined, but the extensive deformation of the specimen caused by the temperature gradient during the rapid cooling is considered to be responsible for generating acoustic emissions at or near the foam-aluminum interface. It was clearly indicated that these spurious emissions were generated whenever a deformation takes place at the foam-aluminum interface. They are very small in strength at their origin, but some of them may occur in such a close range of a sensor that the observed amplitude may be large. These spurious emissions remained to be a cause of concern for the environmental test of the actual tank.

Sensor Mounting Analysis

Selection of Sensor - Initially, it was established that the sensors to be used for this study must meet the following requirements: (1) maintain high sensitivity over a temperature range from -100°F (-73°C) to +350°F (+176°C); (2) generate no internal noise with temperature variations; (3) be waterproof; (4) be noncorrosive; and (5) function in a vacuum. Several transducer manufacturers were contacted to find if any transducer which met these requirements was commercially available. The effort was fruitless. Consequently, it was decided to use sensors developed in our own laboratory.

A detailed description of the transducer is found in Ref. 6. The transducer element used in this acoustic emission sensor is a lead-zirconate-titanate piezoelectric plate of 0.05 in. (1.27 mm) thickness, polarized to the thickness direction, and cut to a 0.2 in. (5 mm) square. The fundamental free resonant frequency of the sensor element for the thickness-mode vibration is 1.54 MHz, and its static sensitivity is approximately 1.0 V/N. The transducer element is enclosed in a brass housing and, when the sensor is mounted on a test specimen, the transducer element touches directly to the specimen with minimal amount of back loading.

The transducer requires two additional materials for its operation: the material to couple the transducer element to the test specimen and the material to bond the transducer housing to the test specimen. Therefore a test program was undertaken to determine the best available materials for these purposes.

Test Setup and Procedures - The setup of the test equipment used in the evaluation of the coupling and bonding materials is shown in Fig. 10. The test arrangement consisted of a 1/8 x 9 x 12-in. 2219-T81 aluminum sheet specimen with one transmitting and two receiving transducers mounted on the specimen. The specimen was positioned in a Tenney Mite 3 environmental test chamber which had a temperature of $-85^{o}C$ to $+175^{o}C$, with automatic temperature control of $\pm 2^{o}C$ and the capability of maintaining an absolute pressure of 10^{-2} mmHg.

A quartz thermometer sensing element was positioned on the surface of the test specimen halfway between the two receiving transducers. The temperature measured at this position was that of the surface of the test specimen and not necessarily the temperature of the transducer.

The electronic equipment consisted of one transmitting channel and two identical recording channels. The transmitting channel consisted of a transducer and a pulse generator, which produced a repetitious pulse of one microsecond duration and 10 volts amplitude into 50 ohms. Each receiving channel consisted of a preamplifier, an amplifier, a passive rectifying and integrating circuit, and a strip-chart recorder.

The transmitting channel stimulated the transmitting transducer with a repetitive (100 pps) pulse of one microsecond duration. The acoustic signals arriving at the receiver transducer were similar in frequency and envelope to acoustic emissions detected from crack growth in materials. The output signal from the receiving transducer was amplified by a preamplifier having a gain of 150 (43 dB). The output signal from the preamplifier was processed by an additional stage of amplification and this signal was used to drive a passive integrating circuit which produced a dc output voltage proportional to the integrated amplitude of the acoustic signal and to the recurrence rate. These integrated signals were recorded on strip charts. The signals from the two receiving transducers were processed by identical methods.

Test Results - For materials to be used to couple the transducer to the test specimen, two important factors considered were a constant viscosity with temperature variations within the expected range and immobility of the material with temperature cycles. To insure that the method of bonding the sensor case to the test specimen was not contributing to any sensitivity change during the check of the coupling materials, the sensor cases were clamped to the test specimen with a non-metallic clamp.

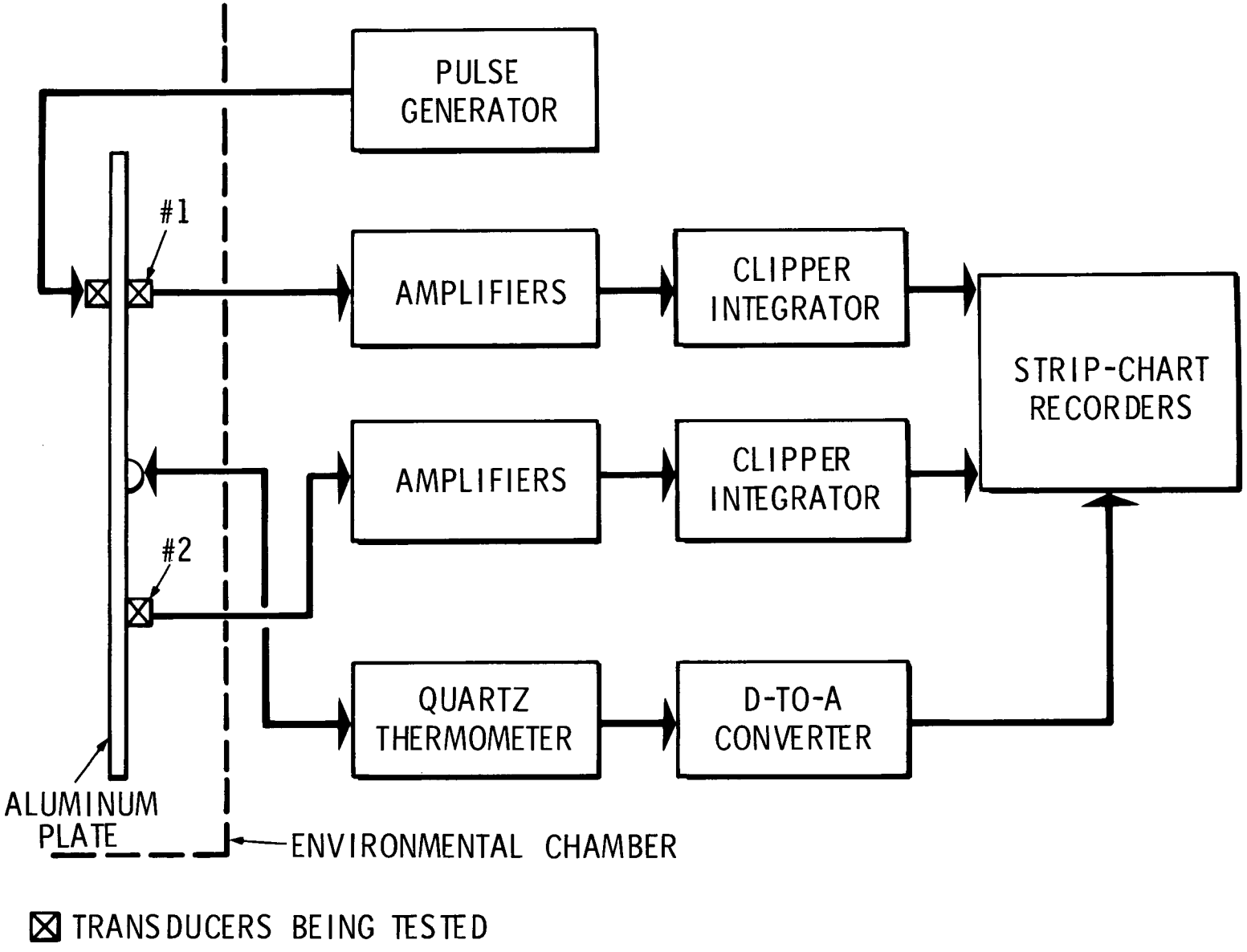

Fig. 10. Setup for testing acoustic sensor mounting.

Several materials were examined for use in coupling the transducer to the test specimen. These materials were in three categories: (1) silicone greases; (2) dry lubricants; and (3) epoxy resin without the catalyst. Each material was used as a coupling agent and the change in sensitivity and reproducibility of the sensor were recorded for evaluation. Constant sensitivity of the sensor during heating when the silicone greases were being tested and constant sensitivity during the cooling cycle when the dry lubricants were being tested indicated that a mixture of these materials would possibly perform well over the wide range of temperatures. A check of these mixtures showed that light consistency Dow-Corning 33 wide temperature bearing grease and Cerac SP102 fluorocarbon telomer dry lubricant performed satisfactorily.

A literature survey showed that silicone rubber would more nearly meet the requirements for bonding the sensor to the specimen than any other commercially available product. Dow-Corning 92-024 aerospace adhesive/sealant was chosen, because it was noncorrosive. Although the specification sheet on this material shows it to be operational to only -70°F (-57°C), a test of this material proved that it functioned in this application at -100°F (-73°C).

Two sensors were bonded 6 in. (15 cm) apart on one side of the test specimen using this material and the sensor coupling material described above. After the Dow-Corning 92-024 adhesive had cured for 48 hours, a transmitting transducer was positioned opposite to one of the sensors (#1) and the signals from the sensor were monitored during two temperature cycles from -73°C to +176°C. Visual examination after these temperature cycles were completed showed no debonding of the sensor cases. After 24 hours of additional curing of the 92-024 adhesive, data were obtained on these sensors during two additional temperature cycles for the same temperature range.

After the proof test of the tank, in an effort to improve the coupling of the transducer to the specimen, a mixture of heavy consistency Dow-Corning 33 bearing grease and Cerac SP102 fluorocarbon telomer dry lubricant was tested using Dow-Corning 94-024 adhesive to bond the receiving and transmitting transducer cases to the specimen at 6-inch separation. These transducers were monitored for three environmental cycles.

The results are presented in Fig. 11 showing the sensitivity change of each sensor as a function of temperature. These data were interpolated from the strip chart recordings for each acoustic emission sensor, assuming 0 dB to be at a temperature of 20°C.

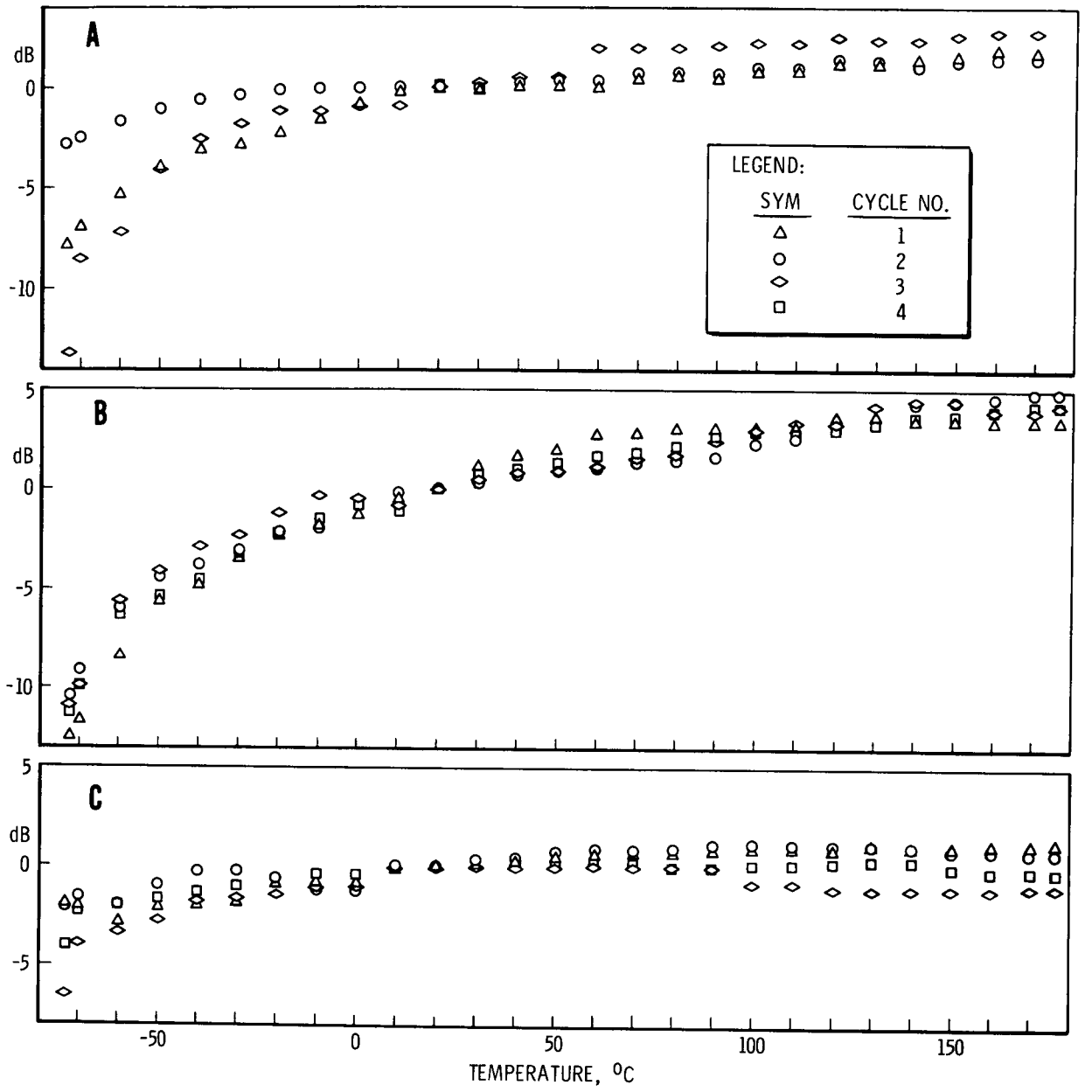

Fig. 11. Variation of sensor response with temperature. (A) Sensor #1, transmitter-receiver distance 15 cm, heavy consistency grease. (B) Sensor #2, transmitter-receiver distance 15 cm, light consistency grease. (C) Sensor #1, transmitter-receiver distance 3.2 mm, facing each other across aluminum sheet, light consistency grease. Response at 20°C is set to 0 dB.

When a mixture of light consistency 33 bearing grease and SP102 dry lubricant was used to couple the transducer to the specimen, the reproducibility between cycles was very good for both sensors. When the transmitter-receiver separation was just the thickness of the specimen (1/8 inch), the average sensitivity change was approximately 6 dB. For sensor #2 (transmitter-receiver separation of 6 inches) the reproducibility between cycles was within 4 dB at all temperatures. The greatest change in sensitivity of this sensor was -12 dB in a temperature range of +20°C to -73°C and an increase of 2.5 dB in the temperature range of +20°C to +176°C. This change occurred during the first temperature cycle.

When a mixture of heavy consistency 33 bearing grease and SP102 dry lubricant was used to couple the transducer and test specimen, there was some variation in the sensitivity between temperature cycles. The greatest differences were during the cold portion of the environmental check. The sensor sensitivity decreased 8.5 and 13.2 dB during cycles 1 and 3, respectively, from +20°C to -73°C, while the sensitivity decrease during cycle 2 was only 3 dB in the same temperature range. A 5 dB decrease in sensitivity from -70°C to -73°C during the third cycle indicated a malfunction of this sensor. However, the temperature was controlled at -73°C for 20 minutes and no further decrease was observed. Also, the sensitivity of the sensor reproduced previous reading when the test specimen was heated to 20°C. It was concluded that the difference between the light consistency bearing grease and the heavy consistency bearing grease was not large enough to choose one from the other for the present applications.

The sensors and the mounting were also functionally checked for operation in a vacuum. The result was satisfactory. The frequency response of the sensors was also monitored by exciting a transmitting transducer with a short duration pulse and analyzing the signals detected by the receiving transducers by a spectrum analyzer. No significant change in response was observed over a temperature range of -40°C to +160°C.

Initial Equipment Setup

The monitoring equipment used for the tank structure tests in San Diego was initially prepared and functionally checked in Fort Worth prior to disassembling for shipment to San Diego. A simplified block diagram of the setup is shown in Fig. 12. It should be noted that, because of the experimental nature of the present program, the setup was only temporary, and it was not intended to keep all the components of the monitoring equipment in this

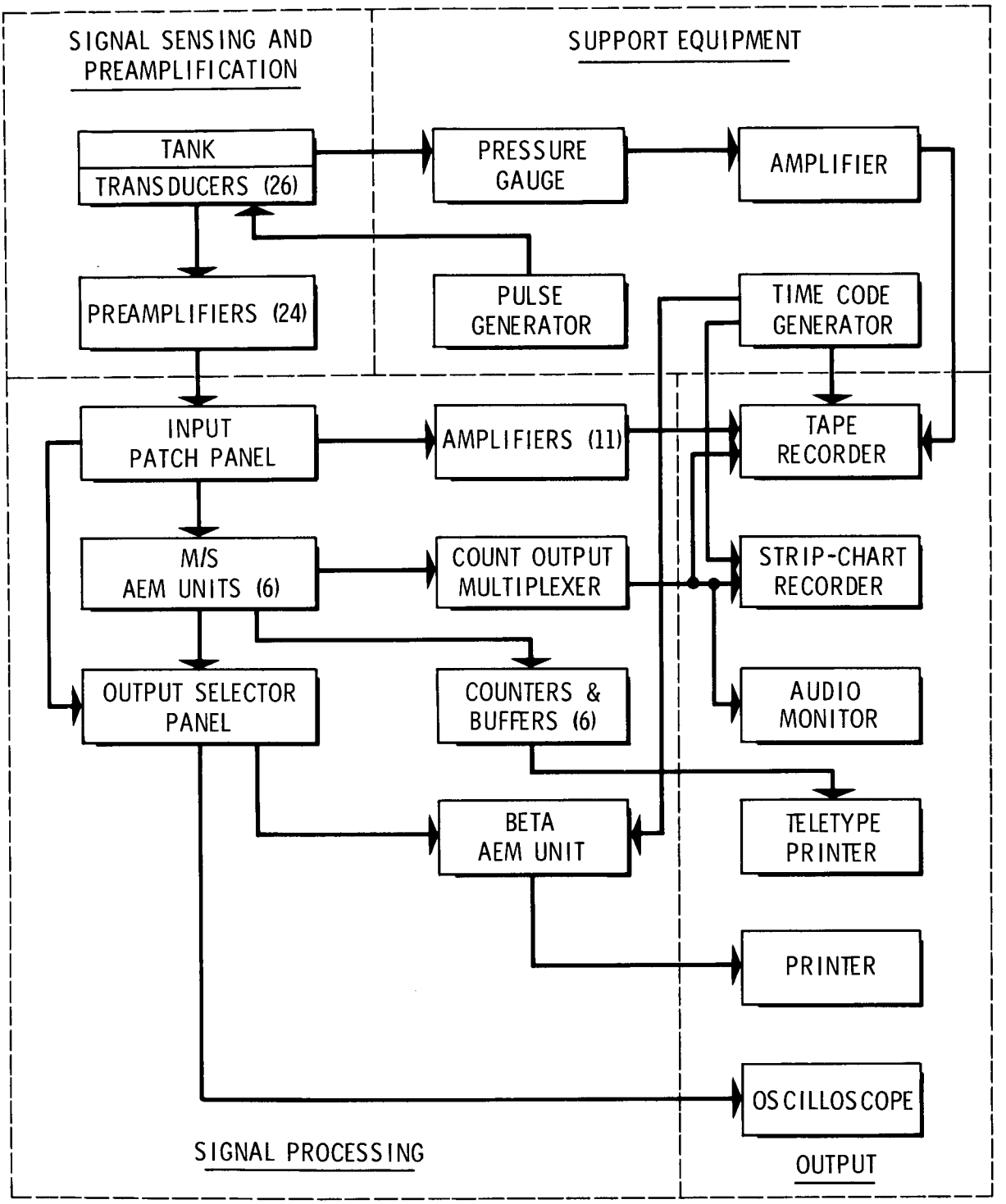

Fig. 12. Block diagram of initial monitoring setup.

arrangement throughout the test. In fact, several modifications in the detailed arrangement of components were made during the test. The basic arrangement, however, remained the same.

The basic setup consisted of signal sensing devices, signal processing devices, and output devices. The signal sensing devices, i.e., acoustic transducers, used for this study have been described in the preceeding subsection. Signals detected by the transducers and amplified by the preamplifiers were fed into various signal processing devices through the input patch panel: (1) Up to 12 channels of signals were further amplified by linear amplifiers to obtain an overall gain of 60 dB, and were recorded on a 14-channel magnetic tape recorder for the post-test analyses of the data. The system frequency response of these recorded channels was normally limited to a range of approximately 50 kHz to 600 kHz, the lower limit being determined by the preamplifier response and the upper limit by the tape recorder response. (2) Signals were also fed into several AEM (Acoustic Emission Monitor) units for a real-time selection of emission signals from background noise. The units selected for the initial setup were those using the master/slave noise-rejection logic. Using these units with overlapping arrays of sensors as will be described later, a spatial filtration of signals was intended. Count outputs from up to six AEM units, indicating occurrence of selected emission events were multiplexed by the count output multiplexer, and were recorded (a) on the tape recorder as event marks, (b) on a strip-chart recorder, and (c) were also fed into the audio monitor as an aid in identifying, in real-time, the general locations of emission sources. The count output multiplexer is an electronic unit to accept count output pulses from up to six AEM channels and to produce output square pulses of constant duration, but of various heights depending upon the channel number. The audio monitor is simply a combination of a voltage-controlled oscillator, audio power amplifier, and a speaker. The multiplexed count outputs thus produce short duration tones of up to six different pitches from the audio monitor, which are easily separable by experienced ears. The count outputs from the AEM units were also accumulated on counters, and the accumulated counts were printed out periodically on the teletype printer. (3) Signals from a selected sensor were fed into the Beta AEM unit for the determination of signal amplitude distribution. The amplitude distribution data were then printed out periodically on a printer. (4) Signals from selected sensors were fed into the oscilloscope, which served as a real-time visual aid for identification of signals.

All the recorded data were synchronized by the time-code generator. The pulse generator was used for the functional checkout of the overall system and for setting the system sensitivity.

The tank pressure was initially recorded on the magnetic tape recorder during the proof test, but was later moved to the strip-chart recorder for the environmental test. Figure 13 shows a photograph of the equipment setup taken during the environmental test.

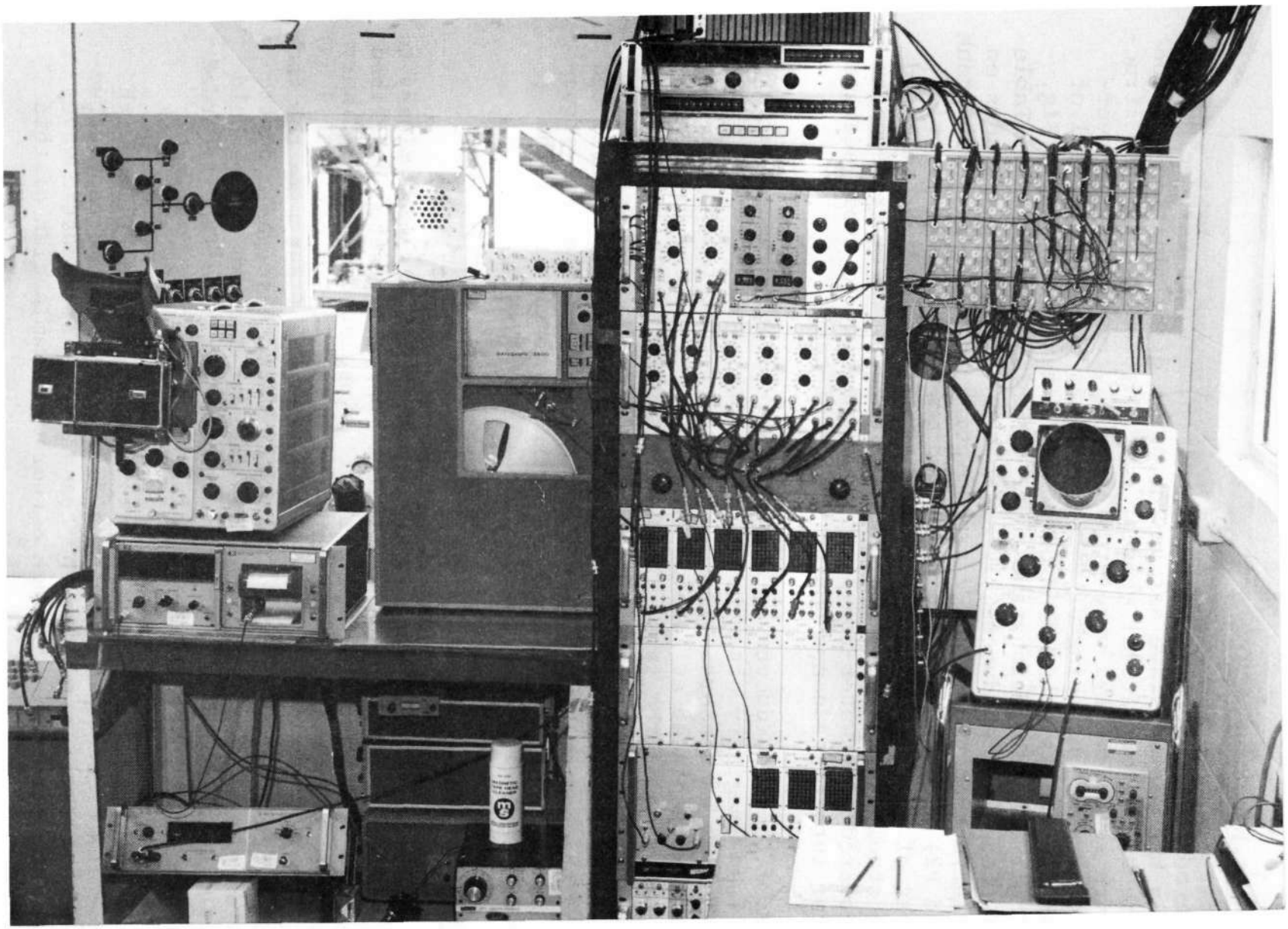

Fig. 13. Photograph of the monitoring setup taken during the environmental test.

III. PROOF TEST

Transducer Locations

Based on the results of the specimen test, it was decided to use only the master/slave arrays for noise discrimination for the proof test. After several ways of covering the entire tank structure with sensor arrays were studied, a coverage with six overlapping arrays consisting of 24 sensors was chosen. A total of 26 transducers was mounted on or near the tank as shown in Fig. 14. Their exact locations and their functions are given in Table 4. Of these 26 transducers, 12 sensors on the tank, 4 sensors on the inlet/outlet pipes, and 2 transmitting transducers on the tank (P1 and P2) were of the type described in the preceding section. The rest of the transducers were of old design, and were mounted on the steel supporting structure with magnets. All transducers were covered with water-repellent modeling clay to avoid seepage of water into transducers during the proof test.

Half the transducers on the tank were located near the corners of an imaginary octahedron in the tank, thus assuring even distribution of sensors. The other half of the transducers on the tank were placed at locations symmetrical to the first six about the axis of the tank. The sensors were then paired with the closest neighbor to establish six pairs of sensors for six arrays. In this arrangement, one each of the arrays covered the top and the bottom hemi-ellipsoidal bulkheads of the tank structure, and four arrays covered the cylindrical section of the structure including the welded circular frame areas.

Preliminary Tests

Preliminary Leak Test - A leak test, which was preliminary to the proof test, was monitored with the monitoring setup described above. In this test, the tank, still uninsulated and in ordinary atmosphere, was pressurized by gaseous helium to 20 psi (137.9 kN/m^2) in 5 psi (34.5 kN/m^2) steps. This was the first time the tank was pressurized above 5 psi. Throughout this test, no acoustic emission signal was detected either in real-time at a threshold sensitivity of 115 microvolts or during a replay of the recorded data at a threshold sensitivity of 50 microvolts.

Wave Propagation through Tank Immersed in and Filled with Water - The presence of water inside and outside the tank structure was expected to affect the transmission of acoustic waves through the structure. Though a thorough examination of this

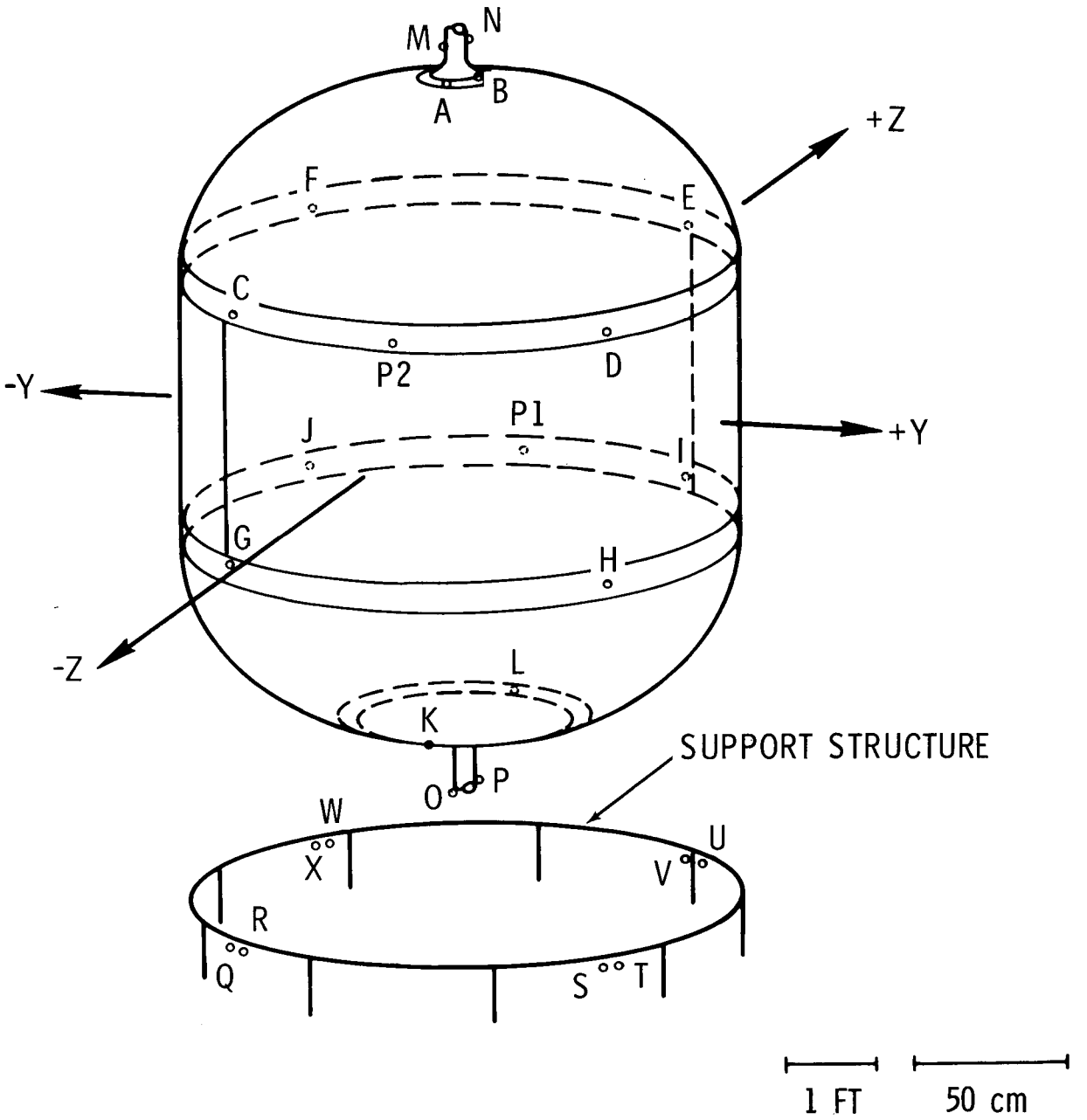

Fig. 14. Transducer locations for the proof test. Lines on the tank represent welding lines.

Table 4

TRANSDUCER LOCATIONS AND THEIR FUNCTION IN PROOF TEST

Transducer No.	Azimuth deg.	Water Line in.	Function*
A	180	90.0	1-M, 3-S, 4-S
B	0	90.0	1-M, 2-S, 5-S
C	224	63.7	3-M, 5-S, 6-S
D	134	63.7	4-M, 2-S, 6-S
E	44	63.7	5-M, 3-S, 6-S
F	314	63.7	2-M, 4-S, 6-S
G	224	32.2	3-M, 1-S, 5-S
H	134	32.2	4-M, 1-S, 2-S
I	44	32.2	5-M, 1-S, 3-S
J	314	32.2	2-M, 1-S, 4-S
K	180	7.5	6-M, 3-S, 4-S
L	0	7.5	6-M, 2-S, 5-S
M	On upper pipe		1-S
N	On upper pipe		1-S
O	On lower pipe		6-S
P	On lower pipe		6-S
Q	On support structure		3-S
R	On support structure		3-S
S	On support structure		4-S
T	On support structure		4-S
U	On support structure		5-S
V	On support structure		5-S
W	On support structure		2-S
X	On support structure		2-S
P1	179	32.2	Pulser
P2	359	63.7	Pulser

*1-M means master sensor for array No. 1, 3-S means slave sensor for array No. 3, etc.

property in the laboratory was desired, no time was available before the proof test because of the tight schedule of the test. The first opportunity to look into this property was when the tank was being lowered into the pool of water while being filled with water. At that time, one of the transmitting transducers was excited with a short duration square pulse thus simulating an acoustic emission source and signals were observed at all the sensors.

In Fig. 15, the observed signal at one of the sensors is compared with that taken when the tank was in air. The difference is striking. When the tank is in air, a large number of modes of vibrations, each of which attenuates very little, combine to make a long, continuous train of waves which lasts for several milliseconds after an impulsive excitation is applied to a transmitting transducer. The largest amplitude arrivals in the wave train are the fundamental longitudinal mode, M_{11}, and the fundamental flexural mode, M_{21}. From the nearly exponential decay of the tail portion of the signal wave train, the overall attenuation factor, Q, of the tank structure was estimated to be 3700 at 300 kHz, i.e., on the average only $2\pi/3700$ of the total acoustic energy was lost during each cycle of vibration.

When the tank is in water, many modes of vibrations are so heavily attenuated because of the leakage of energy into water that only those modes whose attenuation is relatively small can be expected to reach far distances. As a result, the observed signal from an impulsive source is a series of impulsive arrivals representing those modes which have efficient transmission characteristics, as seen in Fig. 15(b).

Some of the observed characteristics of the simulated signals are the following:

(1) When the major transmission path is in thin wall sections of the tank, the first arriving signal is a short duration signal with an impulsive beginning, representing the fundamental longitudinal mode, which travels at a speed of approximately 5.4 mm/μs. The attenuation of this mode is about two orders of magnitude greater than that with the tank in air.

(2) When the transmission path is along one of the circular frames, the first arriving fundamental longitudinal mode is less well-developed than that for the thin wall section, and is followed by several closely-spaced arrivals representing various wave paths along the circular frame.

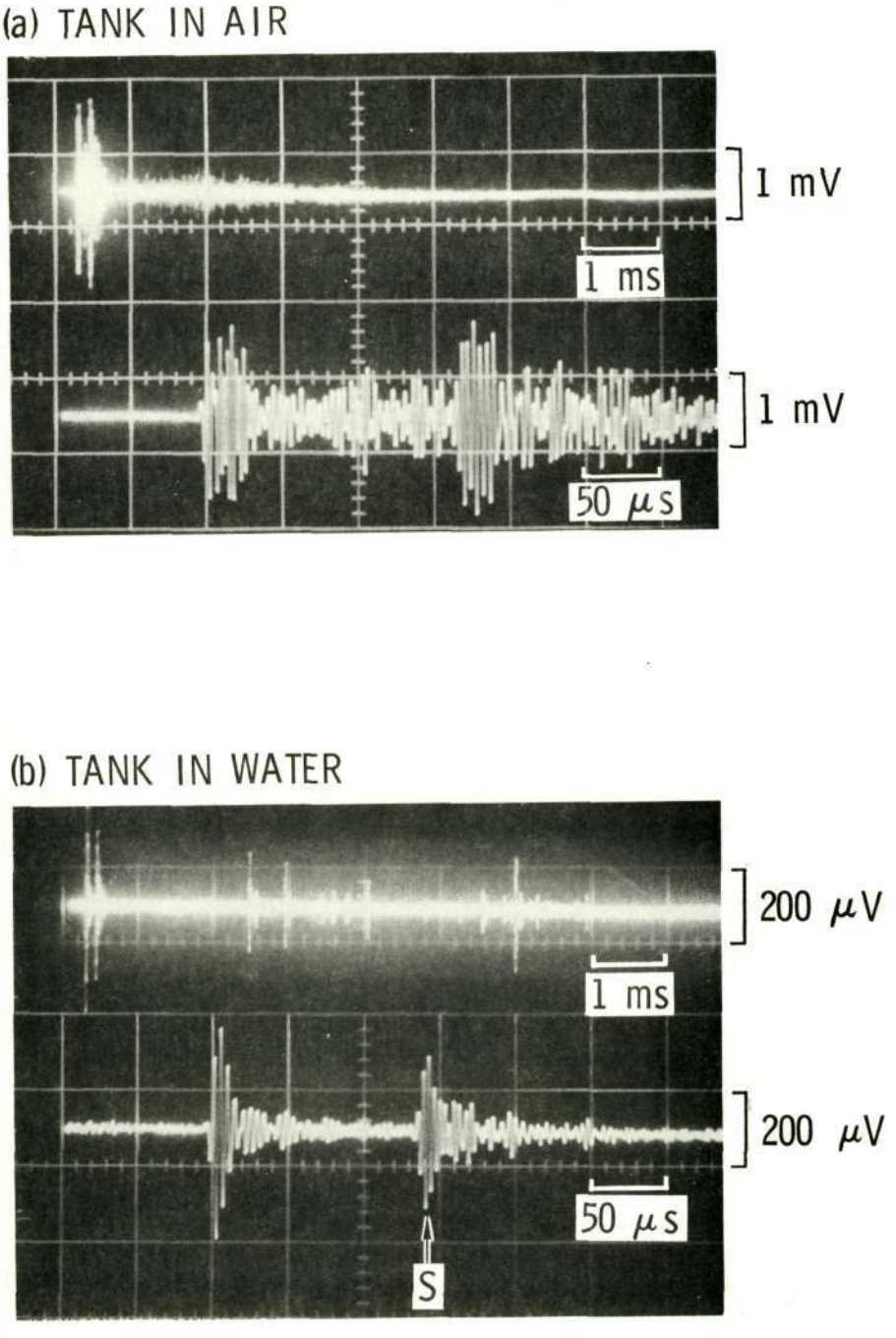

Fig. 15. Comparison of simulated signals with the tank in air and in water. The same signals for each are shown in two different sweep speeds. Note the distinct shear-converted arrival, marked S, when in water.

(3) When the source is in one of the circular frame areas and the detector is in another, a strong impulsive arrival, e.g., S in Fig. 15(b), follows the initial fundamental longitudinal mode arrival. From the transit time of this arrival, it was determined to be a shear wave arrival which was generated near the source, probably at the boundary between the thick circular frame section and the thin wall section, transmitted through the cylindrical section of the tank as a shear wave polarized in the plane of the sheet, converted again into a longitudinal wave at the boundary between the thin cylindrical wall and the circular frame on which the sensor is mounted. Since the energy of a shear wave polarized in the direction of the plane of the sheet can leak into water only by viscosity of water, the attenuation of such a wave is expected to be small, thus very efficient transmission of such a wave is expected.

(4) The fundamental flexural mode, M_{21}, which is the largest amplitude arrival when the tank is in air, is attenuated much more severely than the fundamental longitudinal mode when the tank is in water, and the former is not observable across the thin wall section of the tank.

(5) In all cases, a long series of impulsive arrivals follow the initial arrival for more than 10 msec. These are determined to be waves transmitted through the water and multiply reflected inside the tank.

The transmission of acoustic waves through a thin plate in water has been studied theoretically by Osborne and Hart (Ref. 7). The above results are in general agreement with their results.

Proof Test Monitoring

The proof test of the uninsulated tank was conducted first by filling the tank with water, at the same time lowering the tank into a pool of water very slowly, and then by pressurizing the tank in three cycles. The filling of the tank was a slow process, taking nearly four and a half hours. The pressurization of the tank was done at a rate of approximately 0.3 psi/sec (2.3 kN/m^2 sec), holding at every 10 psi (69 kN/m^2) level for 10 to 65 seconds. The maximum pressure levels were 30 psi (207 kN/m^2), 60 psi (414 kN/m^2), and 75 psi (517 kN/m^2) for the first, second, and third cycles, respectively. The results of a chemical analysis of the pool water is given in Table 5 below.

Table 5

CHEMICAL ANALYSIS OF POOL WATER USED FOR THE PROOF TEST

Total Solids	Less than 0.1 mg/l
Dissolved Solids	2100 ppm
Cl^-	1178 ppm
Hydrocarbons	None Detected
pH	6.7
Specific Conductivity	3300 micromho/cm

The monitoring of the proof test was done continuously with the monitoring setup described above, starting at the filling of the tank. The detection threshold for the real-time monitoring was set at 115 microvolts. A large number of acoustic signals was observed while the tank was being filled. These signals were considered to be due to the flowing, splashing, and bubbling of water in the tank. The majority of these signals subsided as soon as the tank was completely filled.

Some signals, however, were still detectable from three of the arrays after the tank was completely filled and while waiting for the pressurization of the tank. During the fifteen-minute interval immediately before the first pressurization cycle, 280 signals were detected in the array at the bottom of the tank, 144 signals were detected in the array at the top of the tank, and 19 signals were detected in the array in the -Y to +Z quadrant of the cylindrical section of the tank. The origins of these signals were not determined, but the fact that these three areas also generated acoustic emission signals during the pressurization cycles at increased rates may suggest existence of flaws which were activated by the presence of water.

Recordings of the emission signals on a magnetic tape were made from 5 to 30 to 25 psi (34.5-207-172.5 kN/m^2) pressure levels, 25 to 60 to 2 psi levels, and 50 to 75 psi levels in the first, second, and third pressurization cycles, respectively. In the later analysis of the recorded data, the signal detection sensitivity was increased to a detection threshold ranging from 20 to 40 microvolts. The higher sensitivity

was possible by the use of a narrow-band filtering of the recorded signals during the playback. The results of the analysis of the recorded data were combined with the real-time monitoring results to determine the acoustic activities in various locations of the tank.

Proof Test Results - At the detection sensitivity used for the post-test analysis of the recorded data, almost all of the sensors detected acoustic signals of various intensities. One of the most significant features of these signals was that all but a small fraction of these signals were too small to be detectable by more than one sensor. For these signals, the exact locations of the signal sources could not be determined, thus making the interpretation of the result extremely difficult. The detected activity, however, varied from one sensor to another, indicating that some areas on the tank were acoustically more active than other areas.

Another significant feature of these signals common to all the sensors was that no clear correlation between the occurrence of these acoustic events and the pressure level was observed, as is seen in a representative plot of cumulative number of events versus time in Fig. 16. This is not in agreement with the expected behavior of acoustic emission signals from crack growth induced by loading. Thus, a cause of these signals other than pressure-induced crack growth is suggested.

One of the important clues as to the nature of these signals is the amplitude distribution of the observed signals. The amplitude distributions were, therefore, determined for all the sensors for which recordings were made. It was found that the distributions were classifiable into the following three different groups, indicating not all the observed signals were from a single type of source. (cf. Fig. 14, p. 33, for sensor locations)

(1) Group 1 - Signals from all but three sensors showed a more or less common amplitude distribution where all signals were of very small amplitude with an extremely steep slope of the log-cumulative distribution curve. A representative example is shown in Fig. 17(a). The extremely steep slope indicates that the signals are not likely from a crack growth. The exact cause of these signals, however, is still unknown.

(2) Group 2 - Signals from sensor J on the lower circular frame in the -Y to +Z quadrant and sensor H on the lower circular frame in the +Y to -Z quadrant showed an amplitude distribution where the slope of the log-cumulative distribution curve was

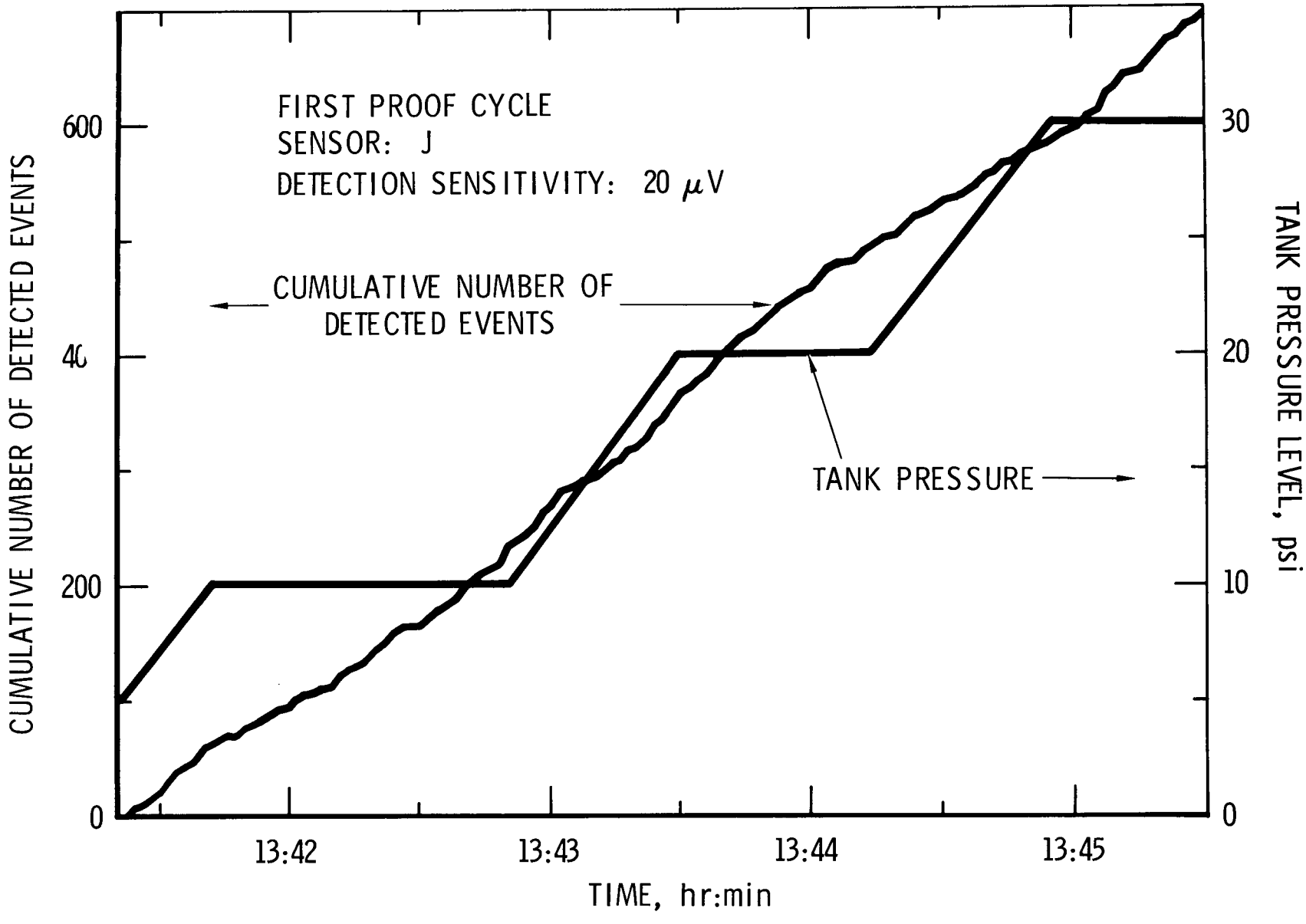

Fig. 16. Cumulative number of detected emission events and loading during proof test.

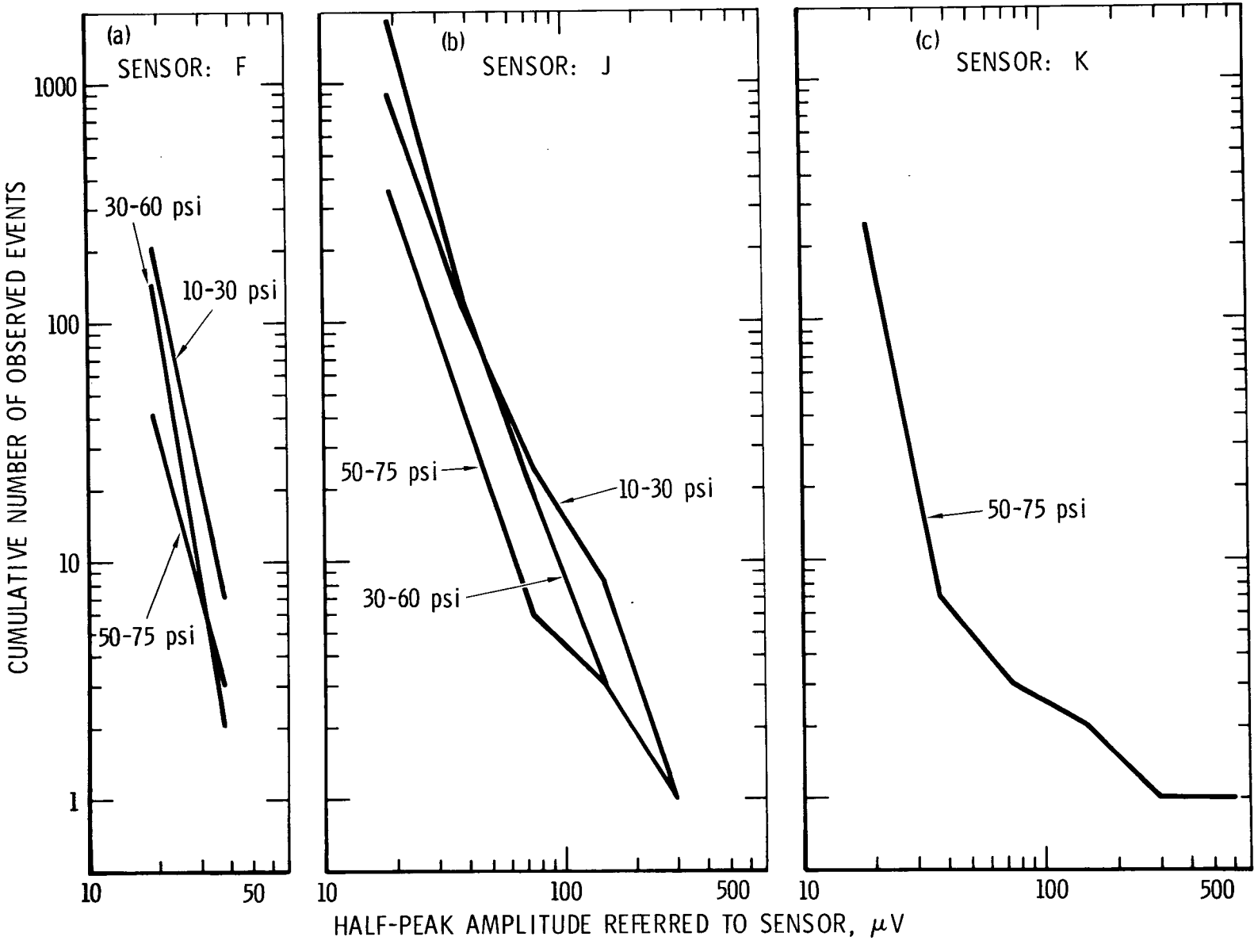

Fig. 17. Amplitude distribution of emission signals observed during the proof test.

distinctly less steep than that for the first group. The distribution for sensor J signals is shown in Fig. 17(b) as a representative example. The activity at sensor H was about one half that at sensor J. The slope of the curves is still relatively steep compared with those observed for a crack growth in a specimen. Thus, it is suggested that, even if they are from a growing crack, the stress intensity level is not critically high.

The signals detected by sensor J also include those from 12 events for which signals were also detected by sensor F on the upper circular frame with a time-of-arrival difference of 150 to 170 microseconds from J to F. A photograph of a typical event is shown in Fig. 18(a). Since the maximum time of arrival difference possible for the fundamental longitudinal mode waves between these two sensors is 148 microseconds, the signals detected by F sensor cannot be the fundamental longitudinal mode wave. The preliminary wave-propagation study, discussed earlier, suggests that these are indeed the shear wave arrivals which are converted to longitudinal waves near the sensor F. Since crack growth is a more efficient generator of shear waves than a thickness-mode transducer used for simulating the emission signals, and since a thin aluminum sheet in water is a better wave guide for shear waves than for longitudinal waves, it is not surprising that only converted shear waves are detected across the thin-wall section of the tank. Thus, the most reasonable interpretation of these signals is that emission sources, likely to be from crack growths, were located from 13 to 25 cm from sensor J on either side of the sensor along the lower circular frame. An x-ray inspection of the tank after the proof test detected a crack at 12.5 cm towards -Y axis from sensor J along the welded joint between the lower circular frame and the lower hemi-eliptical bulkhead. This is in agreement with the above interpretation.

Those events which were detected by sensors J and F were not the largest signals observed at sensor J. Furthermore, they represented a very small fraction of the total number of signals observed at sensor J. This can be interpreted as a result of a large number of emission sources, such as microfractures, distributed in a relatively wide area near sensor J. If microfractures are oriented in various directions, only those emission events whose shear-wave radiation pattern is preferably oriented can be detected by sensor F.

Even for these events, no clear correlation was observed between the occurrence of events and the pressure level. In addition, the fact that emission signals were observed even when the tank was not pressurized, as described earlier, suggests that the

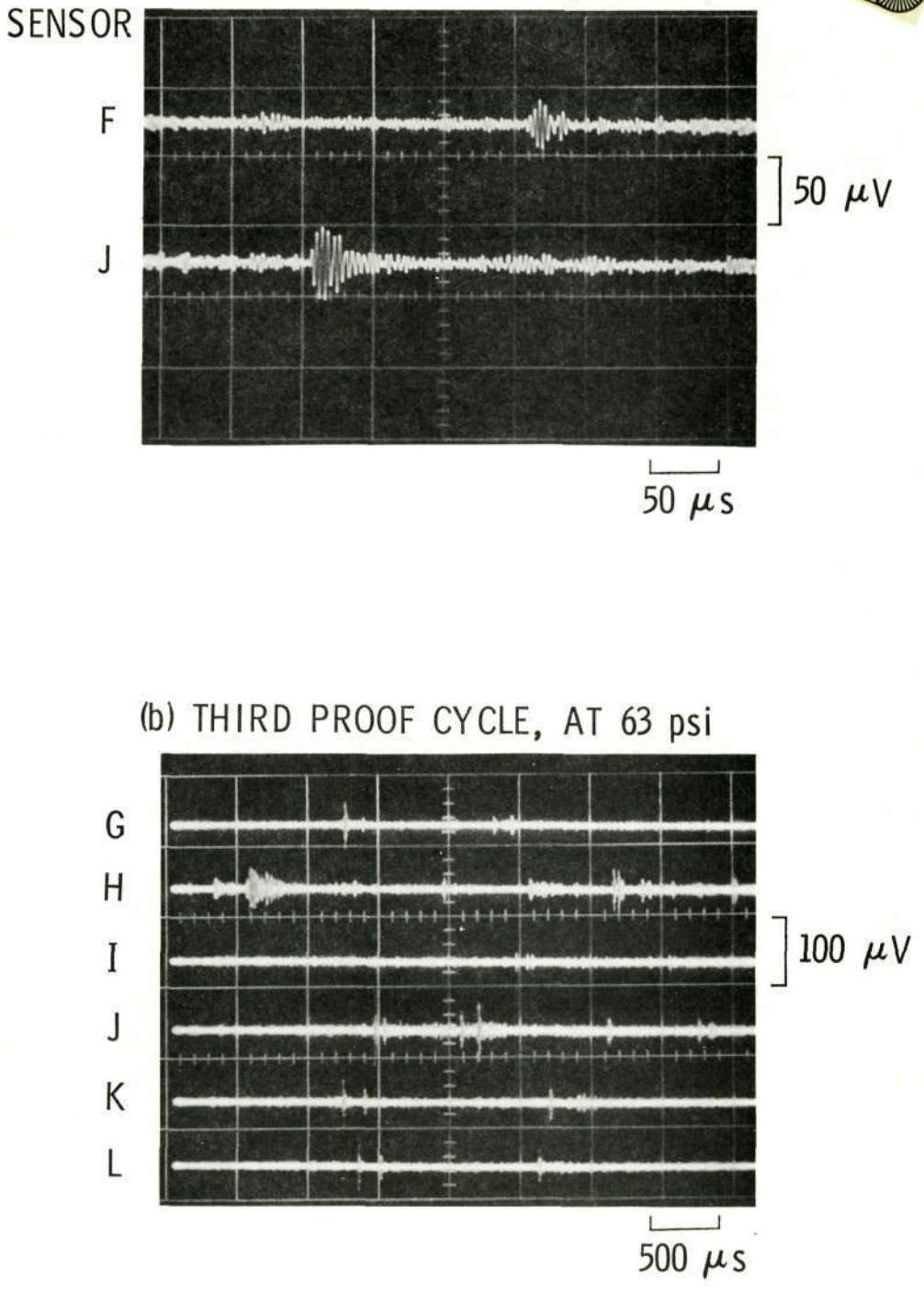

Fig. 18. Oscilloscope photographs of representative emission signals observed during proof test.

reaction of water to the structural material of the tank, particularly to the weld, may be responsible for these emissions.

(3) Group 3 - Signals detected by sensor K near the bottom of the tank showed a quite distinct distribution of signal amplitudes from all the others as seen in Fig. 17(c). The characteristics of some of these signals were different from the others, showing a marked dispersion of the wave train. This is an indication that the sources of these emission signals were more efficient generators of antisymmetrical mode (flexure waves) than of symmetrical mode (longitudinal waves). The exact nature of these signal sources, however, could not be determined.

A unique emission event was observed during the third cycle of the proof test at a pressure level of 63 psi. Dissimilar to all the other signals observed, this event was detected by all the sensors on the tank. The event generated waves through the water inside the tank in such an intensity that the signal was detected by all the sensors on the tank as a series of direct and multiple-reflected pulses as seen in Fig. 18(b). The source of the signal was located on the thin cylindrical wall section of the tank in the -Z to +Y quadrant at water level 58" and azimuth 120°. Uneven distribution of signal amplitudes indicated nonuniform distribution of emission energy from the source into the water. The exact cause of this emission could not be determined.

In summary, the result of the proof test was rather inconclusive. This is primarily because of two reasons: (1) Sensor distribution was not dense enough to permit effective determination of weak signal locations. (2) Interpretation of the detected signals requires more extensive knowledge of the properties of various emission signals than is available at present. The former can easily be solved by increasing the number of transducers used to detect signals. The latter, however, is more difficult to solve because it requires more extensive study of the acoustic emission phenomenon itself. This will be discussed in more detail in a later section.

IV. ENVIRONMENTAL TEST

Pretest Preparations

Setup Modifications - From the results of the specimen tests, it was clear that the setup used for the proof test was not sufficient to monitor the entire insulated tank during the environmental test because of the extremely high attenuation of acoustic waves expected for the structure. Accordingly, several modifications of the monitoring setup were made for the environmental test. The major modifications were the following: (1) Twelve additional sensors were placed on the tank to achieve a denser coverage. (2) Passive bandpass filters were added to the inputs of the AEM units, enabling the use of higher sensitivity in the real-time detection of emission signals. A simplified block diagram of the initial equipment setup for the environmental test is shown in Fig. 19, and the system frequency response from the preamplifier input to the AEM input is shown in Fig. 20. Transducer locations including those sensors which were added after the first 50 life cycles of the environmental test are given in Table 6 and also shown in Fig. 21.

With the passive filters added, the real-time detection sensitivity could be increased by a factor of four to five from the setup for the proof test. This increased sensitivity corresponded to an extension of the range of detection of a single sensor by approximately 30 cm for a PPO insulated tank, thus approximately doubling the area of coverage for the largest emission signals expected from subcritical crack growth.

One of the important but unknown properties of acoustic emission signals from this particular test was the frequency content of the signals. In order to acquire some data on this property, one monitoring channel was modified to cover a lower frequency range than all the other channels. Initially, a commercially-available, low-frequency, high-temperature acoustic emission sensor was planned to be used for this channel. However, the sensor was found to be unsuited for the environmental test because of extremely high impulsive noise generated whenever the sensor was exposed to a slight variation of temperature. Therefore, the same type of sensor as those used for the other channels was used for this channel, although the response of the sensor was not as high at low frequencies as it was at high frequencies. The overall frequency response of this channel excluding the sensor is also shown in Fig. 20.

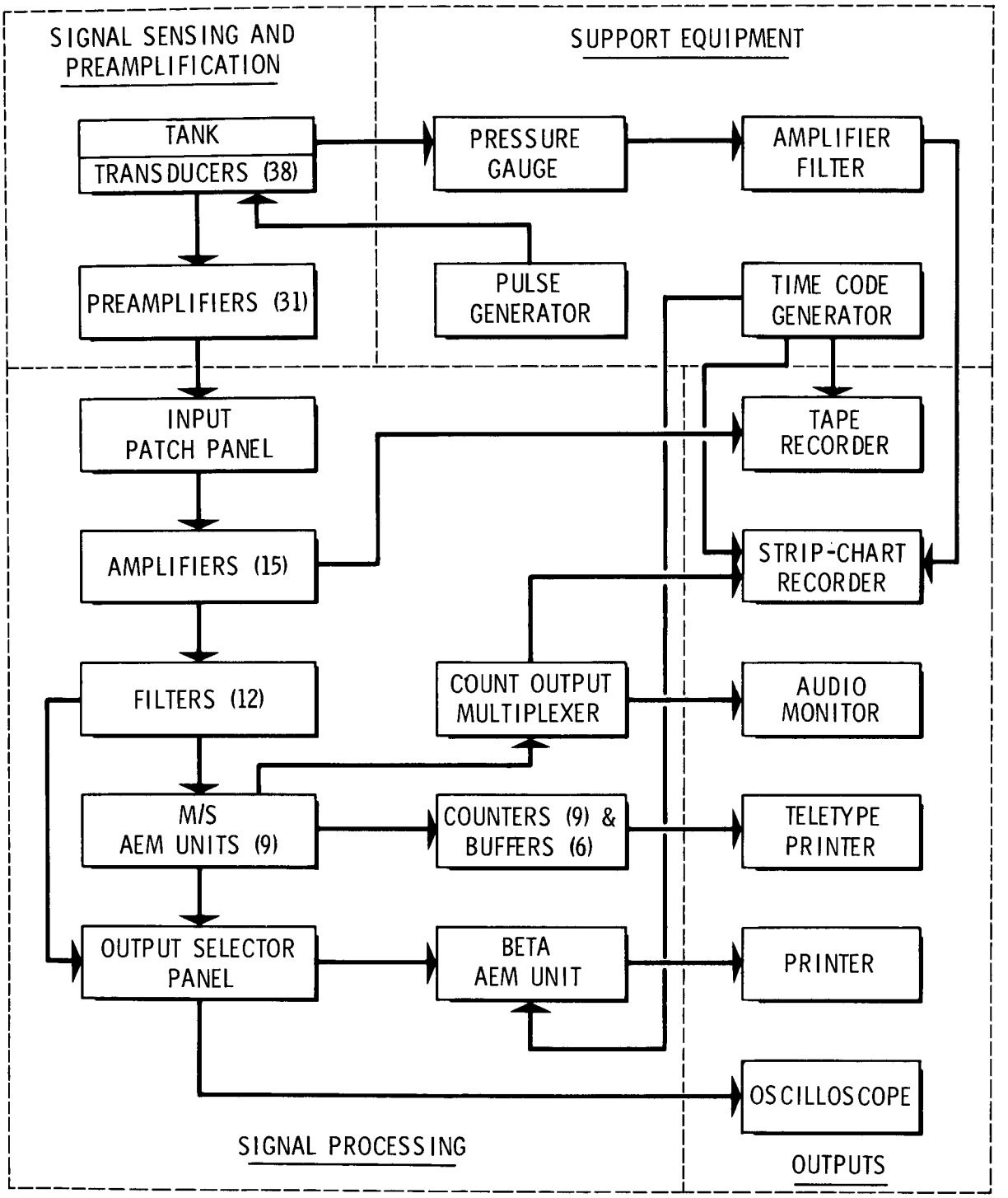

Fig. 19. Block diagram of the initial equipment setup for the environmental test.

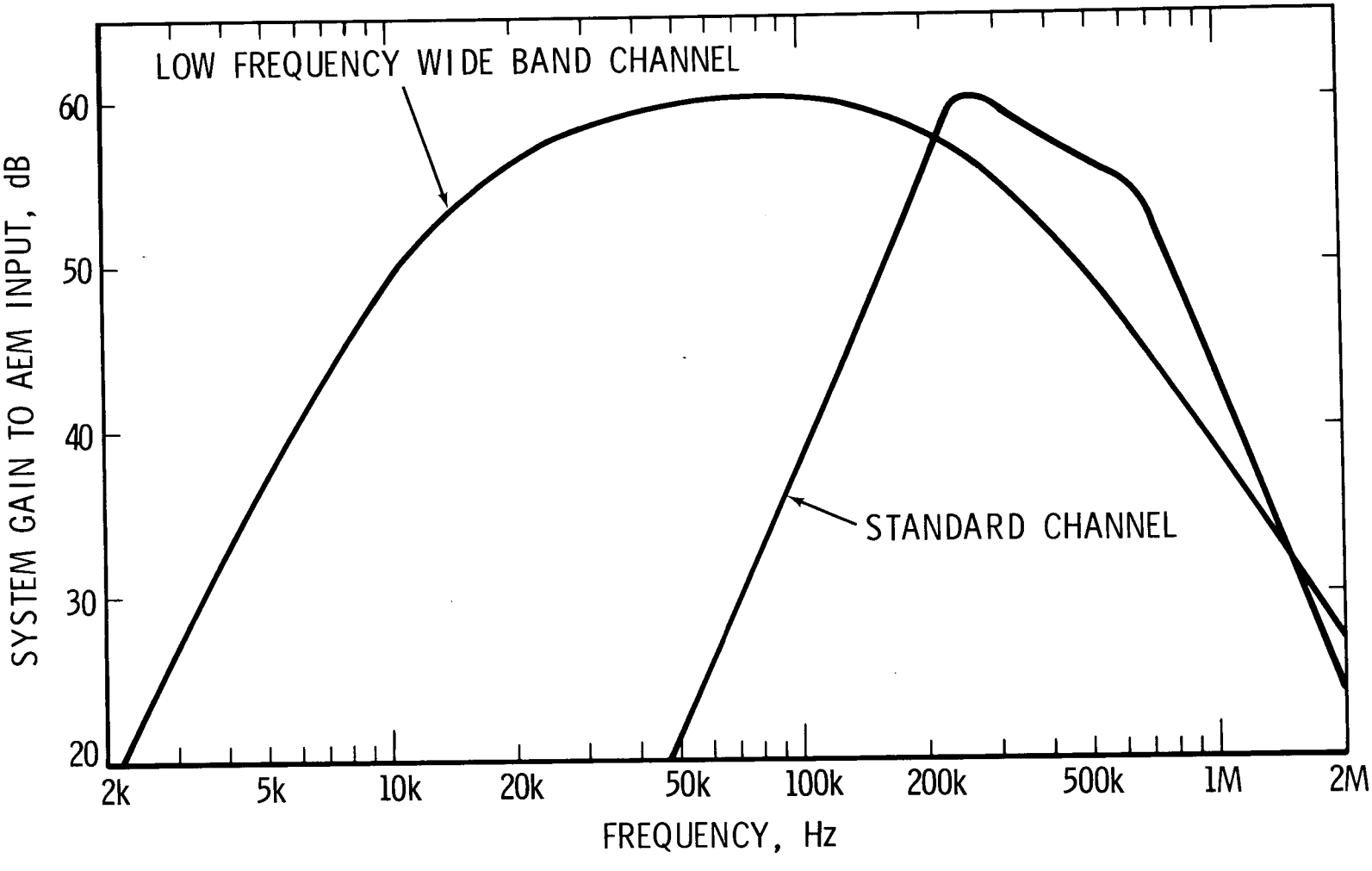

Fig. 20. Frequency response of standard and low frequency channels. The responses are from the input of the preamplifiers to the input to the AEM units, and do not include the response of transducers.

Table 6

TRANSDUCER LOCATIONS IN ENVIRONMENTAL TEST

Transducer No.	Azimuth deg.	Water Line in.	Remarks
A	180	90.0	
B	0	90.0	
C	224	63.7	
D	134	63.7	
E	44	63.7	
F	314	63.7	
G	224	32.2	
H	134	32.2	
I	44	32.2	
J	314	32.2	
K	180	7.5	1-50th cycles
L	0	7.5	
M			On upper pipe
N			On lower pipe
O-V			On support structure
3	179	63.7	
4	89	63.7	
5	359	63.7	
6	269	63.7	
7	179	32.2	
8	89	32.2	
9	359	32.2	
10	269	32.2	
11	270	7.5	1-50th cycles
12	90	7.5	1-50th cycles
13	225	7.5	
14	291.5	32.2	
P1	156.5	63.7	Primarily pulser
P2	336.5	32.2	Primarily pulser
P3	336.5	63.7	Primarily pulser
P4	156.5	32.2	Primarily pulser
11A	302.75	32.2	51-100th cycles
12A	178	32.2	Facing outside, 51-100th cycles
KA	201.5	32.2	51-100th cycles

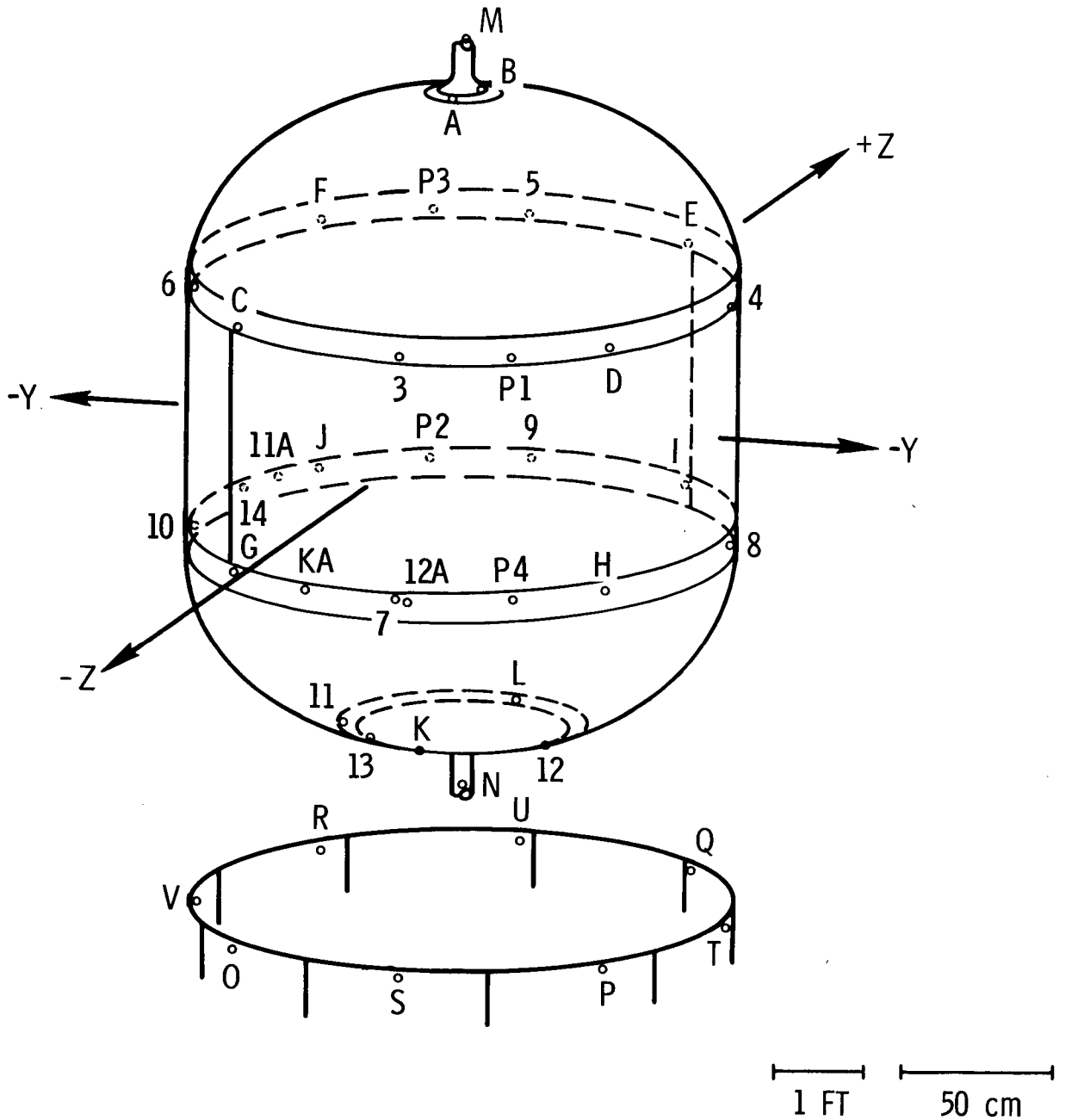

Fig. 21. Transducer location for the environmental test. Lines on the tank represent welding lines.

Wave Propagation Through PPO Insulated Tank - One of the problems anticipated from the result of the specimen tests was the severe attenuation of acoustic waves when the tank was insulated with PPO foam. Therefore, the attenuation property was examined on the real tank before the test began by alternately exciting one of the transducers and by observing the signals received by others. Some representative waveforms of received signals are shown in Fig. 22. The difference of wave propagation characteristics from those in the previous two cases, i.e., in air and in water, Fig. 15, is noteworthy.

The wave propagation characteristics through the PPO-insulated tank can be summarized as follows: (1) The dominant mode of wave propagation through the thin wall sections of the tank (cylindrical skins and bulkheads) is the fundamental longitudinal mode, which shows little wave dispersion and thus appears as an impulsive arrival of short duration. (Sensor 7 in Fig. 22). It is often the only detectable arrival. The attenuation coefficient of this mode was independent of frequency within the frequency range of observation of 50 kHz to 400 kHz. This was in agreement with the result of the specimen test. The value of the attenuation coefficient in the real tank also agreed well with the result of the specimen test. The shear-converted waves observed strongly for the tank in water was not observed for the PPO-insulated tank. This is because the PPO foam can absorb shear wave energy, while water cannot. (2) The wave propagation along the vertical weld section was essentially the same as that for the thin wall section, except that the waves experienced somewhat less attenuation along the vertical weld. This is probably due to a certain guiding effect of the vertical weld section. (3) When both the source and the receiver were located very close to one of the circular frames, a long train of waves was observed. (Sensors 4 and 5 in Fig. 22) This wave train was not attenuated so severely as the first longitudinal mode waves, and therefore was considered to be caused by waves trapped in the frame, which was not covered with PPO foam insulation and thus formed an efficient wave guide. The character of this wave train was complicated because of a large number of possible modes of propagation along the frame. (4) When both the source and the receiver were located on the lower bulkhead ring surrouding the access door, relatively strong flexural waves are observed. This is probably because of the gap in PPO insulation in this area. The observed difference in signal characters was useful in estimating approximate locations of emission signal sources during the environmental test.

Background Emissions - After the monitoring equipment was set up and the functional checkout was completed, the equipment was

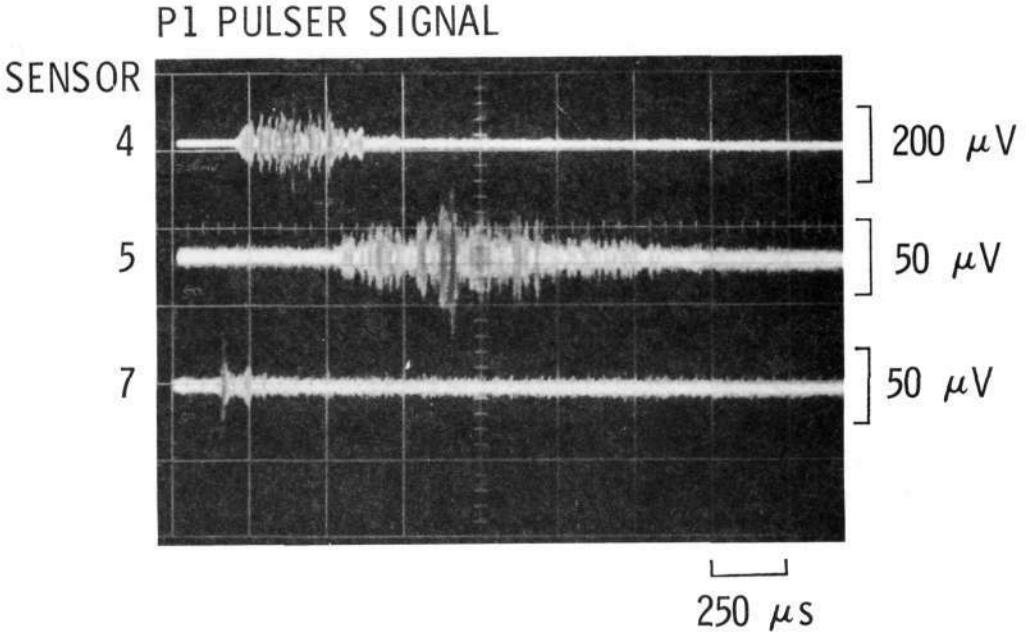

Fig. 22. Simulated signals through the PPO foam insulated tank. The effect of the foam insulation is clear when compared with Fig. 15.

left on for several nights while waiting for the start of the environmental test. During these overnight monitorings, the tank was pressurized at 5 to 6 psig (35 to 40 kN/m^2) with gaseous hydrogen at ambient temperature and was unattended. The detection threshold was set to 30 microvolts referred to the sensor output, a level sufficiently high compared with the preamplifier noise level that practically no output was expected to be caused by the electronic noise.

Although most sensors detected very little or no background activity during these monitorings, a few sensors detected background activities of some interest. A representative result is shown in Fig. 23. In this figure, the cumulative numbers of detected events are plotted against time. Each curve represents two sensors because two sensors shared each detector (AEM unit) for this experiment. As seen in this figure , the activity was sporadic, with periods of high activity lasting for half an hour or so each and separated by several hours of quiet periods. It was also evident that activities detected by different sensors were independent of each other, with no clear temporal correlations among them. This suggested internal origins for these activities rather than such external origins as common electrical noise.

Waveforms of these events, observed on an oscilloscope screen while they occur, had oscillations characteristic of acoustic emission signals. Their amplitudes, however, were mostly very small. A Beta-AEM result for the sensor A indicated that the slope of the log-cumulative amplitude distribution was four to five, which was higher than the slope expected for a crack growth. The largest event detected had amplitude only 12 dB above the threshold of detection.

The true nature of these activities is still unknown. However, it is evident that some extremely weak sporadic activities were taking place in certain limited areas on the tank while it was left slightly pressurized with gaseous hydrogen.

Thermal Performance Test - Preliminary to the environmental life cycle test, the insulated tank was filled with liquid hydrogen for an extended time to examine the thermal performance of the insulation system. Although this test was not acoustically monitored, it gave an opportunity to test the performance of the acoustic sensors in an extremely low temperature environment.

During this test, the skin temperature of the tank, on which the sensors were mounted, dropped to a level ranging from -200°F

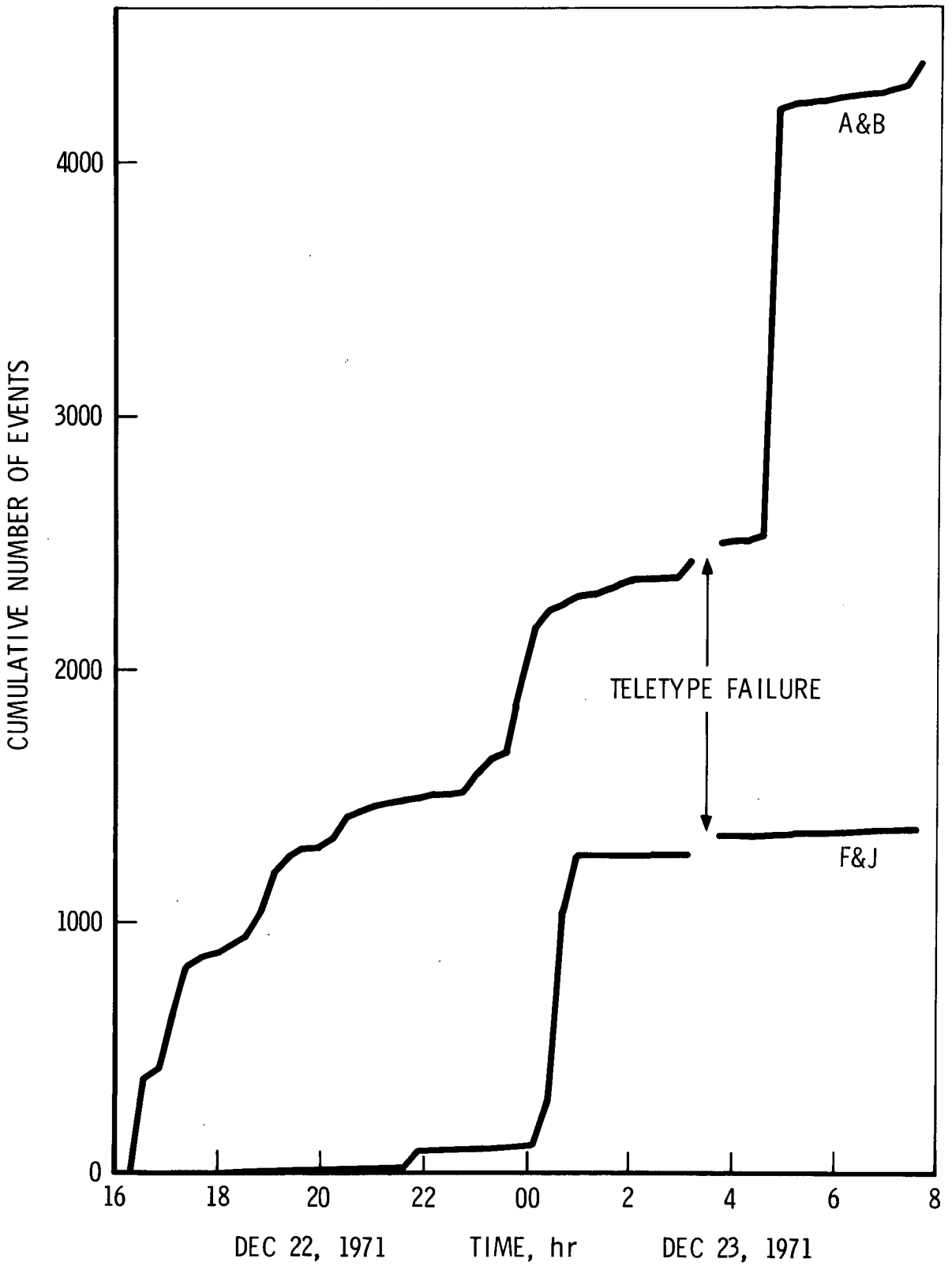

Fig. 23. Cumulative number of background acoustic emission events detected during overnight monitoring of insulated tank. The detection threshold was 30 μV.

to -290°F (-130°C to -180°C). This was much lower than the anticipated temperature of -100°F (-73°C), for which the sensors and their mounting method had been designed and tested prior to the test. As a result, the Dow-Corning 92-024 adhesive used to bond the sensors to the tank either cracked or completely debonded from the sensor or from the surface of the tank.

Aside from the problem with the bonding material, the sensor itself functioned satisfactorily at these low temperatures. This was indicated by the fact that the sensor which was mounted on the lower fill-and-drain pipe showed no malfunction even during the time when the temperature there was lower than -300°F (-185°C). This sensor was mounted directly on the surface of the pipe by taping the sensor case to the pipe with teflon tape without using the Dow-Corning adhesive.

Those sensors for which the bonding material cracked were repaired by supporting each sensor from behind by a phenolic stick, except the two sensors near the top of the tank, for which no convenient way of supporting the other end of the stick was found within the limited time available for this repair. The repaired sensors functioned satisfactorily throughout the environmental test.

Environmental Test, Phase I

Each life cycle of the first phase of the environmental test was conducted in the following sequence: First, the tank was filled with liquid hydrogen to 95% capacity. This took ten to twenty minutes. Then, the skin temperature of the tank was allowed to stabilize for 60 to 70 minutes. During this time, two or occasionally three retoppings of the tank were necessary. About ten minutes after the final retopping, the tank was pressurized to 40 psig (276 kN/m^2) using gaseous hydrogen at a rate of 0.5 psig/sec (3.45 kN/m^2 sec). The pressure was maintained at this level for two minutes, increased to 60 psig (414 kN/m^2) at the same rate as above, maintained at this level for another two minutes, and then reduced to 40 psig at the rate of 0.3 psig/sec (2.07 kN/m^2 sec). The tank was then drained while keeping the pressure at 40 psig. The draining took about three minutes. After the tank was emptied, it was heated by radiant heat from outside to a skin temperature of 250°F (121°C) and was maintained at this temperature for five minutes. After the heaters were turned off, the pressure was reduced to 1 psig (7 kN/m^2) and the tank was allowed to cool until the skin temperature was down to 100°F (38°C). The cool down took slightly over an hour. These procedures were repeated fifty times for the first phase of the environmental test.

Not all the life cycles were monitored by the acoustic emission instrumentation because of the limitations in equipment and manpower. Cycles monitored during this first phase of the environmental test were: 1, 2, 3, 8, 9, 10, 12, 13, 17, 18, 23, 24, 28, 29, 30, 34, 35, 36, 39, 40, 41, 43, 45, 46, 47, 48, 49, and 50 -- a total of 28 life cycles. A few of the cycles were monitored continuously from the beginning to the end, but the monitoring was concentrated mostly during the pressurization period of each cycle.

The First Life Cycle - The first life cycle of the environmental test was monitored with the setup described above. Only the lettered sensors (as opposed to the numbered sensors, cf. Table 6) were monitored with the real time detection threshold of 30 microvolts. The monitoring was done continuously through the entire length of the cycle.

The cumulative numbers of events detected by two of the pairs of transducers are shown in Fig. 24. Sensors were used in pairs because of the limited number of detection units (AEM units) available. As seen in these representative plots, the number of observed events was extremely large. In fact, the detected events were so numerous that the detection units were often saturated and meaningful counts of events were lost.

The noisiest location on the tank throughout the test was at the bottom of the tank. Even while the tank skin temperature was being stabilized, acoustic events were detectable at a rate of 200 to 500 per minute in the area, in contrast to a rate of about 20 per minute from other locations. The cause of these acoustic noise emissions could not be determined during the test, but several causes can be considered, including slight differential movement at the bolted areas of the access door caused by temperature variation and formation of hydrogen bubbles inside the tank in this area. The last cause was likely because the PPO insulation was not complete in this area.

A more serious noise problem was encountered at all of the sensors. Whenever the pressure in the tank varied slightly, a large number of noise events were observed throughout the tank. These noise events were so numerous during the pressurization of the tank that analysis of the data to identify possible crack-generated acoustic emission signals was impossible. These events were detected at an average rate typically of 100 per second in an array on the cylindrical section of the tank, about 250 per second at the top of the tank, and about 200 per second at the bottom of the tank. The rate was higher at lower pressure levels

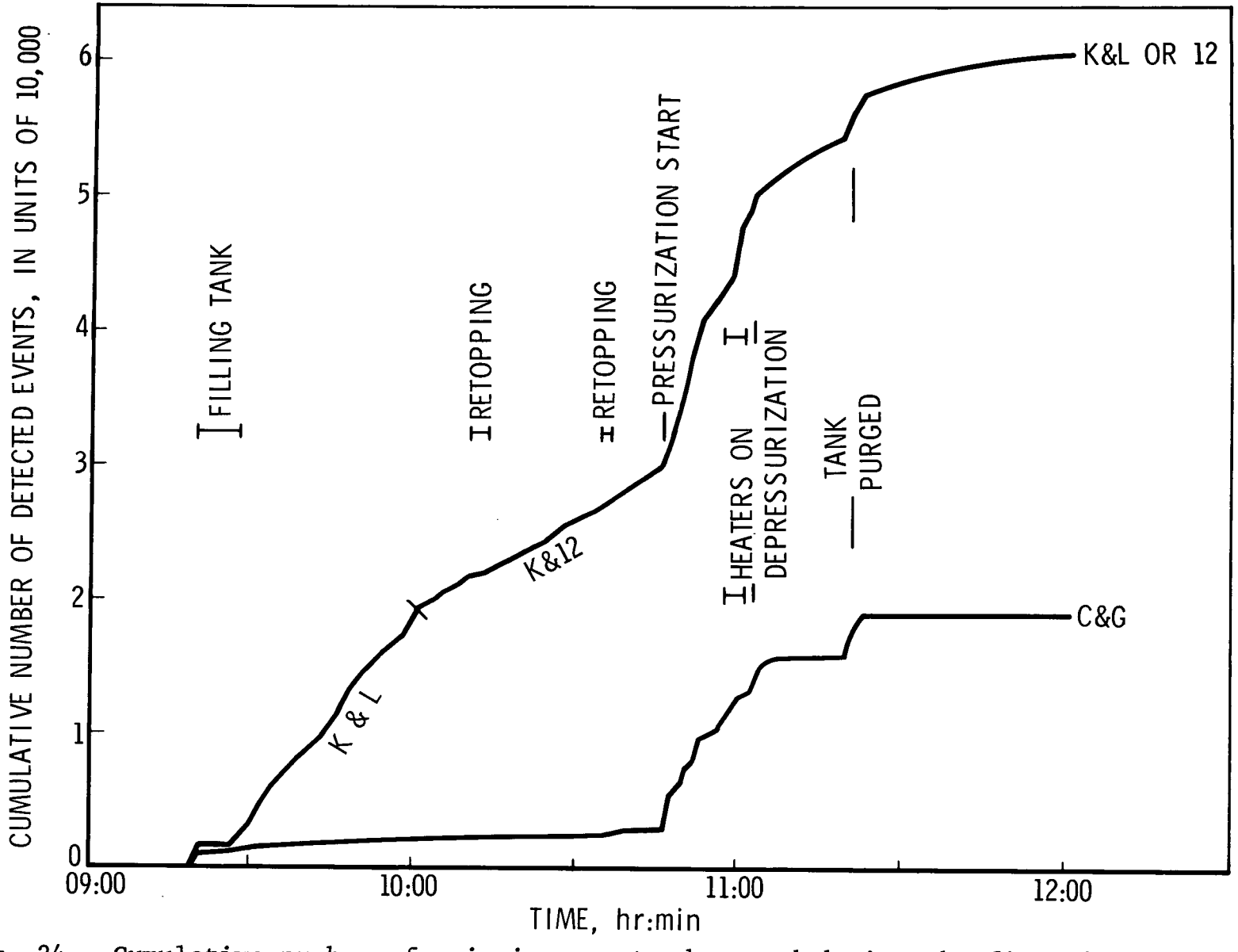

Fig. 24. Cumulative number of emission events detected during the first life cycle of the environmental test.

than at higher pressure levels. Except for a higher concentration of smaller signals as compared with crack-generated acoustic emission signals, each of these noise events had a waveform characteristic of acoustic emission signals. However, no correlation of signals between any two sensors was observed. This indicated that these noise events were generated within very close proximity of each sensor, with a very small amount of energy release for each. The exact origin of these noise events could not be determined during the test. However, inferring from the result of the specimen test, it is likely that a large number of acoustic emission signals were generated at or near the foam-aluminum interface responding to a slight deformation of the material. The fact that these emissions were more numerous at lower pressure levels than at higher pressure levels supports this interpretation because the major bending deformation of the tank structure takes place at low pressure levels.

Another heavy noise was encountered during the heat cycle of the test. Throughout the duration of the time when the heat lamps were on, numerous spikes were observed on all of the sensors. They were probably caused by the extremely high electric current used for the heat lamps, which were located only a few inches from the sensors and sensor cables. Because of these noise spikes, all the counters were completely saturated, making the monitoring for acoustic emission signals impossible.

Temporary Modification of Data Processing Logic - From the monitoring results of the first life cycle, it was clear that the simple master/slave type spatial filtration logic was useless for the type of noise encountered in this structure. Since the noise events encountered during the pressurization of the tank were found to show no correlation between any two sensors separated by a fair distance, some kind of coincidence logic was considered to be helpful in eliminating most of these noise signals. Therefore, a makeshift coincidence-logic network was established using two AEM units and a scaler, as shown in Fig. 25. A simple statistical consideration, however, indicated that these noise events were so numerous that there would be a large number of chance coincidences of two independent noise events being detected as coincident signals between two sensors. In order to reduce this probability, the detection sensitivity was reduced from 30 microvolt to 100 microvolt threshold, referred to the sensor output.

This temporary setup was put to test during the second and the third life cycles of the environmental test. A pair of sensors J and 14 on the lower circular frame in the -Y to +Z quadrant were used. These sensors were separated by a distance of 34 cm.

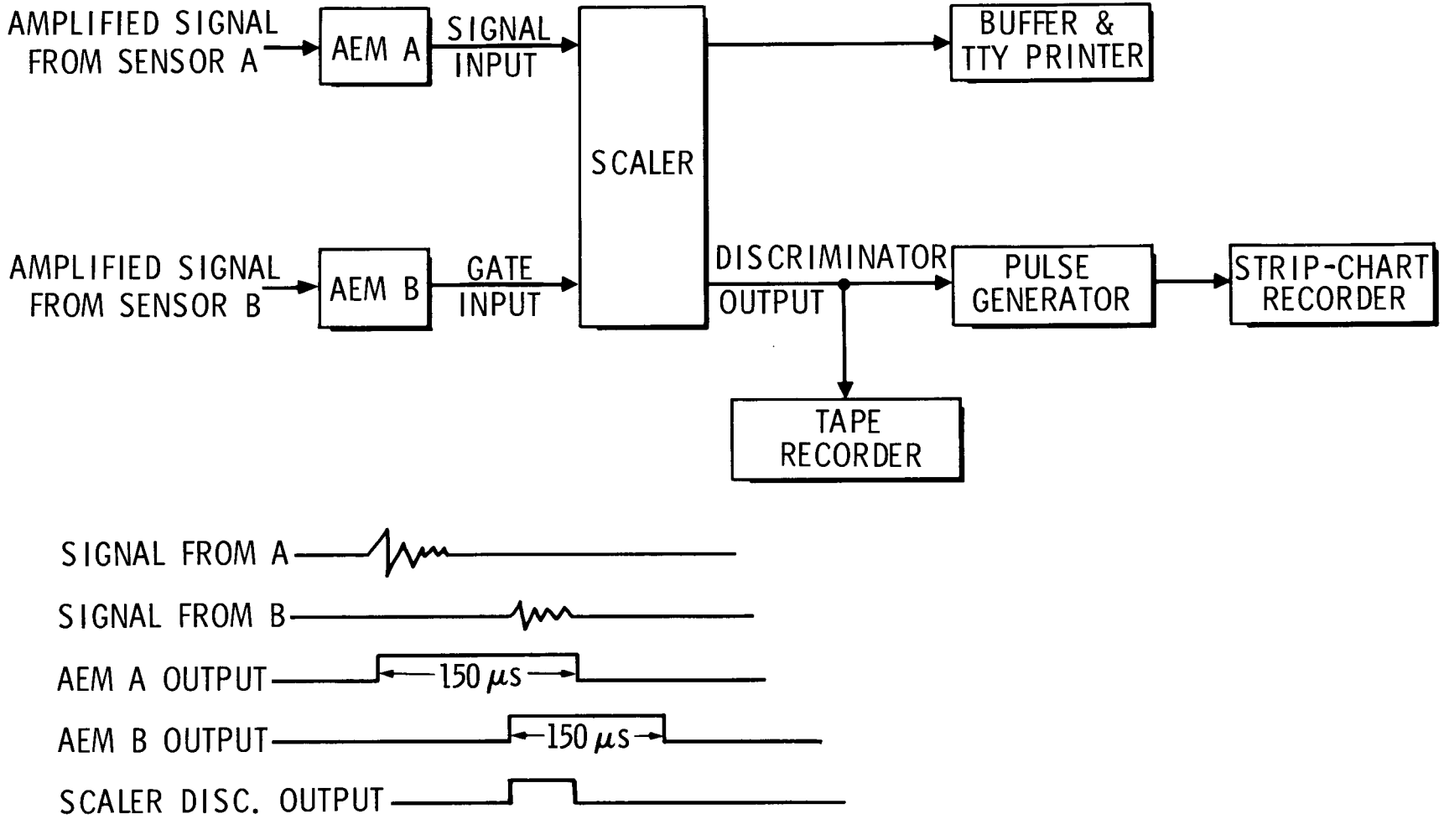

Fig. 25. Temporary setup for the coincidence detection of emission signals. With this setup, discriminator outputs are generated only when the two signal inputs are within 150 μs of each other.

This trial proved to be successful. The number of detected events was reduced by a factor of approximately 30. Although this reduction was not sufficient by itself because the total number of detected events during the pressurization cycle was still too many to be readily analyzable, most chance-coincident noise events were found to occur at pressure levels below 40 psi (276 kN/m^2), when the noise events were extremely numerous, and only few chance-coincident noise events were detected above 40 psi and during the 60 psi (414 kN/m^2) holds, when most crack growths, if any, were expected. The judgment whether a pair of signals observed at a close time separation between two sensors were likely to be of chance-coincidence of two independent noise events or from a single source was made by observing the relationship between their amplitude ratio and arrival-time differential. Other such properties as similarity of waveforms at two sensors, though somewhat subjective, were also used as supporting evidence.

Modification of Setup - Encouraged by the above findings, it was decided to modify the whole monitoring setup by using the coincidence detection logic. Four AEM units were modified to establish four coincidence detection arrays to cover half of the cylindrical section of the tank simultaneously. Each array consisted of three sensors along a circular frame with 68 cm separation between sensors. Two coincidence-detection pairs were established within each array as shown in Fig. 26(A). In the figure, sensors a and b constitute a coincidence pair and sensors b and c constitute another.

The areal distribution of the detection sensitivity around a pair of sensors with this detection logic is different from that for a single sensor. Since an event to be detected by the coincidence logic must be detectable at both of the pair of sensors, the distance to the farther sensor determines the detection sensitivity. Therefore, this detection logic is most sensitive to events which occur at the mid-point between the sensors. Approximate equisensitivity curves for the array with a signal detection sensitivity of 50 microvolts referred to the sensor are also shown in Fig. 26(A). Actual equisensitivity curves are more complicated because of somewhat more efficient transmission of acoustic waves along the circular frame and because of anisotropic distribution of acoustic energy radiation pattern around an acoustic emission source.

The resolution time of the coincidence detection logic for these basic arrays was adjusted to 200 microseconds, which was approximately the time for a shear wave to travel from one sensor of the pair to another. As is the case with most other arrays,

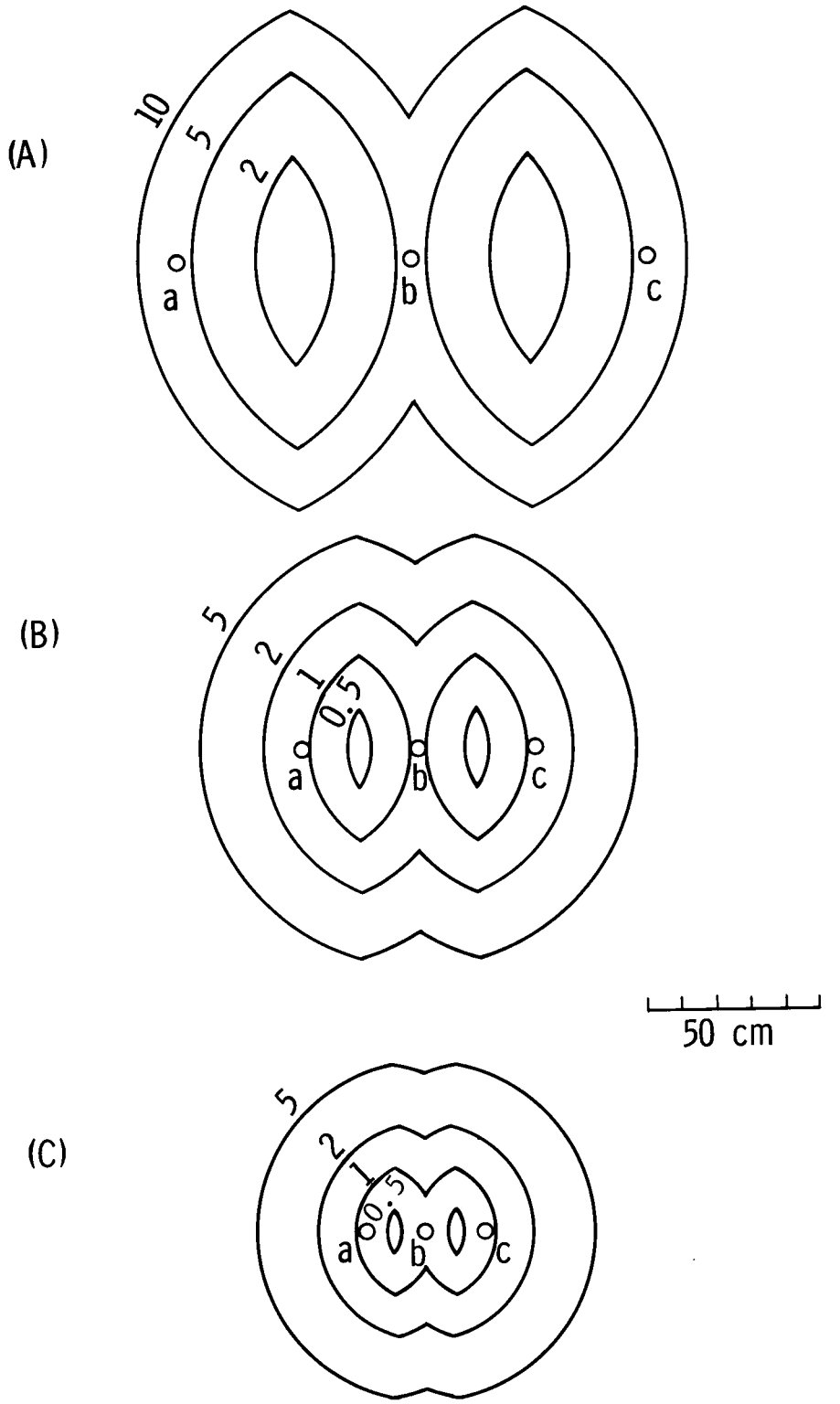

Fig. 26. Coincidence detection arrays and equi-sensitivity contours. Detection sensitivities are given by the amplitude of the minimum detectable signal measured in mV at a unit distance of 1 cm. (A) Basic array with 50 μV detection threshold. (B) Half-size array with 50 μV detection threshold. (C) Quarter-size array with 100 μV detection threshold.

the size of an array must be determined by compromising among several factors. In general, the larger the sensor separation, the larger the areal coverage, but the lower the detection sensitivity. In addition, for the coincidence detection employed in this test, the larger array required the longer resolution time and thus the more susceptible it was to chance-coincident noise events. The sensor separation of 68 cm was not optimum for this purpose, but it was the closest separation that could be used on the tank without any addition of sensors and still accomplishing the total coverage of the cylindrical section of the tank.

Because of the additional work necessary for this equipment modification, the monitoring of the environmental test was suspended temporarily after the third life cycle.

Life Cycles 8 through 50 - The monitoring resumed at the 8th life cycle using the modified monitoring setup described above. The monitoring was done alternately for the +Y side and -Y side of the cylindrical section of the tank for consecutive cycles of the test. In addition to the coverage of the entire cylindrical section of the tank with eight basic arrays, a half-size array was established along the lower circular frame in the -Y to +Z quadrant after the 36th cycle, and used continuously thereafter to monitor this area. This was the area where the post-proof-test x-ray inspection detected a flaw. The equi-sensitivity curves for this array for a signal detection threshold of 50 microvolts referred to the sensor output are shown in Fig. 26(B). It is readily seen by comparison of this figure with Fig. 26(A) that a smaller array gives higher detection sensitivity than a larger array, but in a more limited area. The resolution time of this array was adjusted to 100 microseconds.

The monitoring was done typically in the following sequence: Before the inital filling of the tank, arrays to be monitored for the cycle were selected, and signals from the sensors in these arrays were connected to appropriate amplifier inputs at the input patch panel. One sensor was selected at this time for the measurement of amplitude distribution by the Beta-AEM unit. At the start of the filling of the tank, all the scalers (counters) were reset, and the accumulation of the coincident count outputs from the modified AEM units started. The accumulated counts were printed out periodically on the TTY printer, and the Beta-AEM result for the amplitude distribution was printed out at the same time on a separate printer. These printouts were automatically continued throughout the life cycle. A few minutes before the start of the pressurization cycle, the strip-chart recorder was turned on to record the pressure level and the multiplexed count output with the time code. Just before the end of the pressure

hold at 40 psi, the tape recorder was turned on to record analog signals from twelve of the sensors being used, the multiplexed count output, and the time code. Recording continued till the end of the 60 psi hold. The strip-chart recorder was turned off at the start of the heating cycle. Immediately after the test, the recorded analog signals were played back through an appropriate bandpass filter and displayed on a storage oscilloscope screen for further analysis of the signals using the recorded, multiplexed count output as a guide to locate signals on the tape. Almost all of the detected signals were thus examined carefully for their amplitudes, waveforms, and time relationships, and were tabulated.

In Fig. 27, the number of events detected in each basic coverage array during the pressurization period from 40 psi to 60 psi and during the 60 psi hold are shown against life cycles. This is a direct result obtained from the real-time TTY printout of the accumulated numbers of events. The only prominent feature seen in the figure is the large number of events detected between the 28th and 36th cycles along the upper circular frame, indicating an increased activity in the area during this time interval. Also seen in this figure is the lesser activity along the lower circular frame compared with the upper circular frame area throughout the test. Since the basic coverage array was insensitive to small energy emissions, this simply means that the lower circular frame area generated fewer extremely large emissions than the upper circular frame area.

More detailed results were obtained from the post-test playback of the recorded signals. In Fig. 28, the distribution of the observed time differentials between pairs of sensors used for the coincidence detection is shown for the period of the 12th to the 50th cycles, covering all of the monitored arrays. The histogram shows the number of detected events in the time differential intervals of every 25 microseconds; the mid-point between a pair of sensors means no time differential between these two sensors.

Two prominent peaks can be seen. The large, broad peak covering the wide area between sensors D and 5 along the upper circular frame is due to the extremely high activity in the area during the life cycles 28 through 36. As seen in this delta-t distribution, the emission sources were not concentrated in any one location, but were distributed in a wide area. Typical waveforms of an emission signal from this area are shown in Fig. 29(a). The beginning of the signal is rather gradual, indicating that the source was not in the thin wall section of the tank but in the circular frame area itself. In most cases, the signals were too small to be detectable at sensors on the lower circular frame.

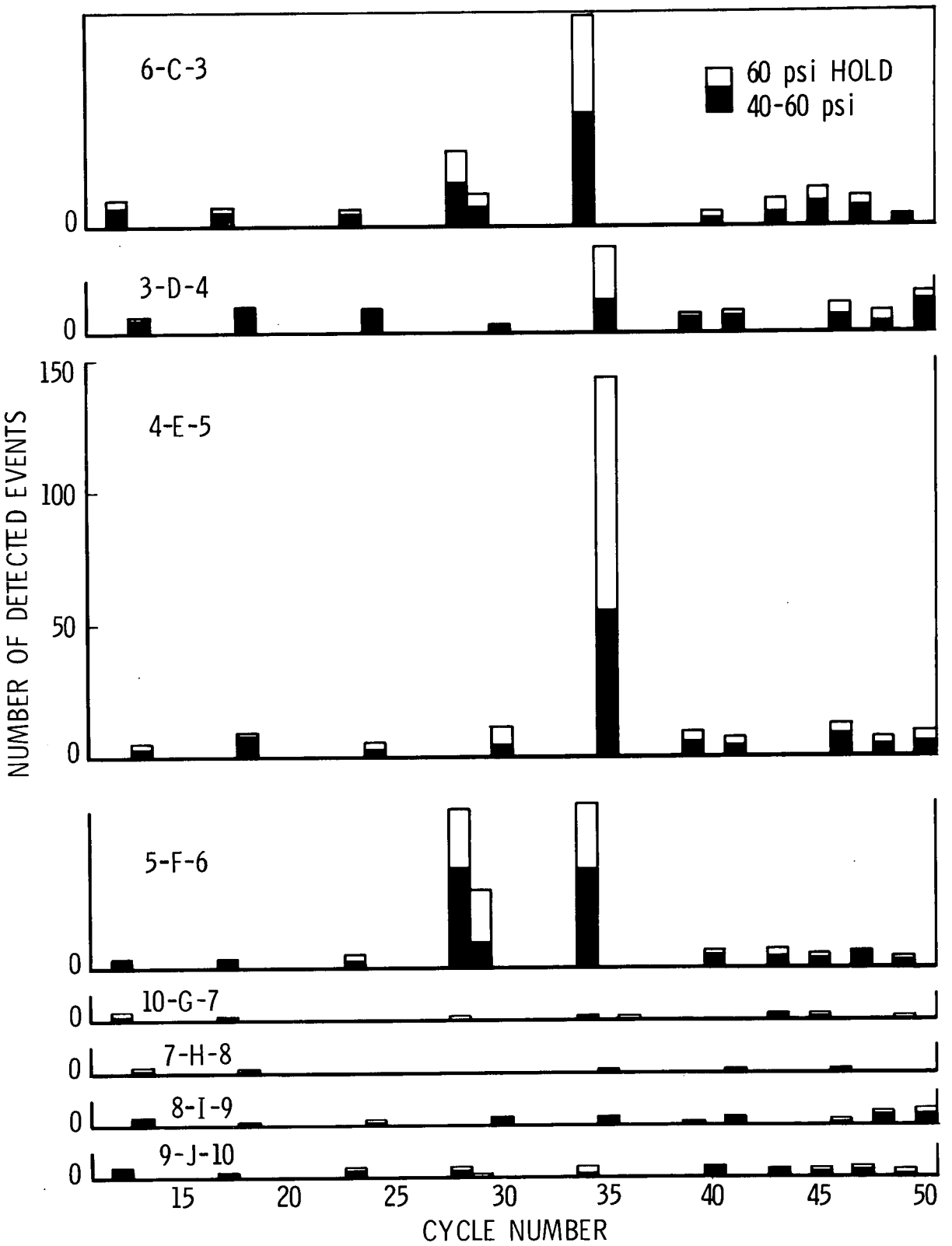

Fig. 27. Number of detected events in each array against cycle number. The top four arrays of the figure are along the upper frame and the bottom four arrays are along the lower frame of the tank (cf. Fig. 21).

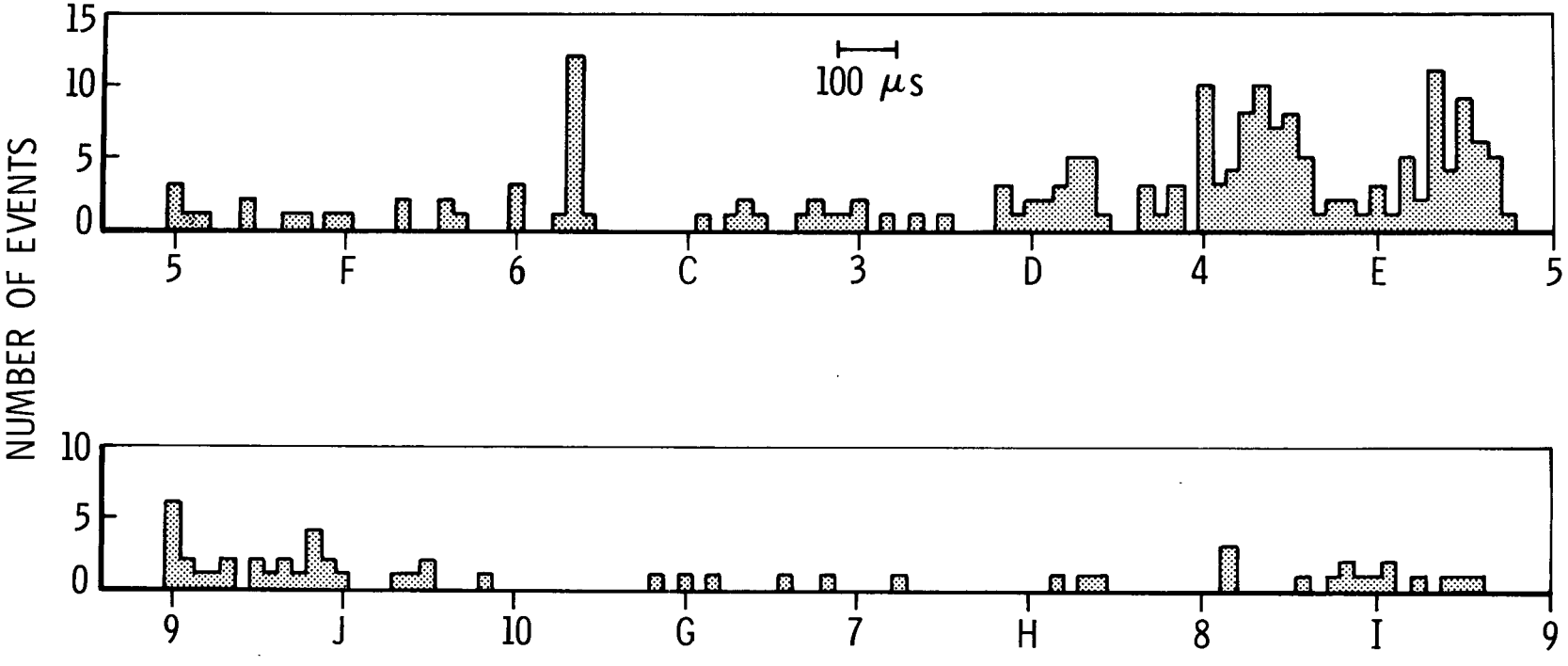

Fig. 28. Delta-t distribution of acoustic events detected during the first phase of the environmental test. The distribution is given in every 25 μs interval of arrival time difference. The delta-t distribution is a measure of approximate locations of signal sources relative to sensors.

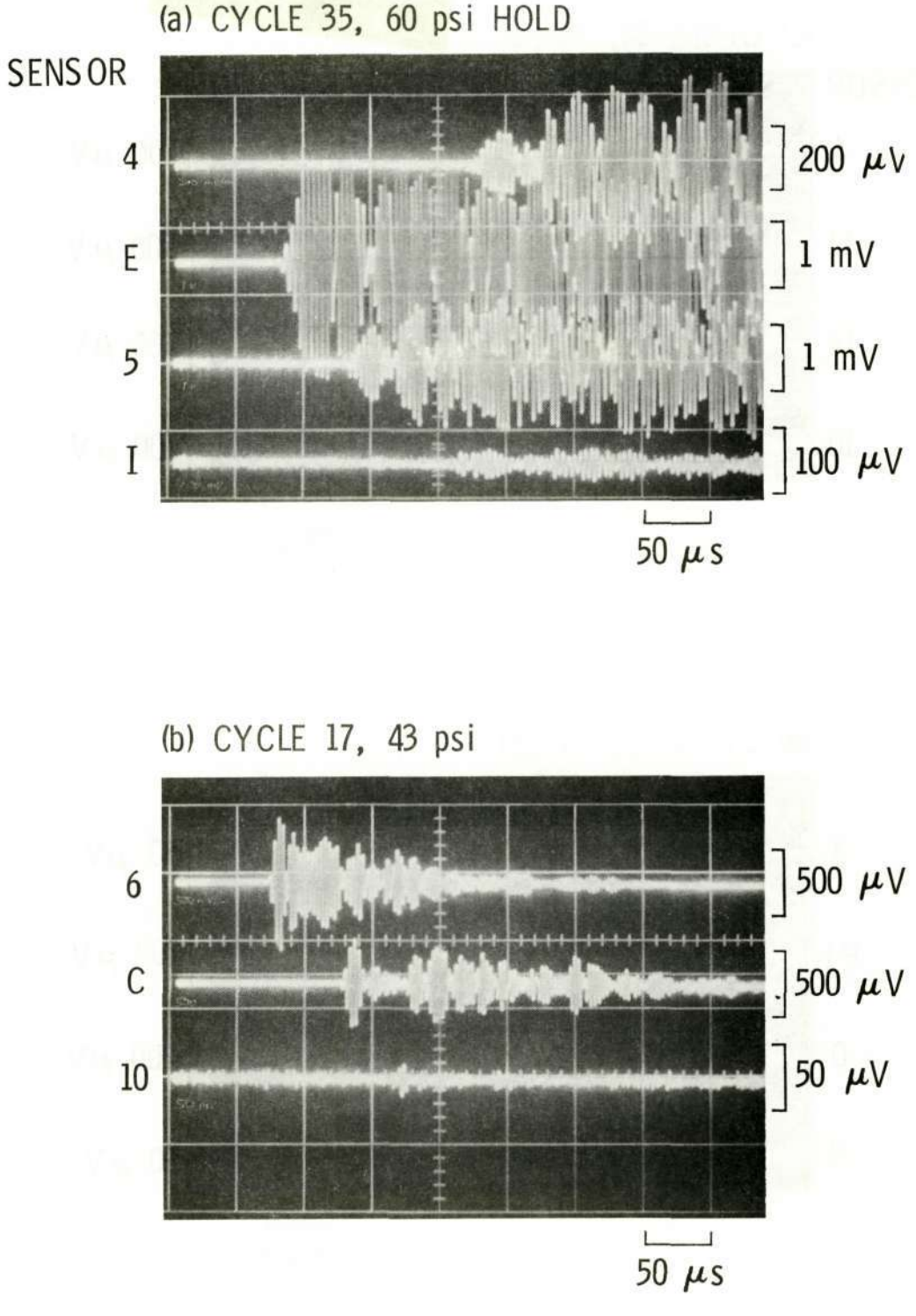

Fig. 29. Representative emission signals observed during the environmental test.

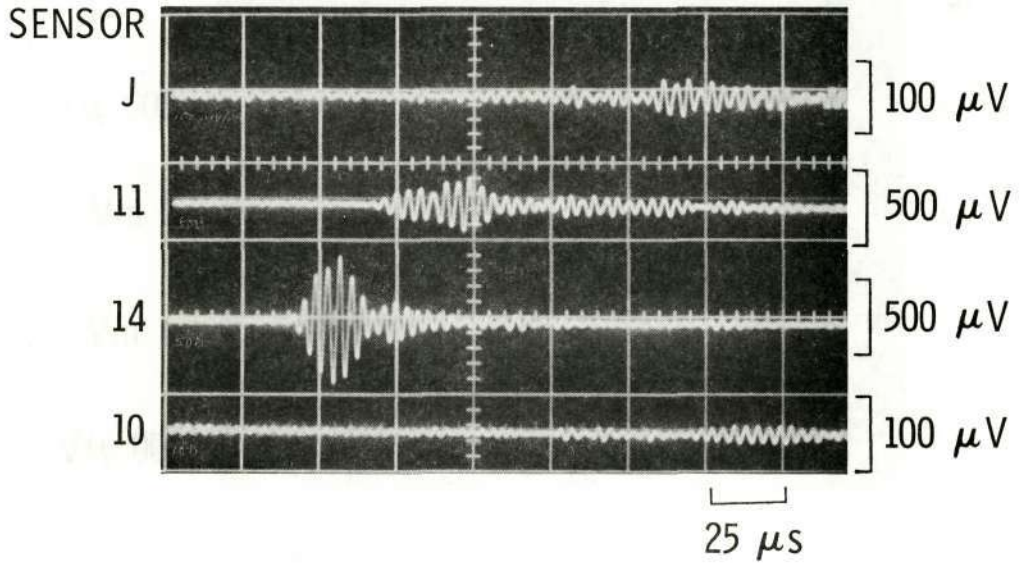

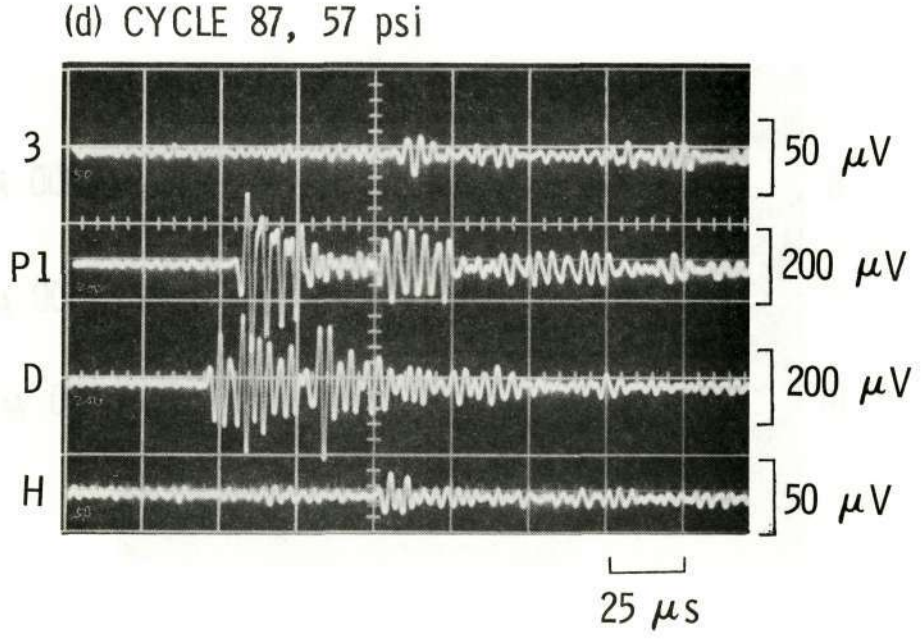

Fig. 29. - Continued

For a few events for which signals were observed by a sensor on the lower circular frame, a triangulation located the emission sources at various places in the upper circular frame area. A representative amplitude distribution of these signals, obtained at sensor D during the 35th life cycle by the Beta-AEM unit, is shown in Fig. 30. The slope of the log-cumulative amplitude distribution curve is less than unity, indicating some kind of fracturing process under high concentrated stress may have been taking place. The absolute value of the observed amplitude, however, was at least an order of magnitude greater than what was expected for a subcritical crack growth, and was too large even for a near-critical crack growth in an aluminum sheet. Therefore, it was not likely to be a result of a crack growth in the tank structure itself. A most likely source of the emissions was a fracturing of a certain material in or near the aluminum-to-insulation interface. Thus, a partial debonding of the insulation was suspected in this area.

The other peak in the distribution of Fig. 28, located between sensors 6 and C is due to large emissions observed during life cycles 12 through 29. Unlike the emissions described above, these emissions originated from a single source located at around the water line 59.5" and angle 254.5°. The impulsive onset of emission signals as seen in Fig. 29(b) also indicates that the emission source was in the thin wall section of the tank. These signals were first observed during the 12th life cycle of the test, but were most frequently observed during the 28th and 29th cycles while the skin temperature of the tank was being stabilized. The amplitudes of these signals were not as large as the largest of the first group of signals described above, but were still too large for a crack growth in the aluminum skin of the tank. The cause of these emissions is still to be determined.

The small array established temporarily during the second and third life cycles and then re-established after the 36th life cycle in the -Y to +Z quadrant of the lower circular frame detected signals continually throughout the monitored period. Almost all these signals were too small to be detectable by the larger basic array in the area. Signal sources were distributed in the area, but mostly concentrated between sensors J and 14. More detailed analyses of these signals were made during the second phase of the environmental test, and will be discussed later in greater detail.

Environmental Test, Phase II

The test procedures of phase II of the environmental test were similar to those of the first phase except the following: During

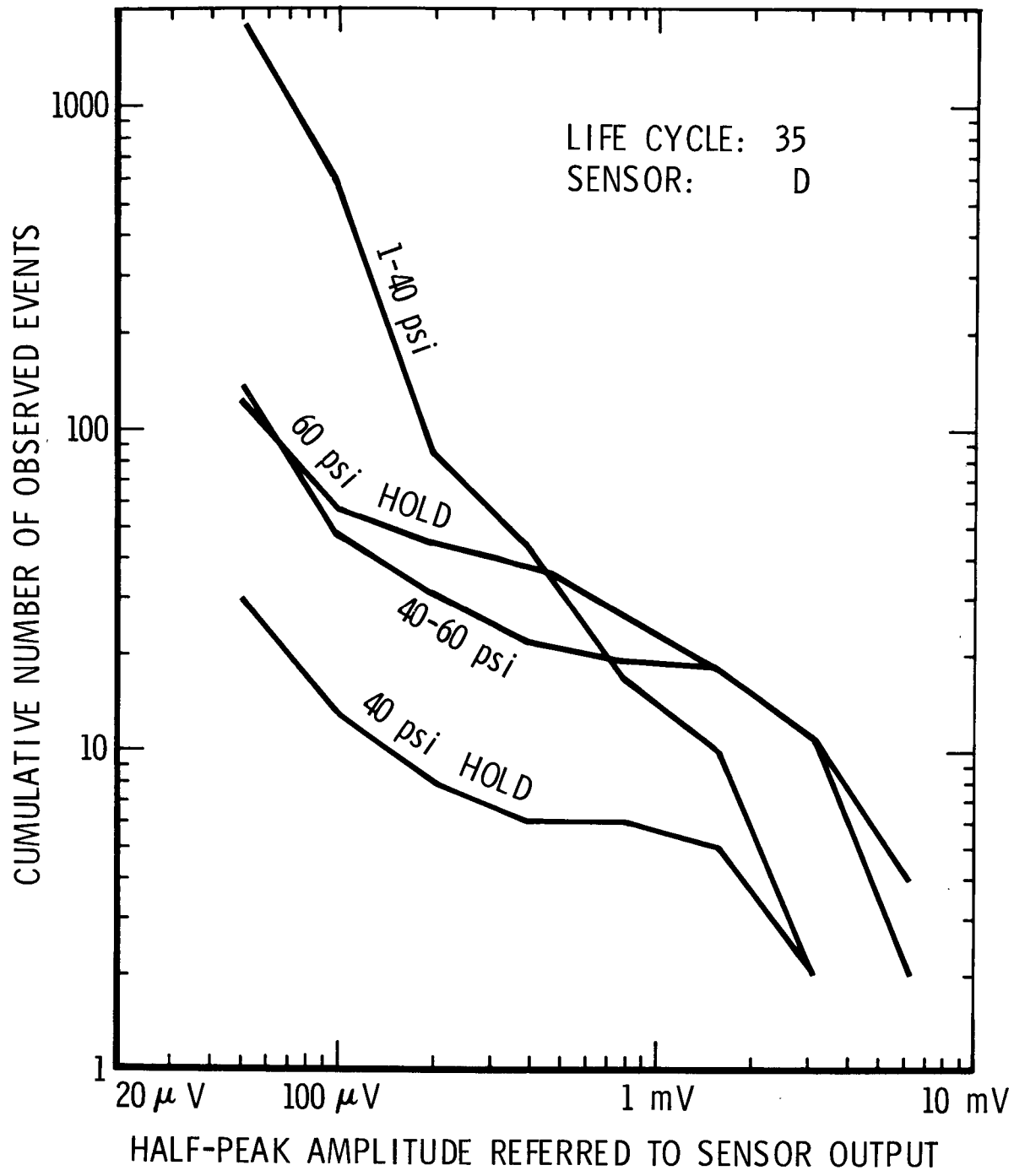

Fig. 30. Amplitude distribution of the extremely large emission signals observed during the 35th life cycle.

the heating cycle of the test, the tank was heated to a skin temperature of 300°F (149°C) instead of 250°F. The temperature was then maintained at this level for 30 minutes, instead of 5 minutes, before the heaters were turned off. Cooldown of the tank consequently took longer. An additional 50 life cycles of test were conducted during the second phase. Cycles monitored during the second phase of the environmental test were: 51-60, 62-64, 66-68, 70-72, 74-76, 78-80, 82-88, 90-92, 94-96, and 98-100; a subtotal of 41 life cycles.

Remodification of Monitor Setup - When one compares the signal detection sensitivity of the large basic array, Fig. 26(A), with the expected signal strengths from crack growths, Fig. 7, it is obvious that the basic array was sensitive enough to detect only large emission signals in the near-failure condition. The sensor separation of 68 cm for the coincidence detection for the basic array was too wide for an effective detection of subcritical crack growth in the tank. A further examination of the results of the monitoring in the first phase of the environmental test indicated, however, that most large emission signals were large enough to be detectable without aid of any elaborate noise-rejection scheme, because extraneous noise signals from far distances were attenuated very effectively by the insulation system. Therefore, it was decided to discontinue the use of the coincidence logic for the basic coverage, and to replace it with a periodic surveillance of the entire tank by monitoring the total activity at each individual sensor location without employing any logic processing.

The monitoring of the total activity at each sensor location was performed by playing out signals recorded on the magnetic tape through a rectifier-integrator circuit, onto a strip-chart recorder. The charge and discharge time constants of the simple RC integrator were 27 μs and 27 ms, respectively. The playouts were made immediately following each monitoring of a pressure cycle for all the sensors for which recordings were made. The entire cylindrical section of the tank was covered in this way in three consecutive cycles.

For monitoring of smaller signals, including possible emission signals from subcritical crack growths, neither the basic coincidence arrays nor the activity playouts were adequate. Consequently, six coincidence detection arrays of smaller sensor separations were established at selected locations on the tank. These arrays are listed in Table 7 below. The equi-sensitivity map of the quarter-size array J-11A-14 is shown in Fig. 26(C) for the signal detection sensitivity of 100 μV referred to the sensor.

Table 7

SMALL COINCIDENCE ARRAYS ESTABLISHED FOR THE SECOND PHASE OF THE ENVIRONMENTAL TEST

Array Elements (Sensors)	Location (Frame & Quadrant)	Sensor Separation (cm)	Resolution Time (μs)
5-P3-F	Upper, +Z to -Y	34	100
3-P1-D	Upper, -Z to +Y	34	100
J-14-10	Lower, +Z to -Y	34	100
G-KA-7	Lower, -Y to -Z	34	100
L-13	Bottom of Tank	30	100
J-11A-14	Lower, +Z to -Y	17	50

Monitoring of the first phase of the environmental test indicated that the majority of the observed noise signals were generated at a very close proximity to each sensor. If this is the case, the signal-to-noise ratio can be improved by placing the sensor not directly on the tank wall but at some distance from the tank wall, because the attenuation of signals is greatest at very close ranges because of the greater geometrical-spreading effect. In order to test this hypothesis, a sensor (12A) was mounted on the outer rim of the circular frame near sensor 7 to compare the signals from both sensors. Signals were recorded by the tape recorder for post-test analysis.

Life Cycles 51 through 100 - These cycles were monitored basically with the monitoring setup described above. Some representative results of the activity playouts are shown in Fig. 31. All three playouts were made at the same sensitivity, thus they gave relative activity levels at each sensor location for each life cycle. The playouts shown in the figure cover from left to right the interval during the pressurization cycle from 40 psi to 60 psi and about 10 seconds into the 60 psi hold. Figure 31(a) shows a type of activity most commonly observed. Activities at most sensors for most cycles were more or less at this relative level. The other two playouts show examples of high activities, which will be discussed later.

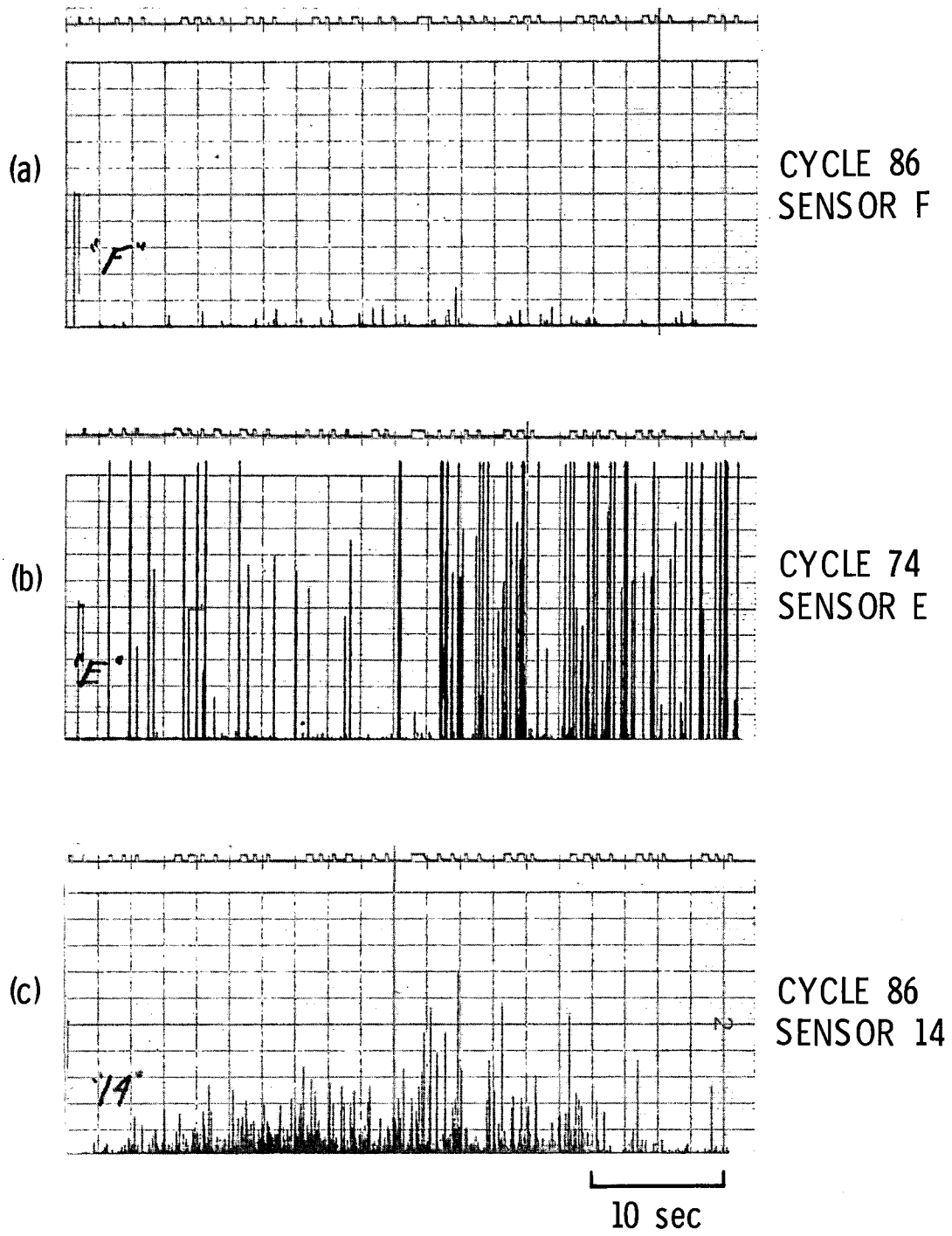

Fig. 31. Representative activity playouts made during the environmental test.

In general, the activity along the lower circular frame was less than the activity along the upper circular frame. This is in agreement with the results of the first 50 cycles of the environmental test. Some sporadic, high activities were observed from time to time at some of the sensors, but most of them were not consistent enough for a systematic analysis to be carried out.

The most prominent activity occurred in the 74th life cycle along the upper circular frame. The activity playout for sensor E during this life cycle is shown in Fig. 31(b). The activity was more than an order of magnitude greater than normal. The analysis of the recorded data clearly showed that this was a recurrence of the high activity during the 28th to 35th life cycles. Emission sources were distributed along the upper circular frame in the +Y to +Z quadrant, and the emitted energy was too large to be from a crack growing in the aluminum structure. The activity did not return again after this cycle.

Smaller signals, the occurrence of which was not apparent on the activity playouts, were detected by the small coincidence detection arrays. The delta-t distributions (distribution of arrival time differences) of detected signals from some of the small arrays are shown in Fig. 32. For the J-11A-14 array, the distribution is given in 5 μs intervals, while for others, they are given in 10 μs intervals. The detection sensitivities used were 100 μV threshold referred to the sensor for the J-11A-14 array, and 50 μV threshold referred to the sensor for others. Both of these gave approximately the same signal detection sensitivity when referred to the emission source as is apparent when one compares Fig. 26(B) with Fig. 26(C).

The most distinct group of signals was observed from the area between sensors 11A and 14, in the azimuthal interval of 290^{o} to 300^{o}. The activity in the area was high enough to be visible on the activity playout as seen in Fig. 31(c). Almost all of these signals, however, were too small to be detectable by any sensor other than those in the array J-11A-14. The waveforms of a representative event in this group are shown in Fig. 29(c). Though the source locations of most of these events could not be determined exactly, the relatively gradual onset of most of the signals indicated that they were in the lower circular frame area. A representative amplitude distribution of this group of signals is shown in Fig. 33. The slope of the log-cumulative distribution is about the same as that of signals observed from this area during the proof test [Fig. 17(b)] . It is relatively steep, indicating that even if they were from subcritical crack growths in the area,

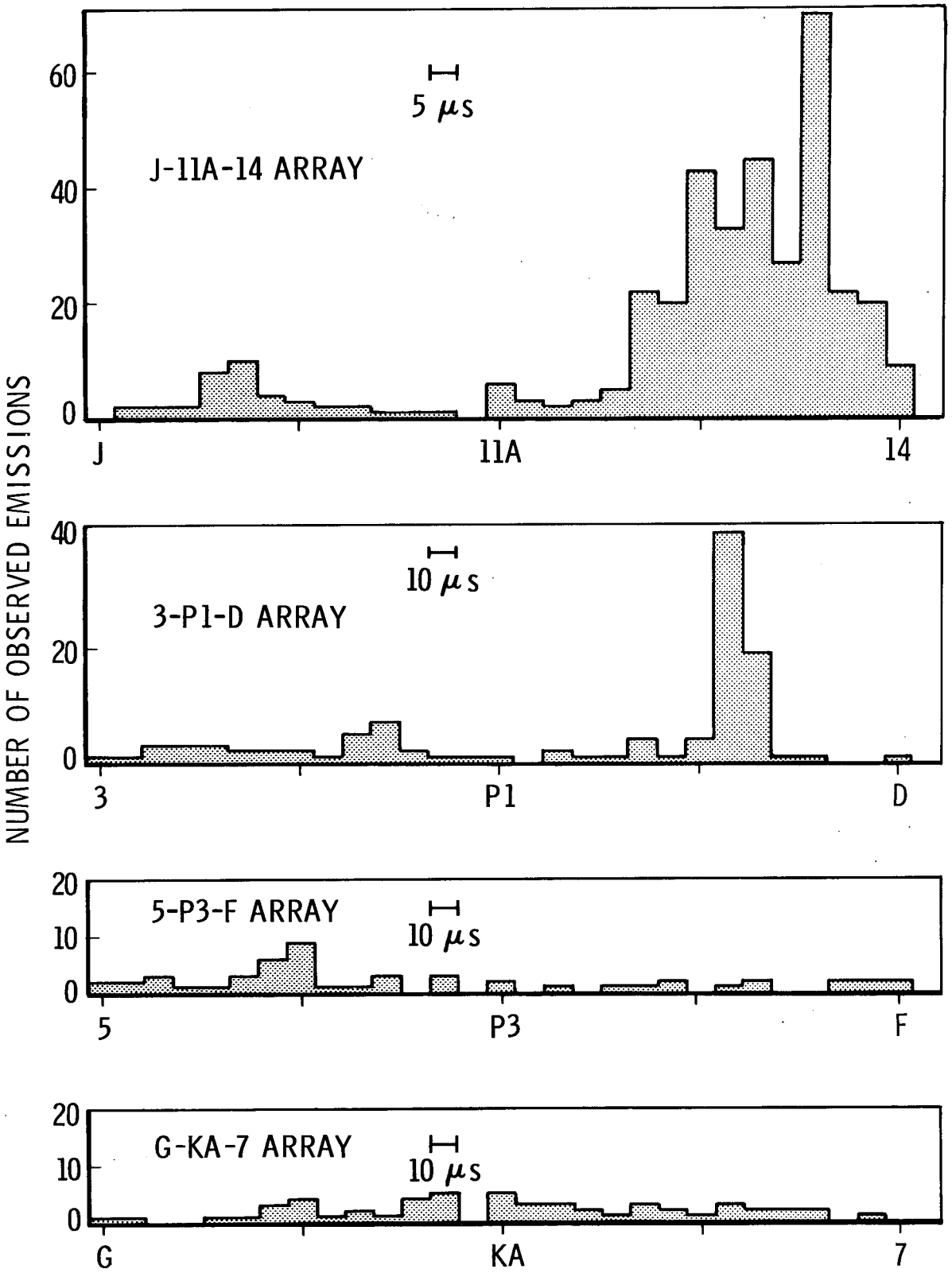

Fig. 32. Delta-t distribution of signals detected by small arrays during the second phase of the environmental test. (cf. Fig. 21, p. 49, for array locations)

D

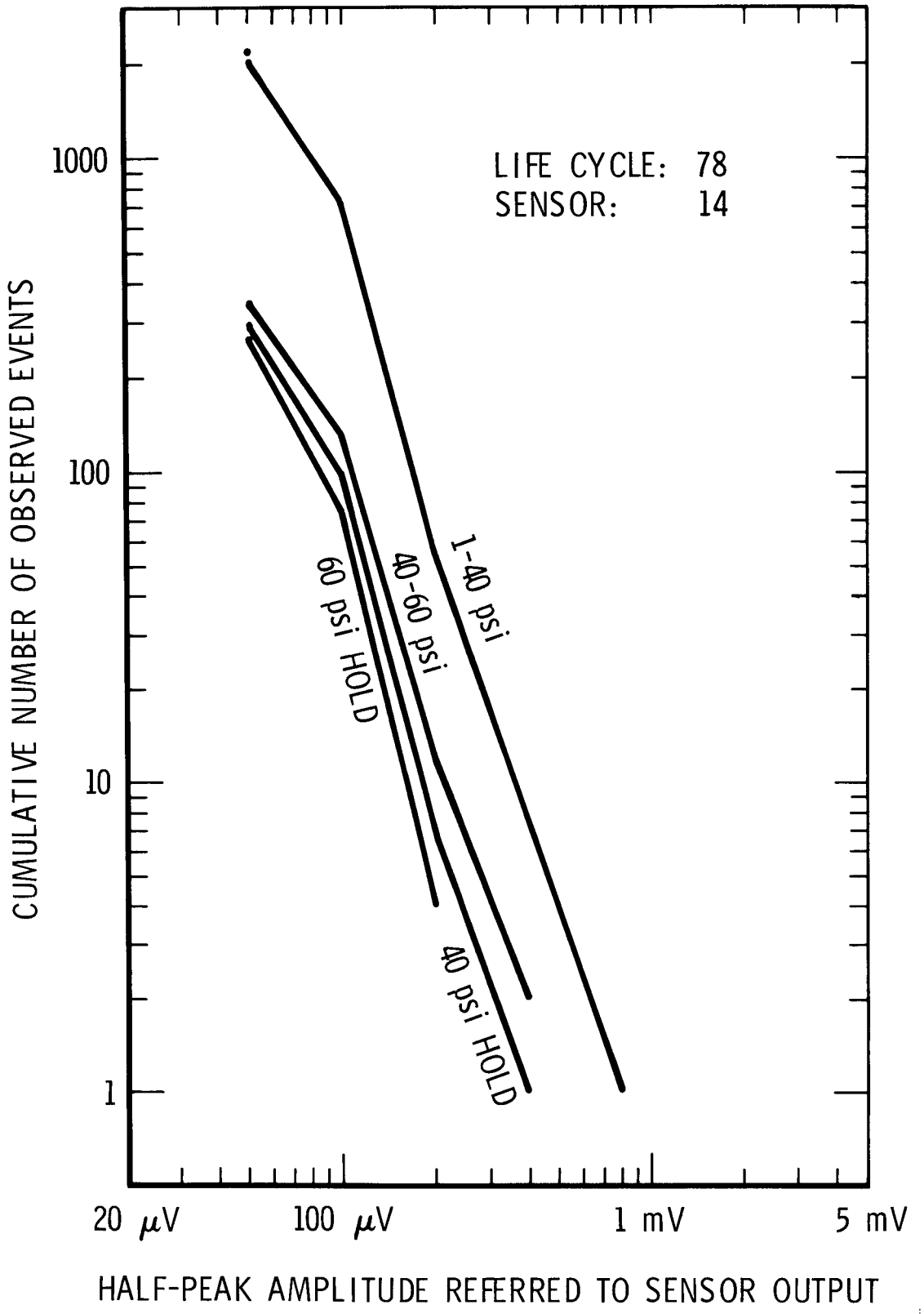

Fig. 33. Amplitude distribution of emission signals from J-11A-14 array.

the stress intensity level was not high. The absolute amplitudes of the signals were in the range expected for a subcritical crack growth in the aluminum structure. No apparent change of activity was observed for this group of signals throughout the test.

Another distinct group of signals was observed between sensors P1 and D as seen in Fig. 32. These signals were first detected immediately after the 3-P1-D array was established, and were observed very consistently in each life cycle thereafter. The signals were not strong enough to be detectable either by the basic array used during the first phase of the environmental test or by the activity monitoring.

This group of signals differed from the group of signals detected near the sensor 14 in several respects. The emission sources of these signals were not distributed in a wide area, but were practically at a single location on the cylindrical thin-wall section of the tank, given by the coordinates: azimuth 142.5^{o}, water line 54". Figure 29(d) shows waveforms of a representative event from this location observed at four sensors. The signals have impulsive beginnings, which are characteristic of events originating on the thin wall section of the tank.

In order to investigate this group of events in greater detail, it was decided to establish a high resolution detection array to detect only this group of signals, spatially discriminating all others. A modification of one of the AEM units to accomplish this was completed by the 94th cycle, and the unit was used thereafter till the end of the environmental test.

Through the aid of this detection array, several additional characteristics of the signals were determined. In each life cycle, one or two emission events were observed from this location, during the filling of the tank at about the time when the liquid level reached this location, approximately ten to twenty events were detectable during the pressurization of the tank, and one or two emissions of very small amplitudes were observed during the heating of the tank. No emission event from this location was observed during pressure holds and depressurization of the tank.

A representative amplitude distribution of these signals is shown in Fig. 34. Though the number of detected signals is not large enough to draw a definite conclusion from this distribution, the slope of the log-cumulative distribution curve is in the range expected for a crack growth, and the observed amplitude also is in agreement with the expected signal strengths from subcritical crack growth as observed during the specimen test.

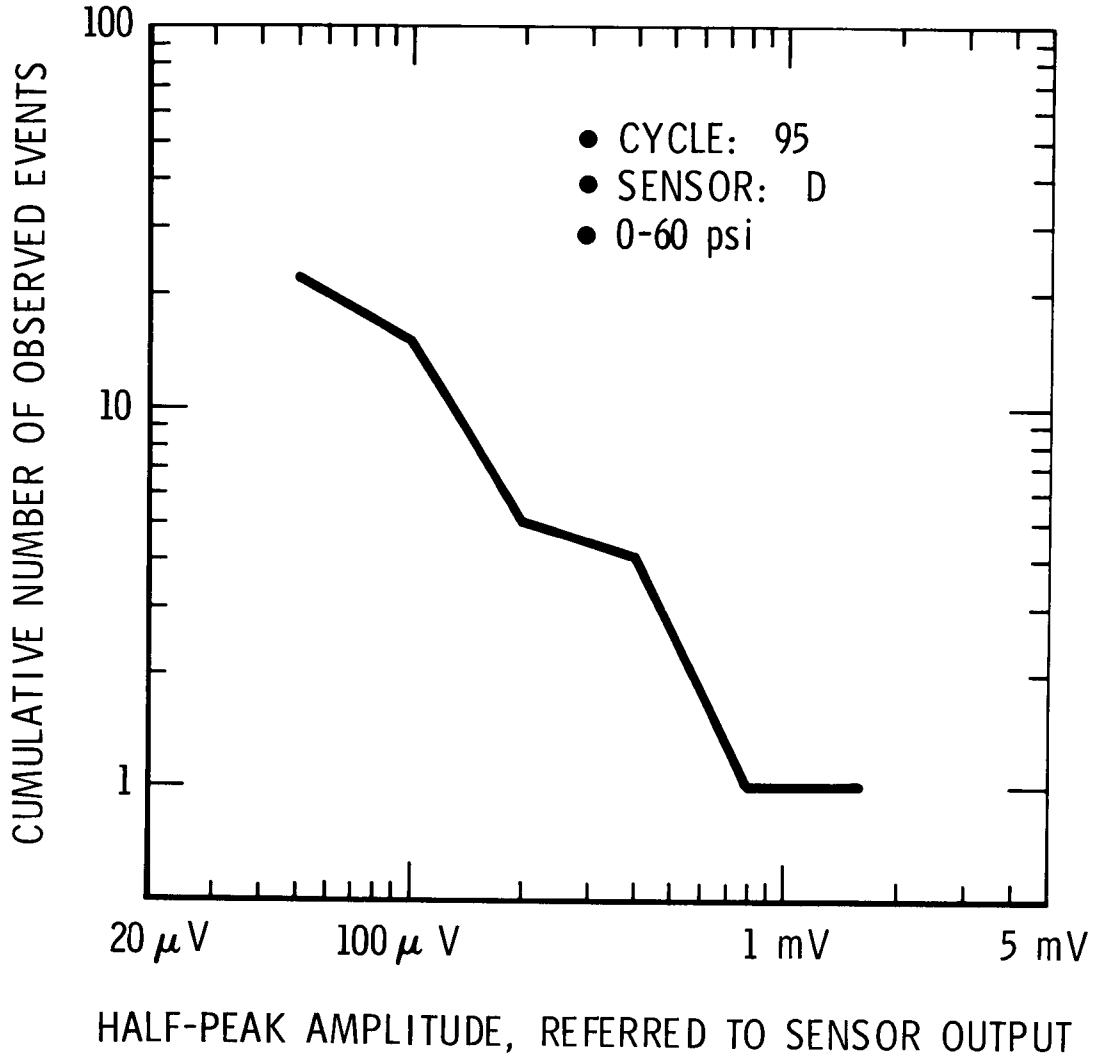

Fig. 34. Amplitude distribution of emission signals from azimuth 142.5°, water line 54".

A slight peak in the delta-t distribution of 5-P3-F array in Fig. 32 at around halfway between sensors 5 and P3 was due to several emission events observed during the 51st life cycle from a location along the upper circular frame. Though this coincides with the location where an ultrasonic inspection found a debonding of the insulation during the inspection performed between the two phases of the environmental test, whether they are related or not is uncertain from the presently available data.

Comparison of Signals at Sensors 7 and 12A - As described earlier, a pair of sensors 7 and 12A were used to compare emission signals detected by a sensor on the tank skin (7) and by a sensor on the outer rim of the circular frame (12A) in order to see if near-range noise events could be suppressed to achieve a better signal-to-noise ratio. Signal amplitudes of events occurring at a wide range of distances were compared. The data reduction is still incomplete, but a tentative result shows that, as expected, the greater the distance from the emission source to the sensor, the larger the amplitude ratio A_{12A}/A_7. The ratio ranged from less than 0.1 for events occurring very close to the sensors to a large, undetermined value (observable at 12A only) for events occurring at far ranges. The cross-over distance where signals were observed at nearly equal amplitudes at both sensors was at around 25 cm. Since almost all of the numerous aluminum-insulation interface noise events were too small to be detectable beyond this cross-over distance, mounting a sensor on the outer rim of the circular frame was found to be effective in minimizing the near-sensor noise interference. However, mounting a sensor on the outer rim degraded the signal quality by making the signal waveform more complex and by deteriorating the onset of the signal because of the more complicated signal transmission through the circular frame. The merit of this technique, therefore,was judged uncertain.

Frequency Content of the Emission Signals - The monitoring system used for the present study had narrow-band characteristics in order to achieve a high sensitivity of signal detection. Consequently, very little information as to the frequency content of emission signals could be obtained from the present data. To supplement this, the frequency response range of one channel of signal train was kept relatively wide open to record emission signals in the frequency range down to about 10 kHz. Only very small fractions of the recorded data have been analyzed to date, but the data examined so far indicates that, although a majority of the observed events have sufficient energy in the few-hundred kilohertz range to be most effectively detectable by the present setup, there are signals which have much less energy in the few-hundred

kilohertz range than in the lower frequency ranges. More extensive data analysis is needed to clarify the nature of these signals.

V. DISCUSSIONS

The present study has demonstrated that acoustic emission signals of the relatively small intensity expected for subcritical crack growth can be detected by using a combination of frequency filtering and appropriate spatial filtering to reduce background noise. For a foam insulated thin-walled tank, the coincidence logic used during the second phase of the environmental test was found to be most effective in spatially discriminating signals from noise. To determine what frequency range to use and how the sensors should be arranged to obtain an optimum monitoring coverage of a tank is a relatively easy task using the data obtained by specimen tests, as has been done in the present study.

A more difficult, and possibly the most difficult, task is to interpret the signals thus detected. As expected, the present monitoring detected acoustic signals of various kinds: some large and some small; some concentrated and some distributed; some consistent and some sporadic. To interpret correctly each of these observed groups of signals requires an extensive knowledge of the expected properties of various possible sources of emission signals.

In the present study, the major features of the observed acoustic signals considered were the following: (1) occurrence of acoustic events in relation to the loading and heating cycles; (2) location of the signal source; (3) absolute intensity of the signal; (4) amplitude distribution of the group of signals; (5) consistency with which events occur. Other such features as waveforms, azimuthal distribution of signal intensity and partition of emission energy into various modes of wave propagation were also considered as supporting characteristics. The frequency content of signals may be a useful feature to consider, but it is more difficult to measure than other characteristics and was not used as a primary feature to look for in signals of the present study.

The emission signals observed during the present study can be classified into two major groups: extremely large amplitude signals and small amplitude signals. The former group of signals was simply too large to be caused by crack growth in the aluminum structure of the tank. The amplitude distribution of these signals, however, indicated that these signals were generated at places where high concentration of stress existed. Thus, a partial breaking of material at or near the aluminum-to-insulation interface was suspected as a cause of these signals. Whether or not

these signals represented a debonding of insulation in a significant amount, however, could not be determined from the available data.

Signals which created most concern to us were the small amplitude signals. Their intensity was right in the range expected for subcritical crack growth in aluminum sheet. Thus, it is possible that they were caused by subcritical crack growths in the structure. There were, however, other possible sources of these small amplitude signals. For example, a small relative movement of the insulation relative to the aluminum skin where the bonding was not perfect could induce acoustic signals of small amplitude into the structure. In case of the proof test, the action of water directly onto the structural material seemed to have caused some of the observed signals. Unfortunately, the present knowledge of the acoustic emission phenomenon is not sufficient to tell one from the other.

One positive result of the present monitoring was that none of the consistently observed groups of small signals showed a steady increase of activity with life cycles. This probably indicated that none of these signals represented crack growth approaching its critical level. The post-test inspection did not find any significant crack growth in the tank structure.

Considering the present difficulty in interpreting the observed acoustic signals, it is obvious that the usefulness of the acoustic emission technique, in the present state of the art, in nondestructive inspection of complex structures is rather limited. In our opinion, two different approaches can be taken with respect to the utilization of the acoustic emission technique to a nondestructive inspection of complex structures. One approach is to use the acoustic emission technique as a surveillance tool. The presently available technology is sufficient to detect and locate, but not to identify, acoustic emission sources. With a proper planning of the locations of sensor arrays, a relatively large region of a structure can be covered simultaneously at a given minimum sensitivity of detection everywhere in the region. The number of detected signal-source locations in an ordinary structure is usually limited to a small figure, as was the case in the present study. Periodic inspection of only these locations using other established nondestructive inspection methods will achieve a considerable saving in inspection time and effort. Two important things to remember in this case are the following: (1) Only active flaws generate acoustic emission signals. (2) The acoustic emission technique is so sensitive that in many cases other presently available techniques cannot detect anything even when an

emission-generating flaw exists. Inspections, therefore, must be repeated until the flaw grows to a sufficiently large size to be detectable. For this approach, the technology is available today, and only such developments as automatic acquisition and processing of data are necessary.

The other approach is to wait until sufficient knowledge of the emission mechanisms becomes available so that correct interpretation of observed acoustic signals may be made. This requires a quite extensive research on the properties of acoustic emission signals. When this is accomplished, however, the acoustic emission technique can be used as an independent tool for a nondestructive inspection of complex structures.

The approach we took for the present study was neither of the two approaches described above. This was because our primary objective was not to detect flaws in the structure, but rather to study how well the acoustic emission technique could be applied to this particular structure. Therefore, the approach and the procedures described in the preceding sections of this report are not recommended to be followed when a detection of flaws is a prime objective.

Whichever approach one takes, it is clear that some interpretations of detected signals are required, or at least quite helpful. To interpret the detected signals requires quite an extensive knowledge of emission mechanisms and wave propagation. For this reason, in our opinion, the most important area of development in the acoustic emission technology today is the training of personnel. This point cannot be over-emphasized considering the great interest expressed recently in the utilization of acoustic emission techniques for nondestructive inspection. To attempt to use the acoustic emission technique without trained personnel only leads to a disaster.

VI. CONCLUSIONS AND RECOMMENDATIONS

The result of the present study, we feel, is rather inconclusive primarily because of two reasons: First, there was less than sufficient time available before the tank test to really think about the planning of the monitoring and to examine thoroughly such anticipated problems as severe attenuation of signals and various expected noise sources. Second, there was less than sufficient time available after the test to analyze the acquired data thoroughly. Nevertheless, some tentative conclusions can be drawn from the present study. The first conclusion below applies specifically to this study, but the rest are also applicable to a monitoring of complex structures in general.

(1) Acoustic emission signals were observed originating at several locations and areas on the tank. None of these was positively identified as originating from a growing crack, and none indicated a critical crack growth. This, however, does not rule out the possibility that some of these signals may have been from subcritical crack growth.

(2) The results of the specimen tests directly oriented towards finding the signal-generation and transmission characteristics in the specific structure were found to be very useful in interpreting the monitoring results.

(3) For correct interpretation of various observed signals, more extensive knowledge of emission characteristics than presently available is needed.

Recommendations resulting from the present study are the following. Again, some of them are specific to the present application, but others are for monitoring of complex structures in general.

(1) As demonstrated in this study, detection and location, but not identification, of acoustic emission signals of relatively small intensity such as would be expected from subcritical crack growth are within the capability of the present technology. Therefore, if immediate use of the acoustic emission technique is desired for nondestructive inspection purposes, it should be used as a surveillance tool. It is recommended that a development effort be started to accomplish this end.

(2) For monitoring of such not-so-familiar structures as the test tank of this study, more extensive specimen tests than have

been made for the present study are recommended because they produce information very useful in interpreting monitoring results. For this specific application, such tests as propagation of acoustic waves in aluminum sheet immersed in water, possible generation of acoustic waves by the direct interaction of water on flawed and unflawed aluminum sheet, dependence of amplitude distribution of acoustic emission signals upon specimen size, and frequency content of emission signals are strongly recommended before attempting to monitor a real tank.

(3) To achieve better interpretation of detected signals, more research effort directed towards obtaining a better understanding of emission mechanisms and thus obtaining a better characterization of various emission signals is recommended.

(4) For the handling of a large quantity of data, as is the case when one attempts to cover entirely a large structure, the use of a small computer for data processing and storage is more economical than the method used in the present study. The use of a small computer, therefore, is strongly recommended to replace the logic processing of data currently handled by several specialized acoustic emission data processing units.

(5) For the interpretation of detected acoustic emission signals, trained personnel are required. It is, therefore, recommended that planning be started for properly training personnel before use of the acoustic emission technique for nondestructive inspection is considered.

(6) Finally, a list of specific items of investigation which are needed to solve some of the seemingly open-ended results of the present study. These items are strongly recommended if further use of the tank is planned as a test bed for acoustic emission investigation because they will supply indispensable back-up data for interpretation of tank-test results. Items are listed in descending order of importance.

i) Testing of PPO-foam-insulated aluminum specimens for characterization of acoustic emission signals generated by debonding.

ii) Testing of welded aluminum specimens in water, and possibly in hydrogen environment, for possible acoustic emissions caused by environmental effect.

iii) Analysis of data for low-frequency content of observed emission signals. The data for this are already available on tape (cf. p. 77).

iv) Testing of flawed and unflawed welded aluminum specimens under tensile stress for acoustic emission characterization.

v) More extensive testing of precracked aluminum specimens for specimen size effect, frequency content of acoustic emission signals, and reproducibility of results.

REFERENCES

1. Acoustic Emission, Proceedings of the Symposium on Acoustic Emission, Bal Harbour, Dec. 1971, American Society for Testing and Materials, STP-505 (to be published in 1972).

2. General Dynamics, Convair Aerospace Division, Space Shuttle Structural Test Program, Final Report - Subtask 1.1, Cryogenic Tank Structure/Insulation Test, Report No. 549-3-092, Contract NAS9-10960, 28 March 1972.

3. W. M. Ewing, W. S. Jardetzky, and F. Press, Elastic Waves in Layered Media, pp. 281-293, McGraw-Hill, New York, 1957.

4. Y. Nakamura, "Acoustic Emission Monitoring System for Detection of Cracks in a Complex Structure," Materials Evaluation, 29, 8-12, 1971.

5. Y. Nakamura, C. L. Veach, and B. O. McCauley, "Amplitude Distribution of Acoustic Emission Signals," General Dynamics Report ERR-FW-1176, 1971.

6. B. O. McCauley, "Development and Testing of a Wide Temperature Acoustic Emission Sensor," General Dynamics Report ERR-FW-1308, 1972.

7. M. F. M. Osborne and S. D. Hart, "Transmission, Reflection, and Guiding of an Exponential Pulse by a Steel Plate in Water, I. Theory," J. Acoust. Soc. Am., 17, 1-18, 1945.